論文 / 著書情報
Article / Book Information

題目(和文)	親指のリハビリテーションのための装着型過拘束パラレルロボットの開発
Title(English)	Development of Overconstrained Wearable Parallel Robot for Thumb Rehabilitation Therapy
著者(和文)	崔 佑赫
Author(English)	Woohyeok Choi
出典(和文)	学位:博士（工学）, 学位授与機関:東京工業大学, 報告番号:甲第12033号, 授与年月日:2021年6月30日, 学位の種別:課程博士, 審査員:武田 行生,菅原 雄介,岩附 信行,岡田 昌史,遠藤 玄,土方 亘
Citation(English)	Degree:Doctor (Engineering), Conferring organization: Tokyo Institute of Technology, Report number:甲第12033号, Conferred date:2021/6/30, Degree Type:Course doctor, Examiner:,,,,,
学位種別(和文)	博士論文
Type(English)	Doctoral Thesis

Development of Overconstrained Wearable Parallel Robot for Thumb Rehabilitation Therapy

by

Woohyeok Choi

DISSERTATION

Presented to
The Graduate major of Mechanical Engineering,
The Department of Mechanical Engineering,
The School of Engineering of Tokyo Institute of Technology
in partial fulfillment of the requirements
for the degree of

DOCTOR OF ENGINEERING

Tokyo Institute of Technology

June 2021

Approved by:

Wataru Hijikata
Associate Professor, Dr. Eng.
Department of Mechanical Engineering
School of Engineering

Gen Endo
Professor, Dr. Eng.
Department of Mechanical Engineering
School of Engineering

Masafumi Okada
Professor, Dr. Eng.
Department of Mechanical Engineering
School of Engineering

Nobuyuki Iwatsuki
Professor, Dr. Eng.
Department of Mechanical Engineering
School of Engineering

Yusuke Sugahara
Associate Professor, Dr. Eng.
Department of Mechanical Engineering
School of Engineering

Yukio Takeda
Professor[Academic Supervisor], Dr. Eng.
Department of Mechanical Engineering
School of Engineering

Development of Overconstrained Wearable Parallel Robot for Thumb Rehabilitation Therapy

Summary

The rehabilitation robot is the robot that aims to recover the human motor function through assisting or reinforced the motion of human movement. This robot is expected to one of the solutions to the lack of therapist. One of the distal parts of the human body, the thumb, is related to the dexterity skill, and it supports other fingers. Because the thumb's damage prevents the dexterity skill and makes the patient uncomfortable, thumb rehabilitation is essential. As the thumb carpometacarpal (CMC) joint structure is very complex, it is hard to allow its mobility to control by the mechanical joint. The misalignment issue, which is the mismatched phenomenon between the robot's axis and the finger joint axis, is the exoskeleton type's challenge point. In previous research, the exoskeleton type designs are proposed to allow the finger joint by the mechanism, but those designs are not for the CMC joint. Moreover, most of those are designed their thumb part to focus on controlling the CMC joint's partial movement. On the other hand, the previous research's end-effector type design is not necessary to design with consideration allowing the rotational mobility between finger and mechanism.

Based on these backgrounds, the (2-RRU)-URR parallel mechanism, which combined each advantage of two design types, is proposed in this thesis. The proposed mechanism is designed to attach its base part to the palm and surface and the output link is attached to the center of the thumb. This mechanism has characteristics such as lower mobility, an overconstrained mechanism, and the providing compound motion that consists of rotational and translational motions. To consider designing for thumb rehabilitation, it should know the characteristics of the mechanism before designing the proposed mechanism through the kinematic analysis. Moreover, since

the proposed mechanism being designed for thumb rehabilitation therapy, considerations such as the mechanical part's placement in hand and the anatomical or the kinesiological information are necessary to design the mechanism. In this thesis, a parallel mechanism was proposed for thumb rehabilitation therapy. The basic kinematics of the proposed mechanism, such as displacement analysis, velocity analysis, static analysis, and workspace analysis, were carried out. Furthermore, the geometric design with the human hand and the user test with the prototype were described. This thesis is consisting of six chapters.

In chapter 1 "Introduction", the background of this research, the related previous research, the objective of the research, and the thesis composition were introduced.

In chapter 2 "(2-RRU)-URR parallel mechanism", the structure of the proposed mechanism was explained, and the kinematic analysis such as the mobility of the mechanism, displacement, and velocity were carried out. Through Grubler's formula and the inspection of the constraint condition through the screw theory, the mobility analysis results revealed that the proposed mechanism is overconstrained mechanism, and its mobility is three DOF, which consist of two rotational and one translational mobility. To understand the position relationship between the input and the output, the displacement analysis was considered by dividing it into two parts, respecting the structure of the proposed mechanism, and its calculation process of each part was derived. Combining each result of the calculations, the whole displacement analysis was derived. Besides, the overall Jacobian matrix, which indicates the constraint and the output velocity, was derived. Those analysis processes are proof through numerical examples.

In chapter 3 "Static analysis", the method of the static analysis and its verification experiment were described. The method of the static analysis is using the overall Jacobian for deriving the required actuation torque when the external loads are given. To confirm this method, the simulation result and the experimental result with the experimental apparatus were compared. From the comparing result, it is confirmed that this method can be used to derive the required actuation torque of

the proposed mechanism.

In chapter 4 “Workspace analysis and dimensional synthesis”, the definition of the effective workspace and its application for dimensional synthesis were described. The effective workspace, which has the required input torques to satisfy the safety requirement by the proposed mechanism’s geometrical condition, is defined from the reachable workspace. The dimensional synthesis method finds the suitable condition that has a broad coverage of the effective workspace in the required workspace and a small link length from the design candidates. Based on this method, the numerical example is calculated for the sake to understand.

In chapter 5 “Prototyping and experiment with users”, the prototype design procedure for thumb rehabilitation with consideration of the thumb measurement data and its user test was described. The thumb measurement data is used for determining the required workspace and the input trajectory of the prototype. To consider the hand’s attachment, the placement of actuators and their effects on the workspace are examined. Based on the preliminary works, the prototype for thumb rehabilitation was manufactured. The purpose of the user experiment is to confirm the possibility of the prototype controlling the rehabilitation movements. As the result of the user test, the prototype shows the performance to generate the required movement and the adaptation to fit on any hand size even though the limitation of the lack of the actuator torque exists.

In chapter 6 “Conclusion and discussion”, discussing this thesis’s whole achievements, the remaining points, the conclusion, and future works are described.

Contents

List of Figures

List of Tables

Chapter 1

Introduction

1.1 Background

1.1.1 Rehabilitation and rehabilitation robot

Physical rehabilitation(rehabilitation) is a type of therapy for assisting in the restoration and recuperation of the motor functions of a patient. It is done primarily for patients who have had their motor functions impaired by ailments such as cerebral hemorrhages, brain tumors, Parkinson's disease, or other brain diseases. In conventional rehabilitation therapy, a rehabilitation therapist must be near the patients, and all the processes of rehabilitation therapy must be done manually. Furthermore, the therapist provides the required external force during therapy, the magnitude of which depends on the degree of paresis of the patient. In the therapy, an external force is used to stimulate the body motor systems of impaired parts. Since rehabilitation therapy requires being able to continuously apply a stronger force than the stiffness of the affected part, therapists must be well trained and physically capable. The effect of the rehabilitation depends on various factors such as the timing of the therapy, the intensity of the therapy, the number of the therapists, the attention of the therapist, the number of repetitions, and the attitude of the patient towards therapy, among numerous others [1–3]. However, because of the aging population, the number of therapists and patients is becoming increasingly

disproportionate, and the workload of each therapist is increasing rapidly [4]. This shortage in therapists relative to patients is a critical issue, as it affects the recovery of the patient's motor function. Even if the therapist fully prepares for each patient, the amount of time for therapy is limited (only 5.2% of daytime in two weeks take the care from the therapist [5]).

A rehabilitation robot was proposed as one of the solutions to alleviate the issue of the lack of therapists. Because robots do not experience fatigue, rehabilitation robots can provide continuous and consistent external force. For this reason, the robot can not only provide a given constant force continuously but also can provide a consistent motion trajectory. This advantage can help reduce the workload of therapists and can increase the number of repetitions a patient receives. Repetitive training helps recover a patient's motor function after the intensive rehabilitation process. It induces brain plasticity in stroke patients and helps maintain its activation [6]. Furthermore, this training is also used as a warm-up process before the primary therapies.

1.1.2 Hand and thumb

The human hand is a crucial organ, and it is critical to human dexterity in daily life. In particular, the role of the thumb is to support the other fingers during grasping and picking-up movements [7]. These movements, which involve the cooperation of the thumb and the other fingers, cover about 40% of all finger movements [8]. Because these movements provide manual dexterity skills to humans, the loss of the thumb function severely hinders daily activities. The transplantation and recovery of the thumb has a higher priority than other fingers because of its critical role. Thumb rehabilitation is important to help patients recover their thumb function and restore overall hand functionality.

The thumb exhibits five movements, namely, abduction, adduction, flexion, extension, and opposition as shown in Fig. 1.1. Abduction refers to the movement of the thumb moving away from the palm from its resting position. In detail, two

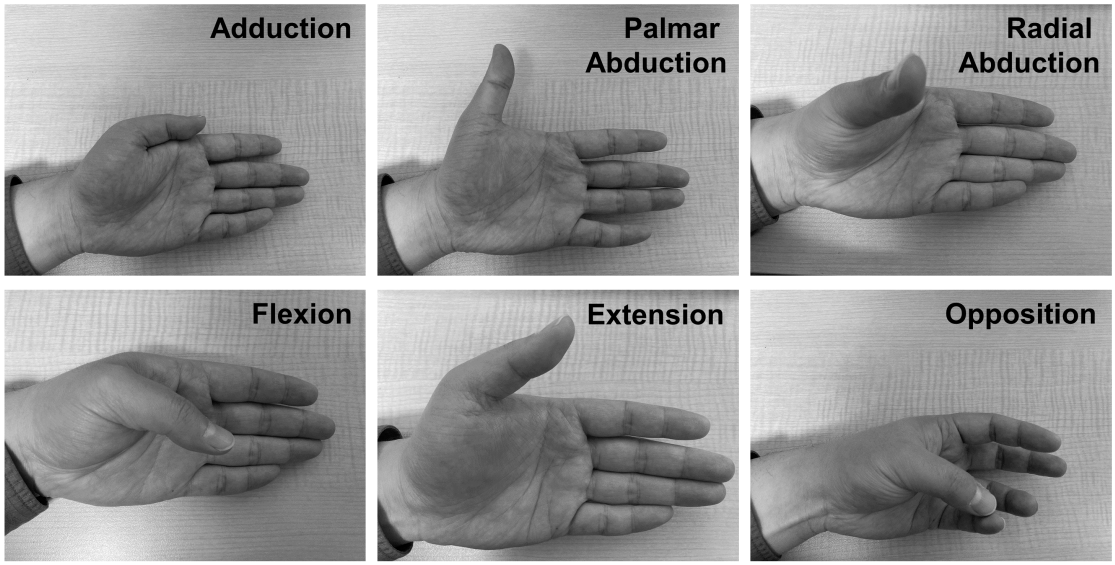

Figure 1.1: Thumb movements: Adduction, Palmar Abduction, Radial Abduction, Flexion, Extension, Opposition. This figure was drawn by the author adapted from [9] (hereafter, such figures will be presented "adapted from [*]" like this case)

kinds of abduction exist regarding the thumb direction [10]. Palmar abduction is the thumb movement wherein the thumb moves perpendicular to the palm. Radial abduction is the movement wherein the thumb extends away from the palm's surface. In this paper, abduction refers to radial abduction. Adduction is the movement of the thumb making it aligned with the palm plane. Flexion is the bending movement of the thumb from the resting position to the surface of the palm. Extension is the movement of the thumb from the flexion state to the resting position. Opposition is the movement of the thumb's tip to the tip of the other fingers. Because the role of the CMC joint is the same in opposition and flexion, the movements are jointly termed as flexion in this work. In terms of the continuous movements such as adduction-abduction (AA) and flexion-extension (FE), the role of the AA is to control the position of the thumb, and FE serves to grasp an object. These roles can be easily visualized considering the situation of catching a ball in one hand. In general, the range of motion about the CMC joint is reported as follows: 50 degrees in the flexion-extension(FE) movement, and 40 degrees in the adduction-abduction(AA) movement [11, 12]. Thus, the range of motion of the developed robot should be

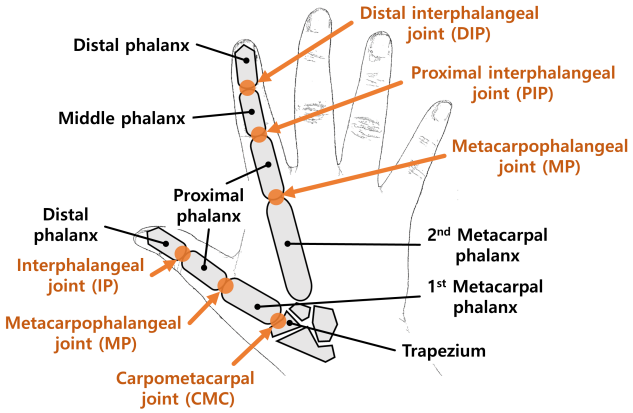

Figure 1.2: Location of joints and bones of the thumb and index finger.

designed to be larger than this.

In the anatomical structure of the hand, the thumb has three joints, called the interphalangeal(IP) joint, the metacarpophalangeal(MP) joint, and the carpometacarpal(CMC) joint. Figure 1.2 shows the location of each joint and bone in the thumb and index finger. When the hand is in the anatomically resting position, the thumb MP joint axis is oriented approximately 90° to the MP axis of the other fingers [7]. As shown in this figure, the other fingers have two IP joints but thumb has only one IP joint.

The thumb's CMC joint exhibits a biconcave-convex surface between the first MP phalanx and trapezium. This joint is usually known as a saddle joint because of its saddle-like shape. Owing to this shape, an additional sliding movement occurs when the thumb moves because the human joint which can not be perfectly classified according to the various kinds of mobility like mechanical mobilities. This sliding movement is not independent of the thumb movements; and thus, although the number of degrees of freedom (DOF) of the thumb is two, the sliding motion has an effect on the position of the thumb. This motion is caused by the cartilage, which is between two bones. The cartilage keeps the distance between two bones stable, but tolerance in the joint exists. The additional slide movement occurs due to this tolerance during joint motion. Figure 1.3 shows the sliding motions of CMC joint and the saddle surface of the trapezium. These anatomical features make it

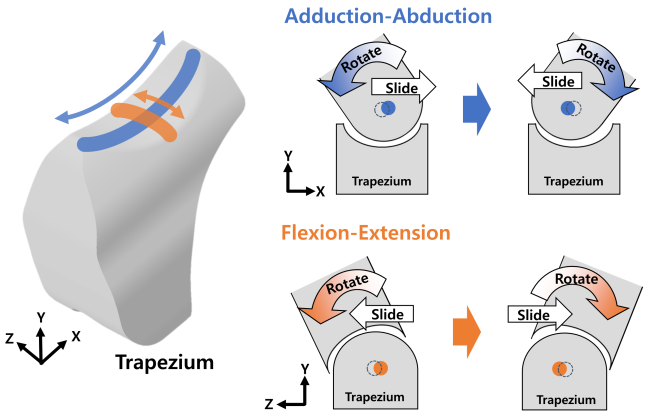

Figure 1.3: Explanation of CMC joint and its motions. This figure was drawn by the author adapted from [7].

difficult for the mechanical joints to perform the required movement, as there is a possibility of misalignment between the mechanical joint and the patient's hand joints. This misalignment remains a challenging point in the development of thumb rehabilitation robots. Such challenges are often observed in the field of rehabilitation robots.

1.1.3 Paresis of the hand

Muscles in the arms and hands fulfill the following roles: flexor and extensor. In normal conditions, the extensor and flexor muscles work in proportions proportions of 45% and 55%, respectively [13, 14]. However, in a paralyzed condition, the flexor muscles work significantly more than extensor muscles. The usage rate of flexor and extensor shifts to about 80% and 20%, respectively [13, 14]. This means that the required torque in the extensor direction is greater than in the flexor direction during rehabilitation therapy. For this reason, the patient's wrists, arms are bent towards the side of the body. Furthermore, the fingers are always bent towards the palm. Therefore, the paralyzed thumb generally ends up in a position between the palm and other fingers. This pose completely blocks the thumb, making a paralyzed thumb very hard to attach instruments to as compared to the other fingers. Since the paralyzed limbs are not used regularly by the patient, the surface of the skin

Table 1.1: Brunnstrom Stage [15]

Stage	Description
1	Flaccidity period: In the post-stroke period, no limb movement on the affected side occurs.
2	Recovery begins: Spacticity begins to occur, reflexes increase, partial or all synergy movements through response to stimuli can be observed.
3	Limited control of movement: Spasticity becomes more pronounced, and synergies become strong. The patient gains a limited range of voluntary control.
4	Less limited control of movement: Spasticity and synergy effect decline. The patient can move with fewer restrictions.
5	Increasing ability of movement: Continuously decreasing spasticity. The patient can move more freely than before and is able to perform more complex movement combinations.
6	Near-normal: No spasticity. The patient is able to move their limbs to near-normal to normal movement and coordination.

becomes weak. This factor further increases the difficulty of attaching mechanisms to the hand.

As the criterion of the paresis, the Brunnstrom stage is widely used. This classification method describes the recovery of the patient's motor function with a six-stage scale [15–18]. Table 1.1 shows the six-stages of a paralyzed situation. The stages are considered from the initial situation of paresis to the final stage, a near-normal situation. Moreover, it is commonly used as a tool for evaluating body function impairment [17–23]. This simple six-stage assessment system allows patients to not only understand their paresis situation but effectively communicate with the professionals in charge of their treatment, such as their doctors and therapists. Furthermore, an engineer who is developing a rehabilitation robot can better understand the patient's paresis condition, which helps determine the requirements. Moreover, it also helps in determining the target specifications when developing the rehabilitation robot. Rehabilitation therapy is adapted for the periods from stage one to five, but the spasticity of the fingers in stage one is too high, and it makes it difficult to apply an external force. To reduce the spasticity, a botulinum toxin (Botox) injection is

sometimes used before therapy. This injection is used to reduce stiffness and make the patient feel a slight resistance at the distal area of the hand [24]. Therefore, it is assumed that patients experiencing a high degree of spasticity in their hand muscles uses a botox injection before using the rehabilitation robot, so that it is not necessary to develop the robot to be able to apply a very large force.

1.2 Literature review

To specify the challenging point of this research, the literature research was done. In this thesis, the literature research was focused on the two points. The first point is the hand wearable robot/mechanism and its type. Through the analysis of this point, the definition of the design types regarding hand rehabilitation (the exoskeleton and the end effector), and those advantages and disadvantages were clarified. Additionally, the misalignment issue is explained in detail to clarify the existing challenging point. This is the additional explanation of the first point. Another point is the design of the thumb part, and its structural characteristic. From this, the adaptation method of the mechanism design regarding the thumb anatomical mobilities was clarified and those limitations were analyzed.

1.2.1 Types of hand rehabilitation robots

A number of hand rehabilitation robots have been developed, and these can be divided into two main types: the exoskeleton type and the end-effector type [25, 26].

An end-effector type interacts with the movement of the patient using a single attachment part on his/her distal end [27]. This type of robots is designed to externally locate their main parts on the patient's body. Moreover, its end-effector is designed to attach with the distal end of the user's body. Due to this characteristic of the design, this robot controls only the position and orientation of the end-effector. Furthermore, those mechanisms have the advantage of a simple structure and easy adaptation to different sizes of the patient body, though the robot cannot directly control each joint angle of the patient's limbs or fingers. Figure 1.4 shows three con-

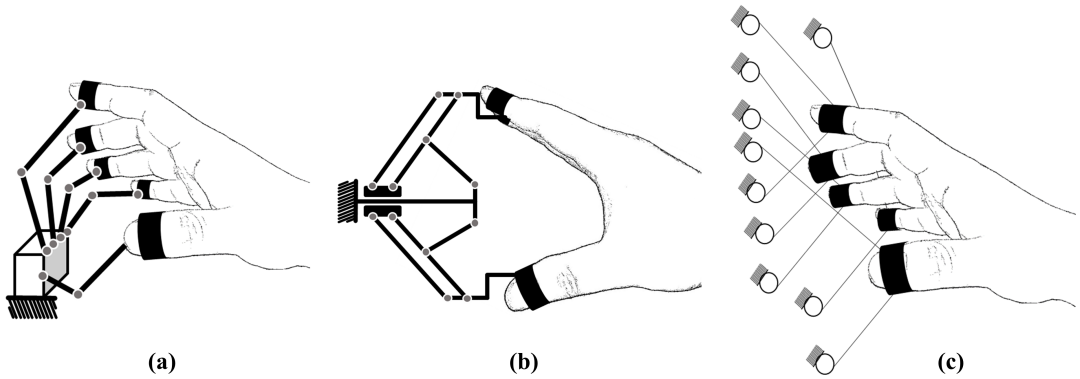

Figure 1.4: Previous mechanisms of the end-effector type: (**a**) Serial linkage adapted from [28], (**b**) Closed-loop linkage adapted from [29,30], (**c**) Cable driven from fixed base adapted from [31]

ceptual drawings of end-effector type mechanisms. In this figure, the first type is the end-effector type that uses serial linkages, in which each joint is actuated, as shown in (a) [28]. Figure 1.4 (b) [29, 30] shows the case where a closed-loop mechanism is used and (c) [31] shows the case where a cable driven mechanism is used.

An exoskeleton-type mechanism independently provides the required angle and force to each joint of through the use of various attachments. The axis position of each joint is determined when it is attached to the patient. If the patient's joint axes are not aligned with the robot's joints, a mechanical singularity of the total system composed of the robot and patient occurs [32]. In addition, a hybrid-type robot, which is the intermediate structure of the two types, has been reported [25]. For example, one of the parts of the mechanism was designed as an exoskeleton and is attached to the patient body. It is also connected to another part of the end-effector type. In another case, the base of the mechanism is attached to the patient's body similar to an exoskeleton, but the structure of the mechanism is of the end-effector type. However, this terminology and concept are only reported in the research of upper limb rehabilitation robots, and there were no cases found regarding the fingers. In this thesis, this classification is adapted to explain this research more intuitively.

1.2.2 Misalignment issue

In the case of exoskeleton-type robots, the distance between the link and patient's bone caused by the muscle and skin becomes the cause of misalignment when the patient's joints move. In other words, even though the kinematic joints are precisely aligned with the patient's joints in the home position, the axes of the kinematic joints of the exoskeleton cannot respond to the changes in the human joint axis during performance. The whole configuration of an attached finger with the exoskeleton is similar to the overconstrained mechanism. In the practical manufacture of the overconstrained mechanism, the DOF of the mechanism is affected by the tolerance. When some joint axis is unexpectedly moved, the DOF of the overconstrained mechanism is lost or reduced. Because the finger joint is not perfectly rotating like a kinematic revolte joint, the finger joint axis is moved. It occurs with the same effect as like as the joint tolerance in the overconstrained mechanism. Figure 1.5 shows a situation of misalignment in an exoskeleton type robot. In this thesis, the misalignment is defined as follows: the reducing mechanism's DOF by the interaction of the finger and its movement. In opposition, the normal state is that keeping the DOF of the mechanism even though it works.

To solve this issue, various designs have been reported. Figure 1.6 shows the linkage structures proposed by previous studies. In Figure 1.6 (a), a redundant linkage structure was reported [32, 33]. This structure aligns the rotational center of the joint by providing more points of mobility than required. For example, only one

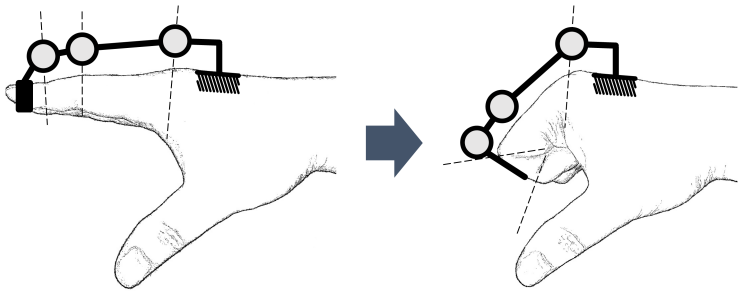

Figure 1.5: Misalignment situation of an exoskeleton type robot.

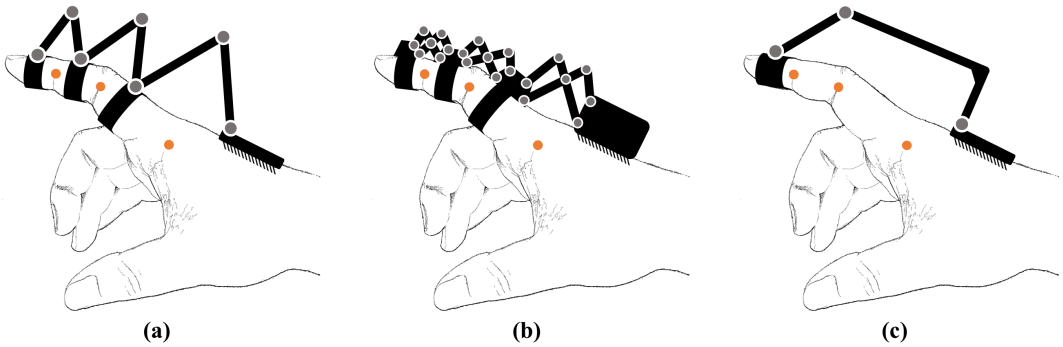

Figure 1.6: Structures of previous studies for matching the center of rotation for alignment: (**a**) Redundant linkage adapted from [32,33], (**b**) Remote center of rotation adapted from [34–37], (**c**) Serial linkage adapted from [38–40].

mobility is needed in the proximal interphalangeal (PIP) joint of the index finger, but this type of mechanism was designed to have two joint mobility. The additional mobility is constrained by the overall constraint condition to include the hand when the mechanism is attached. The remote center of rotation structure was designed to comply with the rotational center by using a mechanical closed-loop linkage, slider, etc [34–37]. However, those two types, the redundant linkage structure and the remote center of rotation structure, are structurally very complex and bulky. Furthermore, those structures were designed so that their mechanism is attached to fix the center point of each finger node as shown in Figure 1.6 (a), (b). Moreover, any cases adapted for use on the CMC joint have not been found. Even if those designs are adapted to the CMC joint, it is predicted that those structures cannot be easily designed to provide full mobility of CMC joint.

On the other hand, the end-effector type was designed such that its attachment part is connected to the tip of the finger, and the mechanism's joints do not control each finger joint angle. For this reason, the consideration of misalignment is not necessary because this mechanism's design does not align its kinematic joints with the finger joints [41,42]. This type of mechanism design provides a number of advantages. One such advantage is that this mechanism can easily adapt to the different sizes of various patient hands. Furthermore, the attachment part does not have a heavy weight because its base part, where the heaviest part of the mechanism is

located, is usually installed on a table or stand. However, this type of mechanism results in lower mobility than the exoskeleton type. Furthermore, the attaching point is mostly the distal part of the finger, and sensitive control for the individual finger joint angles is not necessary.

1.2.3 Design cases of the thumb part

Assorted thumb parts of the exoskeleton system have been developed for rehabilitation, virtual reality, or teleportation [38–40, 43]. Most of these are designed with the end-effector type mechanism attached to the distal point of the finger. The advantage of this structure is that there is a focus on the distal movement of the finger when designing the mechanism, and it is relatively easy to attach to the hands compared to the exoskeleton type. These factors allow this structure to adapt well to the mobility of the CMC joint.

Due to the complex structure of the CMC joint, most exoskeletal robots have been designed to actuate the flexion–extension movements of fingers other than the thumb. Only a few robots have been designed for the thumb. For example, the isolated orthosis for thumb actuation (IOTA) was proposed in [44]. This mechanism had 2-DOF, and was designed to have two actuated joints for the CMC joint and MP joint. This mechanism was reported to have a maximum efficiency of 44%. However, the CMC motion was restricted to permit the palmar abduction-adduction movement. On the other hand, a robotic hand exoskeleton system that is controlled by the electromyography(EMG) was reported [45]. This mechanism has 2 DOFs with and could adapt to different hand sizes. One actuator of this robot was connected to the four fingers (index, middle, ring, and little fingers), and another actuator was used for the thumb movement. For the thumb function, only the flexion–extension movement was considered and designed. An exoskeleton device called a “five-fingered assertive hand” was studied. It achieved motion of five fingers using three driving parts by using a tendon-driven system [46]. The part of the mechanism driving the thumb had two actuated joints. One of the actuated joints controlled the MP joint

and the IP joint. The other actuated joint controlled the CMC joint for flexion–extension movement.

Another previous device named the "Rutgers Master II-ND" was reported. In this device, one pneumatic actuator was used for thumb movement [47]. This actuator is connected to the tip of the thumb from the base of the palm. The device controls the flexion–extension movement using this actuator. The two passive universal joints were connected between the actuator to the fingertip and the actuator to the base. These joints allowed the mechanism to perform the adduction– abduction movement. The thumb exoskeleton reported by Lambercy, et al. [48] was designed to allow the flexion–extension movement of the thumb by use of a passive hinge joint, as well as to control the abduction-adduction using a linear actuator. Furthermore, a passive universal joint connected between the CMC part and MP part allowed for adaptation to the center of the CMC joint. This mechanism was manufactured using a 3D printer, and had a mass of less than 150 g.

An actuated thumb exoskeleton for hand rehabilitation named ATX has also been proposed [49]. This mechanism was designed with 5 DOF in order to control each DOF of the thumb independently. Two of the total DOF were used for the CMC joint, and those were used to control the flexion–extension and adduction–abduction movements. Agarwal et al. have proposed an exoskeleton robot for thumb rehabilitation [50]. This mechanism has four DOF, and was designed for its CMC chain to consist of four revolute joints and one prismatic joint. This chain becomes a 4-bar linkage by the constraint between the hand and chain when the mechanism is attached to the hand. This configuration allows its DOFs of the CMC chain to be reduced to two from five. To control the two DOFs, two actuators were used for controlling each thumb movement.

To sum up, the thumb part design of previous studies can be divided into three categories regarding the movement of the CMC joint. For the first category [44–46], the mechanism design, is focused on the control of only one movement, and other movements are physically limited. However, one movement of the CMC joint (FE or

AA) is neglected, and this is important for control of whole thumb movements such as matching the thumb and other fingers with each other or adapting to different sizes of objects. For example, since the CMC joint is fixed in the home position of the hand, objects bigger than the width of the palm cannot be grasped. This means that this structure is not enough to adequately perform the whole thumb movement.

The second design category [47,48] controls only one of among all the movements (mainly FE movement), similar to the first design, but it allows other movements through the use of passive joints (mainly AA movement). Thus, the end-effector position along the direction of non-actuated movements depends on the movement of the patient. However, the thumb of a paralyzed patient will always be fixed in the inside of the palm, as mentioned previously. For this reason, moving the thumb to the outside of the palm is difficult due to the spasticity of the patient's muscle. Even if they can move in that direction, the range of motion is minimal depending on the recovery condition of the patient. Because of this reason, this design is not able give the whole movement necessary for the rehabilitation.

The third category [49, 50] of the mechanical design controls all movements of the CMC joint through the use of two actuators. Each actuator corresponds to a movement, and this type of mechanism has 2 DOF by the constraints applied when the device is attached to the human hand. The CMC joint's rotations are not completely circular motions, unlike the kinematic revolute joint, because of the additional sliding motion of the CMC joint's saddle shape. Therefore, the kinematic revolute joint does not directly match the patient's movement. However, each movement is matched with one kinematic joint in this category. For this reason, it is questionable whether this design case can provide the full movement of the thumb, including the additional sliding motion, without an additional DOF. Based on this discussion, controlling all DOF of the CMC joint and solving the CMC joint's misalignment issue still exists as the challenge points in the design of a mechanical device that can provide all the DOF of the CMC joint.

1.2.4 Summary of literature reviews

In previous studies of literature, the design of the hand rehabilitation robots is classified into two design types: end-effector and exoskeleton. The most frequently used type of hand rehabilitation robot was the exoskeleton. The exoskeleton type has an issue called misalignment. Misalignment occurs when there is a mismatch between the axes of the human joint and the kinematic joint. In this situation, the actuator of the rehabilitation robot may provide an uncontrolled force to the user's finger, leading to a high possibility of injury. It is a very critical problem for the safety of the users. In the previous researches, the mechanical linkage designs (redundant linkage, remote center of rotation mechanisms, and serial linkage mechanisms) were reported as the solution to the misalignment. However, these linkages only considered the other fingers. Therefore, these designs cannot be considered for thumb rehabilitation due to the difference in DOF and CMC joint complexity. Even if the mechanism would be designed to suit of the DOF of the CMC joint, there is a possibility that the complexity of the mechanism would increase significantly because of the narrow space of the hand. On the other hand, the end-effector type was designed the attachment part is connected to the distal part of the finger and it does not control each finger joint. For this reason, this type is not necessary to the consideration of the misalignment when it designs the mechanism.

Furthermore, the thumb rehabilitation robot's design should consider the sliding motion of the CMC joint for providing accurate finger movement to develop a thumb rehabilitation robot. In the previous studies that have the thumb part, the thumb CMC joint's design mechanism can be divided into three approaches depending on the consideration of its DOF. However, those approaches did not consider the sliding motion of the CMC joint. Furthermore, the mechanism must be designed not to exert an unexpected force to maintain user safety.

1.3 Design requirements of thumb rehabilitation

To design the mechanism, it is necessary to specify the requirements for a thumb rehabilitation robot. Various studies have been conducted regarding the external force or torque provided to the patient for the rehabilitation therapy. The range of forces safe to apply on patients was reported as $0 \sim 800$ g (about $0 \sim 7.8$N) [51]. However, previous work stated that providing a force of more than 5 N may not be suitable for patients with paralyzed hands [31]. Furthermore, the required torque for each joint of the thumb is reported as follows: 0.3 N·m for the CMC joint, 0.26 N·m for the MP joint, and 0.26 N·m for the IP joint [32, 52]. Other prior studies reported the maximum force that could be applied to the patient is 45 N [53] for serious paresis. However, the proposed mechanism user is assumed to have received the proper prior treatment to reduce their muscles' stiffness in this research. For this reason, higher amounts of torque are not necessary. In the literature of kinesiology, the muscle torques, which are connected around the CMC joint, are reported [7, 54]. The maximum torque among them is performed by the adductor pollicis, which is the biggest muscle in the thenar eminentia with a torque of 6 N·m. The required range of motion is determined based on anatomical information. The CMC joint's range of motion is 40 deg in the AA movement and 60 deg in the FE movement [11, 12]. Based on the background study, the requirements of the mechanism design for the thumb rehabilitation are determined as follows:

- The target user is expected to be a paralyzed patient who has received a botulinum toxin injection.
- The required force is determined to be 5N. The required moment is derived to be 0.2 N·m considering the thumb length (36.9 mm [55]) and required force.
- The maximum torque of the actuator is limited to be under 6 N·m.
- The range of the motion for AA movement is $0 \sim 40$ deg and the range of the FE movement is $0 \sim 60$ deg.

1.4 Idea, objective and goal of the research

Based on the background discussed in the previous sections, the main goal of this thesis is to propose a novel rehabilitation robot mechanism that can completely provide the whole thumb CMC movement while considering the complex CMC joint structure. Furthermore, the kinematic analysis to determine the characteristics of the mechanism and the geometric design for considering the attachment situation with the hand are to be carried out. Because these robots interact directly with the human body, safety is an essential factor in their design. The alignment between the human joints and mechanism joints is still a challenge that needs to be addressed. From previous research done on the topic, mechanisms have been proposed and studied to solve the misalignment issue. However, consideration of the misalignment issue for the thumb has still not been studied well despite the importance of its anatomical function. Though thumb movement was achieved in these designs, the motion was limited.

A hybrid mechanism, combining the advantages of the exoskeleton and end-effector types, is proposed. In detail, the design is considered so that multiple linkages connecting only to the attachment point are designed, similar to an end-effector type mechanism, and the base parts of the mechanism are designed to be attached to the hand like an exoskeleton type. More specifically, multiple linkages attached to a center point of the MP bone are proposed and the base part is designed to attach to the palm and surface. It is expected that this design has the potential to avoid CMC joint misalignment. In essence, a simple mechanism will be considered so that it will be able to provide motion to the thumb with less resistance force between the hand and device. Moreover, it is necessary to utilize an ergonomic design to ensure that the patient's hand does not feel uncomfortable and the device adapts their hand size. Therefore, some parts would be ideally designed with many curvilinear forms, complex shapes, and tiny sizes. Thanks to the recent progress of the Additive Manufacturing (AM), fabrication of these parts can be done at a low cost. For this reason, some parts will be designed in consideration of manufacturing by AM in this

research.

To design the thumb rehabilitation robot with respect to the ideas mentioned above, the requirements for the design of the mechanism were determined as follows:

- Two required movements: Adduction-Abduction(AA)
  and Flexion-Extension(FE).
- The trajectory of one point in the thumb is focused on as the target movement.
- The user is considered as a paresis patient rated at levels 2 or 5 in the Brunnstrom stage and their hand muscles have already been provided a Botox injection to soften them before the use of the device.
- The mechanism is designed to solve or avoid the misalignment problem caused by the CMC joint's complex structure.
- Actuators must have less torque than the human hand.
- The design strategy of the mechanism must consider adaptation to different hand sizes.
- The shape of the output link must be designed so that it is easy to attach with the user's fingers.

To realize the goal, idea, and requirements, the objectives of this thesis are determined as follows:

- The proposed mechanism is designed to control the two target movements: AA and FE.
- Kinematic analysis and performance analysis of the proposed mechanism are conducted with numerical examples.
- Static analysis, a verification experiment, and the calculation for actuator selection are conducted with numerical example.

- Determining the design requirements is conducted from data measured from human performance and dimensional synthesis for link length selection.
- Design of a practical mechanism is conducted based on the results of the analysis.
- Experiments with actual users and evaluation of the results are carried out.

1.5 Composition

This thesis is organized as follows: In chapter 2, a novel mechanism for control of the CMC joint for rehabilitation is introduced, and its mobility analysis, displacement analysis, and kinematic performance analysis are described. In chapter 3, static analysis and actuation selection for the mechanism are described. In chapter 4, workspace analysis and dimensional synthesis of the mechanism are described. Based on these results, a prototype was manufactured, and an experiment with users is described in chapter 5. Finally, the conclusion and discussions are detailed in chapter 6.

Chapter 2

(2–RRU)–URR parallel mechanism

2.1 Introduction

In this chapter, a mechanism called (2–RRU)–URR parallel mechanism is proposed. The mobility of the proposed mechanism is described with respect to the movement of the thumb, and its mobility is verified with theoretical equations. The proposed mechanism is an overconstrained mechanism. To clarify the constraints of the mechanism and derive the actual mobility, screw theory is applied to derive the Jacobian matrix. To understand the characteristics of the proposed mechanism, the displacement analysis is done by dividing the mechanisms into two parts. Moreover, based on the formulation for the displacement analysis, the reachable workspace and sensitivity are analyzed.

2.2 Configuration and mobility

2.2.1 Structural configuration

This mechanism was designed so that its output link can be attached to the center point of the proximal phalanx to assist and reinforce the required movements of the

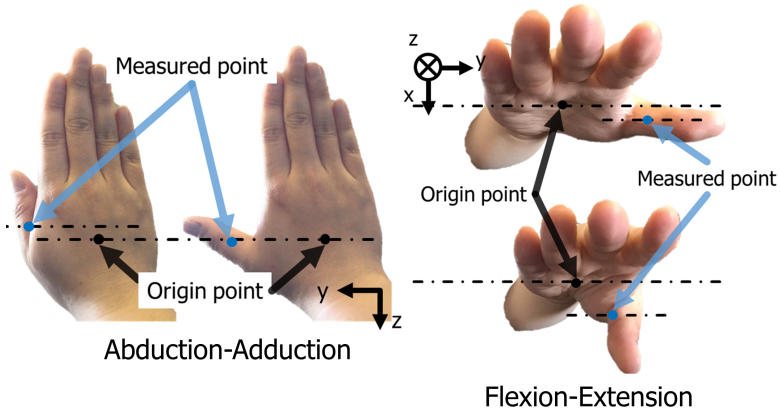

Figure 2.1: (a) Thumb movements where origin and measured points are set to palm and center point of thumb proximal phalanx. (b) Conceptual drawing of an application of proposed mechanism as an exoskeleton robot for thumb rehabilitation.

MP and CMC joints. Figure 2.1 shows the movements of the thumb considered in this thesis: AA and FE. When the coordinate system is defined as shown in the figure, the FE movement of the measured point moves in the yz plane and it consists of a translation along the y axis and a rotation around the x axis. In observations of the thumb movement, the displacement of the z axis caused by the two mobilities mentioned above is measured to be within a small range ($1 \sim 3$mm based on motion capture measurements).

To simplify the required mobility of the thumb for the mechanism design, the small displacement of the z axis was assumed to be negligible. For this reason, the required mobility of the FE movement is a translation along the y axis. Moreover, the rotation around the x axis at the measured point (relative rotational mobility) is should adapt to the thumb's orientation angle. On the other hand, the AA movement consists of a rotation around the z axis and translation along the y axis. Both mobilities mentioned above are related to the movement of the CMC joints, and the relative mobility is related to the MP joint. In summary, this mechanism is proposed for a rehabilitation device to perform the motions of the thumb, and is shown in Figure 2.1.

The components of the (2–RRU)–URR mechanism are the base frame, output link, two RRU chains, and one URR chain [56], are shown in Figure 2.2 (R refers to

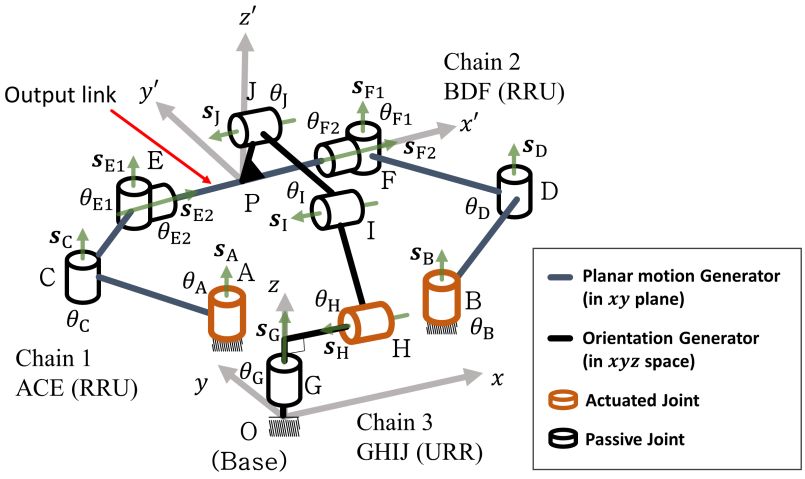

Figure 2.2: Parallel mechanism of (2–RRU)–URR including offset link GH. Mechanism consists of three kinematic chains that connect the output link with the base frame. Joints A, B, and H are actuated joints.

a revolute joint and U refers to a universal joint). The parentheses in the mechanism name are used to denote multiple chains in the same plane. For convenience, the chains ACE, BDF, and GHIJ are denoted as chains 1, 2, and 3, respectively. Chains 1 and 2 move in the xy plane, and have the same kinematic structure, in which four R joints are arranged from the base to the output link. Three successive R joints are parallel, and the fourth joint is perpendicular to these, such that the third and fourth joints form a universal (U) joint. In addition, chains 1 and 2 are arranged so that they are parallel to each other. This means that the six revolute joints A, C, E_1 and B, D, F_1 are parallel, and the two revolute joints in the fourth position, E_2 and F_2, are coaxial. Chain 3 is perpendicular to the xy plane and is composed of four R joints. The second to fourth joints are parallel, and the first joint is perpendicular to the others, forming a U joint with the second joint. The joints A, B, and H are actuated, while the other joints are passive. Based on this structural configuration, the proposed mechanism is composed of two planar chains, namely, the planar motion generator (PMG: ACEFDB in Figure 2.2) and orientation motion generator (OG: OGHIJP).

Based on these ideas, the concept of the mechanism was devised, and is illustrated

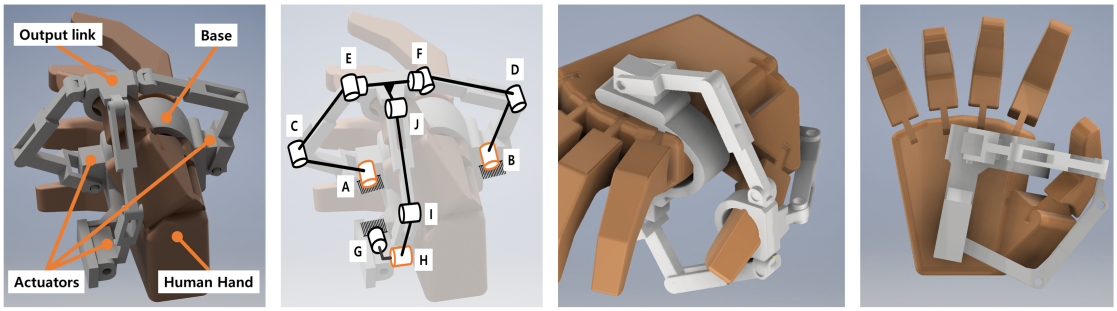

Figure 2.3: Conceptual design of proposed mechanism for the thumb rehabilitation: (**a**) Three dimensional side view, (**b**) Joint placement, (**c**) Top view, (**d**) Bottom view.

in Figure 2.3. In this figure, the hand is in the middle of the base frame of the mechanism. Thus, the joints in the base frame are in the palm, at the back of the hand, and near the wrist. When the placement of each actuator is fixed, the mechanism maintains its structure and characteristics as a parallel mechanism. With respect to the thumb movement, the chains (especially chain 3) which are located near the surface of the thumb, may collide with the wrist or the thumb. To avoid collisions with the wrist or the hand, an offset was added to create distance between the joints to avoid collisions in chain 3. In Figure 2.1, the offset is the link in the x-axis direction between joints G and H. Due to the offset, the fixed-point position of joint O was changed from near the wrist to the palm.

As for mobility of this mechanism, there is a rotational mobility along the x'-axis, another rotational mobility along the z-axis, and a translational mobility is along the y-axis. The mechanism achieves the target movement of AA and FE by combining the three mobilities of the mechanism as shown in Figure 2.4. In the case of AA, when the thumb is far away from the palm and returns, its position is controlled by the y translational mobility. Simultaneously, the orientation of the thumb is changed, and this is controlled by the rotational mobility along the x'-axis. Regarding the FE movement, assuming that the orientation angle is not changed, the rotation mobility along the x'-axis is set as constant. Furthermore, the thumb position is controlled in the xy plane by combining motion from two mobilities of

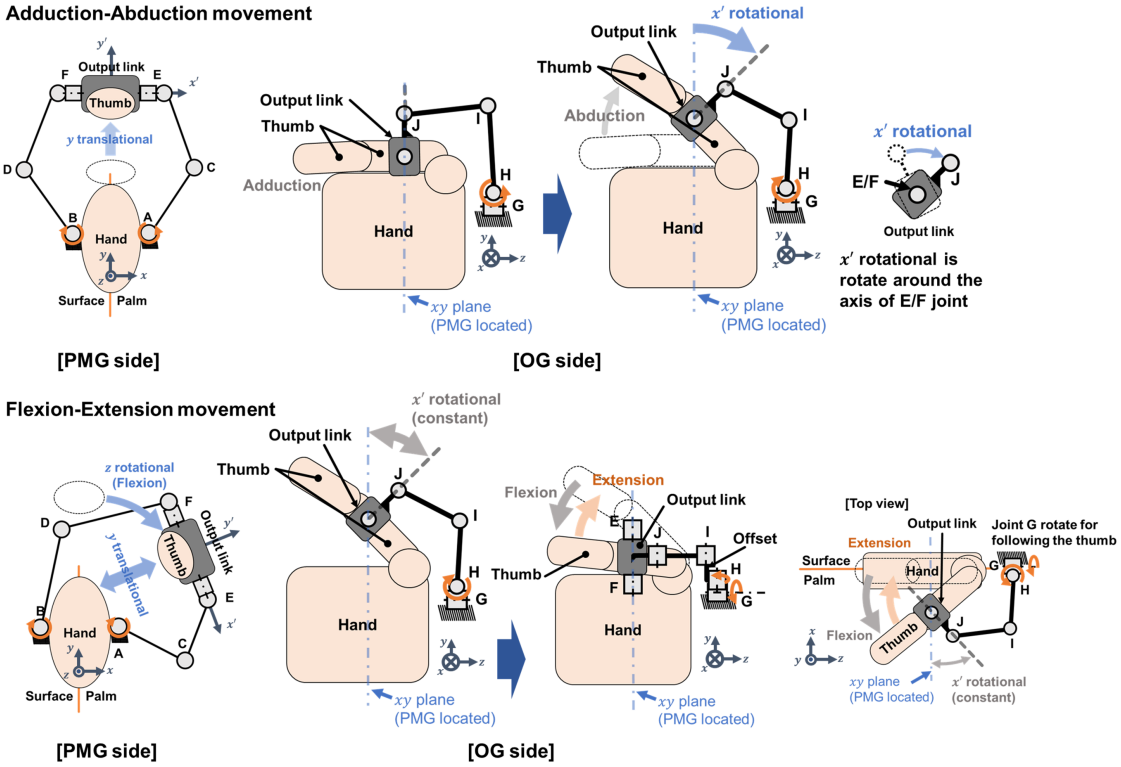

Figure 2.4: Explanation of the proposed mechanism's mobility in the cases of AA and FE movement. This figure illustrates the movements in the side of two parts such as PMG and OG.

the rotational mobility along the z-axis and the translational mobility in the y-axis. Through these structural characteristics, the proposed mechanism can simply assist the thumb motions by controlling the position of the attachment point like an end-effector type mechanism, and the complex motion of the CMC joint is not considered. However, because the attachment point is in the Proximal phalanx of the thumb finger, the motion of IP joints can not be controlled. Moreover, a sliding motion between the thumb finger and the attachment may occur depending on the size of the hand due to the controlled motion provided in the xy-plane.

2.2.2 Comparison with the parallel mechanisms

This proposed mechanism achieves a compound motion that consists of a rotational and translational motions, which differ from the motion of well-known parallel

robots such as the Stewart-Gough platform, DELTA, and Agile eye [57–59]. In addition, The parallel robot with the presented compound motion has the possibility of various applications, but it is usually not commonly applied in the fields where most parallel robots are used. In a previous study, Liu, X. J., and Wang, J., reported a spatial parallel robot with two rotational motions and one translational motion [60, 61]. This robot has three nonidentical kinematic chains that connect its base to the output link, and it is actuated by three prismatic actuators. In comparison to the aforementioned proposed robot, this robot is similar from a functional point of view. However, there are differences in the presented motion, actuator type, and structural characteristics.

2.2.3 Mobility analysis

To investigate the mobility of the proposed mechanism, Grubler's mobility formula is applied. Its result shows that the DOF is calculated as zero as follows:

$$\begin{aligned} &6(L-J-1)+\sum_{i=1}^{J} f_i = \\ &6(8-9-1)+(1\times 8)+(2\times 2)=0 \end{aligned} \tag{2.1}$$

where J, L, and f_i are the number of joints, number of links, and DOF of the joints, respectively. However, this calculation result is different when compared to the real behavior from the observed mobility of the prototype. In real observation, three DOFs were confirmed in the proposed mechanism: rotational motion around the z axis, translational motion in the HP direction, and rotational motion around the x' axis. To clarify the actual DOF of this mechanism, the constraints imposed on the output link by each chain have been accounted for. First, the constraint with respect to the coordinate system $\mathrm{P}-x'y'z'$ is considered according to the structural and observed features of this mechanism. According to the kinematic structure of chain 1 having four DOF, its constrained mobilities are the rotational motion of the output link around the y' axis and the translational motion at P in the z axis. The

same constraint conditions are imposed by chain 2. In the case of chain 3 also having four DOF, the rotational motion around the y' axis and translational motion at O in the x axis are constrained. These constraint conditions are also described from the constraint wrenches of the proposed mechanism ($\$_c$). The constraint wrench is the 6×1 vector, which shows the constraint condition of the output by the structure of each kinematic chain. The number of constraint wrenches is related to the DOF of each chain. This wrench satisfies the orthogonal condition of all joint screws in each kinematic chain [62]. Those wrenches of each chain are described as follows:

$$\begin{aligned}
\$_{ci,1} &= \begin{bmatrix} 0 & 0 & 1 & 0 & 0 & 0 \end{bmatrix}^T (i = 1, 2), \\
\$_{ci,2} &= \begin{bmatrix} 0 & 0 & 0 & 0 & 1 & 0 \end{bmatrix}^T (i = 1, 2), \\
\$_{c3,1} &= \begin{bmatrix} 1 & 0 & 0 & 0 & 0 & r \end{bmatrix}^T, \\
\$_{c3,2} &= \begin{bmatrix} 0 & 0 & 0 & 0 & 1 & 0 \end{bmatrix}^T
\end{aligned} \tag{2.2}$$

where r is the distance between O and P. In the case of the proposed mechanism, the six constraint wrenches are derived as shown in Equation (2.2). Hence, because each chain has 4 DOFs, there are two constraint wrenches with respect to each chain. In Equation (2.2), $\$_{ci,j}$ refers to the constraint imposed by the ith chain, where $j = 1, 2$. From Equation (2.2), it is found that three of them are independent. Then, the three independent constraint wrenches ($\$'_c$) are obtained as

$$\begin{aligned}
\$'_{c1} &= \begin{bmatrix} 0 & 0 & 1 & 0 & 0 & 0 \end{bmatrix}^T, \\
\$'_{c2} &= \begin{bmatrix} 0 & 0 & 0 & 0 & 1 & 0 \end{bmatrix}^T, \\
\$'_{c3} &= \begin{bmatrix} 1 & 0 & 0 & 0 & 0 & r \end{bmatrix}^T
\end{aligned} \tag{2.3}$$

These wrenches indicate that the output link can perform the rotational motion around the x' axis, rotational motion around the z axis, and translational motion along the y' axis. In summary, the proposed mechanism is a 2R1T mechanism, where

R and T are the rotational and translational outputs, respectively.

2.3 Displacement analysis

The displacement analysis was formulated and analyzed. This refers to the geometrical relationship between the actuated joints and the output link, disregarding the forces/torques that can cause movement. To derive the kinematic equations of the proposed mechanism, the mechanism is divided into two parts: planar motion generator (PMG) and orientation generator (OG). The equations for those parts are derived separately.

2.3.1 Forward kinematics analysis of planar motion generator

The PMG is shown in Figure 2.5. This diagram shows the top view of the xy plane. Part GHP is the projection of the kinematic chain GHIJP on the plane of linkage ACEFDB. If the connection and constraint of link r are not included, the PMG can be considered to be a planar six-bar linkage. In general, planar six-bar linkages with a single closed-loop require three actuators. Because there are only two actuators at joints A and B, this condition cannot be used to solve the forward displacement analysis of the six-bar linkage of ACEFDB. If one of the joints C or D is assumed to be an actuated joint and the angles of θ_{A} and θ_{B} are given, then

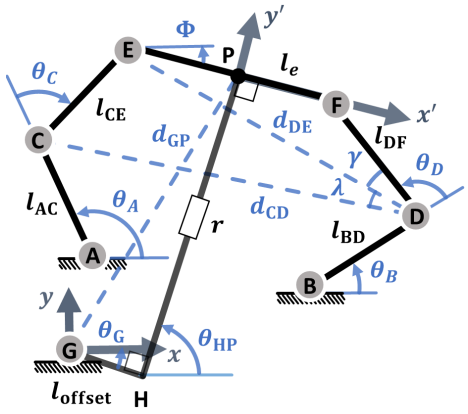

Figure 2.5: Diagram of planar motion generator(PMG).

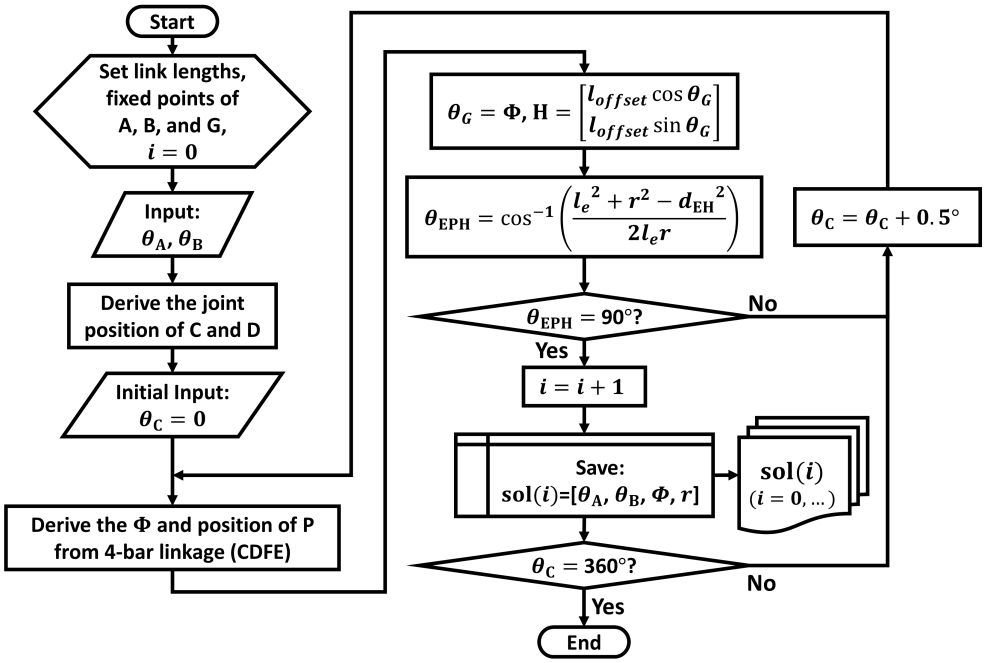

Figure 2.6: Procedure of forward displacement analysis for PMG.

the end-effector point of the six-bar linkage can be calculated. However, according to the constraint given by the chain GHP (details are described in the following sub-section), its value should be adjusted. At this time, the calculation is ongoing with the assumption of joint C as the temporal actuation joint.

Figure 2.6 shows the procedure of the forward displacement analysis of the PMG when joint C was considered to be the temporal actuation joint. As shown in this figure, the pre-allocation of the constant parameters, such as the length of the links and fixed points of the base joints, are defined before the calculation. In detail, all the kinematic parameters are classified as l, θ, and d, which represent the link length, joint angle, and distance between two joints, respectively. As mentioned above, when θ_{A} and θ_{B} are given, the positions of joints C and D are fixed, and other chains such as CDFE can be considered to be a four-bar linkage. Based on this, when θ_{C} is given, the orientation angle Φ and position vector of point P are derived via the general method of the four-bar linkage. Because link EF, r, and link GH are perpendicularly constrained to each other, link EF and link GH are always

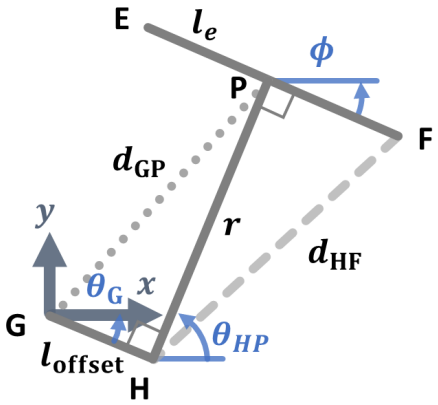

Figure 2.7: Diagram of constraint condition between r, l_{offset}, and link EF.

parallel, and this is described as $\Phi = \theta_{\text{G}}$. Figure 2.7 shows the constraint condition of the GHP. Therefore, r can be derived considering the right-angled triangle condition of r, d_{GP}, and l_{offset}. Furthermore, θ_{EPH}, which is the angle between link EF and r, is derived using the cosine laws, and it should be 90° with respect to the constraint condition. In this process, θ_{EPH} is calculated for each temporal value of θ_{C} value, and these are confirmed to satisfy the above constraint condition. The tolerance of θ_{EPH} is $90 \pm 0.25°$. The overall forward displacement of the proposed mechanism can be derived when θ_{A} and θ_{B} are arbitrarily given.

2.3.2 Inverse kinematics of planar motion generator

Before calculating the forward kinematic analysis of the PMG, the constraint condition of the proposed mechanism is considered. As mentioned in the previous section, chain 3 and link EF are perpendicularly connected to each other. In the case of PMG, chain 3 is represented as the link r and link GH (offset link). As the constraint condition of PMG, link GH and r, and link EF and r, are always perpendicularly connected. Therefore, the relationship between the orientation of link EF (Φ) and the angle of joint G (θ_{G}) is $\theta_{\text{G}} = \Phi$, i.e., Φ is passively determined by θ_{G}, and θ_{G} is perpendicularly determined in the direction of the link r. There are two output components of the PMG: r and Φ. Because these are related to the position of point P, if the position vectors of p_x and p_y are known, then the output

components of r and Φ can be derived. Actually, the trajectory of the real thumb movement is recorded by the measurement system using the position vector of the x axis and the position vector of the y axis. Considering the comparison results or tracking with the real movement, for convenience, the input components of inverse displacement analysis are determined to be p_x and p_y. If l_{GH} and the position of point P ($\mathrm{P} = [p_x, p_y]^T$) are given, then d_{GP} and r are derived by considering the right-angle condition of l_{GH}, d_{GP}, and r as follows:

$$d_{\mathrm{GP}} = \|\mathrm{P} - \mathrm{G}\|\,,\ r = \sqrt{d_{\mathrm{GP}}^2 - {l_{\mathrm{offset}}}^2} \tag{2.4}$$

$$\theta_{\mathrm{PGH}} = \cos^{-1}\left(\frac{{l_{\mathrm{GP}}}^2 + {l_{\mathrm{offset}}}^2 - r^2}{2 l_{\mathrm{offset}} l_{\mathrm{GP}}}\right),\ \theta_{\mathrm{GP}} = \mathrm{atan2}(p_y, p_x) \tag{2.5}$$

$$\theta_{\mathrm{G}} = \Phi = \theta_{\mathrm{PGH}} - \theta_{\mathrm{GP}} \tag{2.6}$$

where d_{GP}, θ_{PGH}, θ_{GP}, and θ_{G} are the distance between joints G and P in the xy plane, angle of PGH, orientation angle of GP from the x axis, and joint angle of G, respectively. From the perpendicular conditions such as those of link r and FP, and link r and GH, the positions of joints H, E, and F can be calculated using Equation (2.6) as follows:

$$\begin{aligned}
\mathrm{E} = \mathrm{P} + \begin{bmatrix} e_x \\ e_y \end{bmatrix} &= \begin{bmatrix} p_x \\ p_y \end{bmatrix} + \begin{bmatrix} l_e \cos\theta_G \\ l_e \sin\theta_G \end{bmatrix}, \\
\mathrm{F} = \mathrm{P} + \begin{bmatrix} f_x \\ f_y \end{bmatrix} &= \begin{bmatrix} p_x \\ p_y \end{bmatrix} + \begin{bmatrix} l_e \cos(\theta_G - \pi) \\ l_e \sin(\theta_G - \pi) \end{bmatrix}
\end{aligned} \tag{2.7}$$

Using the results of the positions of E and F as mentioned above, the angles of the joints of each chain are calculated using the cosine law. Figure 2.8 shows the triangle of chains ACE and BDF. If the case of chain ACE is considered, the detailed equations used to determine the angle of joints A and C can be described as follows:

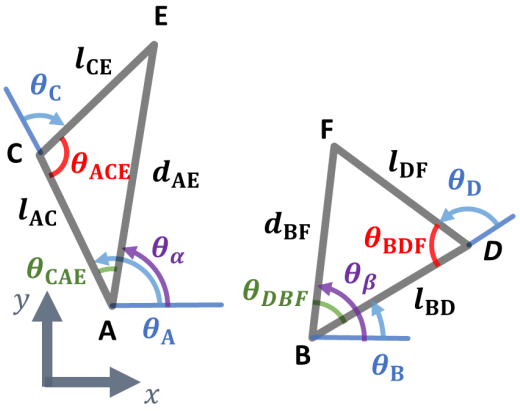

Figure 2.8: Triangles for inverse displacement analysis of planar motion generator model.

$$\begin{aligned} \theta_{CAE} &= \cos^{-1}\left(\frac{l_{\mathrm{AC}}^2 + d_{\mathrm{AE}}^2 - l_{\mathrm{CE}}^2}{2 l_{\mathrm{AC}} d_{\mathrm{AE}}}\right), \\ \theta_{\mathrm{ACE}} &= \cos^{-1}\left(\frac{{l_{\mathrm{AC}}}^2 + {l_{\mathrm{CE}}}^2 - d_{\mathrm{AE}}^2}{2 l_{\mathrm{AC}} d_{\mathrm{CE}}}\right) \end{aligned} \tag{2.8}$$

$$d_{\mathrm{AE}} = \|\mathrm{E} - \mathrm{A}\|, \ \theta_\alpha = \operatorname{atan2}(e_y - a_y, \ e_x - a_x) \tag{2.9}$$

$$\theta_{\mathrm{A}} = \theta_\alpha + \theta_{\mathrm{CAE}}, \ \theta_{\mathrm{C}} = \theta_{\mathrm{ACE}} - \pi \tag{2.10}$$

where l_{AC}, d_{AE}, l_{CE}, θ_α, θ_{A}, θ_{C}, θ_{CAE}, and θ_{ACE} are the link length of AC, distance between joints A and E, link length of CE, orientation angle of AE from the x axis, angle of joint A, angle of joint C, angle of CAE, and angle of ACE, respectively. Because chains ACE and BDF have the same kinematic structures, each joint angle of chain BDF can be derived using the same method. Figure 2.9 shows the procedure of the inverse displacement analysis of the PMG.

In the results of the displacement analysis, there are four types of solution, as shown in Figure 2.10. Each solution is classified by the angle values of θ_{C} and θ_{D}. Considering rehabilitation, the user's hands will be located inside the chain ACEBDF. To prevent collisions with the hands, solution (a) is considered suitable for the application in this study.

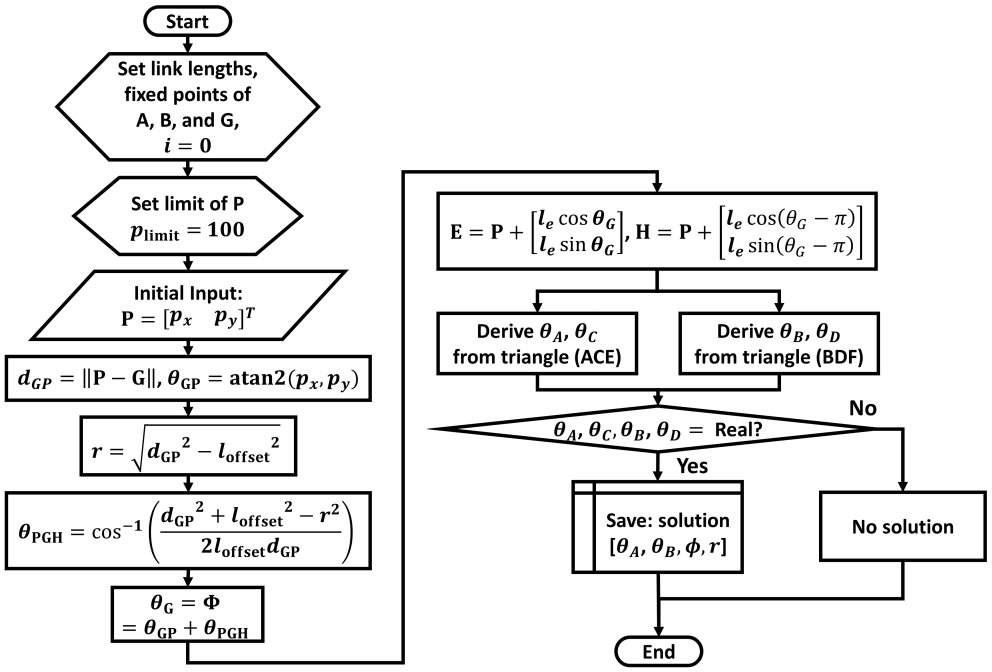

Figure 2.9: Procedure of inverse displacement analysis for PMG.

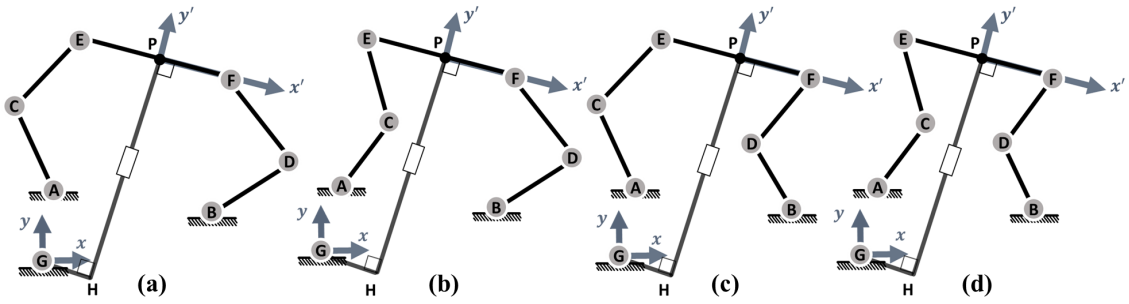

Figure 2.10: Four solutions to inverse displacement analysis for each pattern: (a) negative/-positive, (b) positive/positive, (c) negative/negative, and (d) positive/negative. (These results depended on values of angles θ_C and θ_D.)

2.3.3 Forward and inverse kinematics of orientation generator

If the OG is projected on the $y'z'$ plane of the P-$x'y'z'$ coordinate system, it can be considered to be a four-bar linkage even though an offset was adopted in the proposed mechanism. Figure 2.11 shows a diagram of the OG in the plane. Then, the OG can be considered to be a planar four-bar linkage. Because joints G and H overlap at the same position in the $y'z'$ plane, and the rotational mobility of joint G

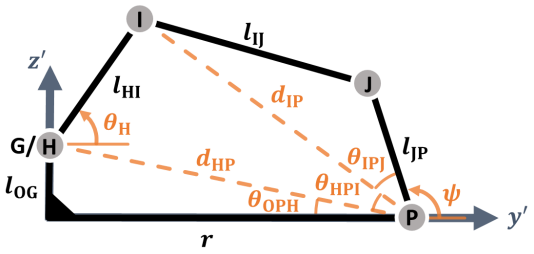

Figure 2.11: Diagram of orientation generator.

does not affect the other links of the OG on this plane, only the motion of joint H needs to be considered. Because the link length r is calculated from the PMG, it is considered to be a known value. With respect to the forward displacement analysis, θ_{H} is given as the input angle. Based on these, θ_{OPH}, θ_{HPI}, θ_{IPJ}, and Ψ are derived. These symbols indicate the angle between r and link HP, angle between link HP and link IP, angle between link IP and link JP, and the orientation angle of link JP from the y' axis, respectively. The equations are summarized as follows:

$$\begin{aligned} &d_{\mathrm{HP}} = \|\mathrm{P}-\mathrm{H}\|\,,\ d_{\mathrm{IP}} = \|\mathrm{P}-\mathrm{I}\|\,, \\ &\theta_{\mathrm{OPH}} = \operatorname{atan2}(r, l_{\mathrm{OG}}),\ \theta_{\mathrm{H}} = \theta_{\mathrm{IHP}} - \theta_{\mathrm{OPH}} \end{aligned} \tag{2.11}$$

$$\begin{aligned} \theta_{HPI} &= \cos^{-1}\left(\frac{d_{\mathrm{HP}}^2 + d_{\mathrm{IP}}^2 - l_{\mathrm{HI}}^2}{2 d_{\mathrm{HP}} d_{\mathrm{IP}}}\right), \\ \theta_{IPJ} &= \cos^{-1}\left(\frac{d_{\mathrm{IP}}^2 + l_{\mathrm{KP}}^2 - l_{\mathrm{IJ}}^2}{2 d_{\mathrm{IP}} l_{\mathrm{KP}}}\right) \end{aligned} \tag{2.12}$$

$$\Psi = \begin{cases} \pi - (\theta_{\mathrm{IPJ}} + \theta_{\mathrm{HPI}}) - \theta_{\mathrm{OPH}} & 0 \le \theta_{\mathrm{IHP}} \le \pi \\ \pi - (\theta_{\mathrm{IPJ}} - \theta_{\mathrm{HPI}}) - \theta_{\mathrm{OPH}} & -\pi \le \theta_{\mathrm{IHP}} \le 0 \end{cases} \tag{2.13}$$

With respect to the inverse displacement analysis, because the method mentioned above can be adapted if the input is changed from θ_{H} to ϕ, then the output angle of θ_{H} can be derived.

2.4 Overall Jacobian matrix

To understand the relationship between the input and output velocity of the proposed mechanism, the overall Jacobian matrix of the lower-mobility parallel mechanism is derived using the screw theory [62]. Considering the actuated wrenches($\$_a$), those wrenches are obtained as follows:

$$\$_{a\,1} = \begin{bmatrix} 1 \\ 0 \\ 0 \\ 0 \\ 0 \\ 0 \end{bmatrix},\ \$_{a\,2} = \begin{bmatrix} 0 \\ 0 \\ 1 \\ -r \\ 0 \\ 0 \end{bmatrix},\ \$_{a\,3} = \begin{bmatrix} 0 \\ 0 \\ 0 \\ 0 \\ 1 \\ 0 \end{bmatrix} (i = 1, 2, 3) \tag{2.14}$$

The constraint wrenches and the actuation wrenches are respectively classified as the force and moment components as follows:

$$\$'_{c\,i} = \begin{bmatrix} s'_{c\,i,f} \\ s'_{c\,i,m} \end{bmatrix},\ \$_{a\,n} = \begin{bmatrix} s_{a\,n,f} \\ s_{a\,n,m} \end{bmatrix} (n = 1, 2, 3) \tag{2.15}$$

where the subscripts of f and m in the wrenches respectively represent the components of the force and the moment. Based on $\$'_{ci}$ and $\$_{a\,n}$, the overall Jacobian of the proposed mechanism is described as follows:

$$J_T = \begin{bmatrix} J_{\mathrm{a}} \\ J_{\mathrm{c}} \end{bmatrix} = \begin{bmatrix} \left(\frac{s_{a,1,m}}{(\$_{a,1} \circ \$_{\mathrm{A}})}\right)^T & \left(\frac{s_{a,1,f}}{(\$_{a,1} \circ \$_{\mathrm{A}})}\right)^T \\ \left(\frac{s_{a,2,m}}{(\$_{a,2} \circ \$_{\mathrm{B}})}\right)^T & \left(\frac{s_{a,2,f}}{(\$_{a,2} \circ \$_{\mathrm{B}})}\right)^T \\ \left(\frac{s_{a,3,m}}{(\$_{a,3} \circ \$_{\mathrm{H}})}\right)^T & \left(\frac{s_{a,3,f}}{(\$_{a,3} \circ \$_{\mathrm{H}})}\right)^T \\ {s'_{c,1,m}}^T & {s'_{c,1,f}}^T \\ {s'_{c,2,m}}^T & {s'_{c,2,f}}^T \\ {s'_{c,3,m}}^T & {s'_{c,3,f}}^T \end{bmatrix} \tag{2.16}$$

where J_{c}, J_{a}, and J_T are the constraint, actuation, and overall Jacobian matrices, respectively. Furthermore, $\$_{\mathrm{A}}$, $\$_{\mathrm{B}}$, and $\$_{\mathrm{H}}$ are the joint screws of the actuation joints. In the six dimensions, the relationship between the input velocity $\dot{\theta}_a$ and output velocity $V = [\omega^T \ v^T]^T$ with the constraint equation is described using the overall Jacobian matrix as follows:

$$\begin{bmatrix} \dot{\theta}_a^T & 0_3^T \end{bmatrix}^T = J_T \begin{bmatrix} \omega^T & v^T \end{bmatrix}^T \tag{2.17}$$

where $\dot{\theta}_a$ and 0_3 are the velocity of the actuation joints $\dot{\theta}_a = [\dot{\theta}_{\mathrm{A}},\ \dot{\theta}_{\mathrm{B}},\ \dot{\theta}_{\mathrm{H}}]^T$ and a three-dimensional zero vector, respectively.

2.5 Kinematic performance analysis

To evaluate the performance of the proposed mechanism, the reachable workspace of PMG, range of the orientation, and Jacobian matrix of the proposed mechanism are analyzed using numerical examples. Kinematic parameters used in the analysis are listed in Table 2.1.

Table 2.1: Kinematic parameters used in numerical example.

Position of joints [mm]		Length of links [mm]			
A(x, y, z)	(16, 36, 0)	l_e	26	l_{JP}	45
B(x, y, z)	(74, 36, 0)	l_{AC}, l_{BD}, l_{CE}, l_{DF}	40	l_{OG}	8.5
O(x, y, z)	(0, 0, 0)	l_{HI}, l_{IJ}	70	l_{offset}	20

2.5.1 Reachable workspace of planar motion generator

The reachable workspace of the proposed mechanism is obtained in the xy plane caused by its constraint conditions. To obtain the reachable workspace, the method of inverse kinematic analysis is applied. At this time, point P's position, such as p_x

or p_y, is given randomly, as listed in Table 2.2.

Table 2.2: Given position of point P.

Parameter	given values [mm]
p_x	-40 ∼120 Interval: 0.1mm
p_y	-20 ∼120 Interval: 0.1mm

The reachable workspace was represented by the points where all the equations as mentioned in Section 2.3 are satisfied. Figure 2.12 shows the obtained reachable workspace. Because the connecting structure between link EF and PH is always perpendicular, the shape of the expected workspace is circular around the origin O. Owing to an asymmetrical placement between joints A and B, the reachable workspace is unequally distributed. The shape of the workspace is deformed owing to the constraint effect by the chains 1 and 2. Furthermore, the empty circular space around the origin is caused by the offset GH.

2.5.2 Rotational capability and sensitivity of orientation generator

To evaluate the rotational performance of the OG, the rotational capability and sensitivity were analyzed. The rotational capability is defined as the relationship

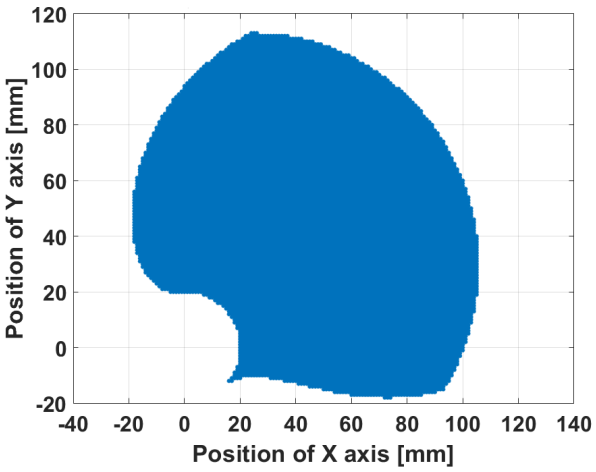

Figure 2.12: Workspace of planar motion generator.

between θ_{H} and Ψ, and the sensitivity is the ratio between their first derivatives. In the calculation, the results are classified by each case of the r value, and the range of minimum and maximum values were determined from the results of the reachable workspace calculation as 0 mm to 119 mm. Considering the thumb rehabilitation, the minimum value of r was redefined as 20 mm.

According to the concept of this mechanism, the OG presents and supports the orientation angle of the proximal phalanx of the thumb, and link JP is designed to be attached to that bone. According to the kinesiology of the thumb movement, the thumb has 50° as the range of angles during the adduction–abduction movement [11, 12]. Assuming that the thumb is located at 0° in the natural posture of the hand, the range is −10° to 40°, and is related to Ψ. Considering the model of the OG, because the thumb CMC joint is located near joint J, the target range of Ψ is determined as 80° to 120°. Based on this, the rotational capability and sensitivity are derived. Then, the displacement results of the OG are selected, where the condition of the period of the target orientation when inputs θ_{H} are randomly given in 0° ∼ 360°, is satisfied. Therefore, the sensitivity is derived using the following equation:

$$s = \frac{\Delta\Psi}{\Delta\theta_{\mathrm{H}}} \tag{2.18}$$

where s is the sensitivity. Figures 2.13 (a) and (b) show the results of the relationship between Ψ and θ_{H} and the sensitivity in proportion to r.

In Figure 2.13 (a), there are six results, where r is kept constant at a certain value shown. The length of each result indicates the range of the orientating performance. Considering the target orientation, the ranges of the input angles vary for each r. These results are used to determine the range of the input angle as it adapts to different hand sizes.

Furthermore, Figure 2.13 (b) shows the maximum and minimum values of the sensitivity for each length of r. In this figure, the sensitivities of each case are stable because there is no unnaturally rapid change between the maximum and minimum

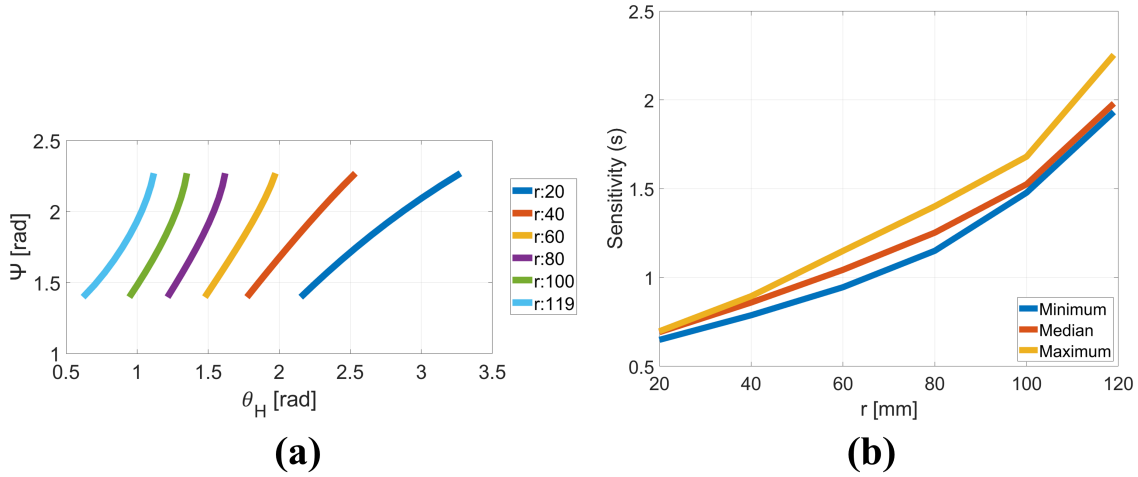

Figure 2.13: Rotational capability and sensitivity results of OG by numerical example: (a) relationship between θ_{H} and Ψ and (b) maximum, and minimum values of s with regard to link length r.

values as the signal of the singularity, but the difference between them increases when r increases. This result can be used for the optimum design of the proposed mechanism by predicting the singularity and understanding changes in the output angle with respect to the input angle.

2.6 Conclusion

To understand the characteristics of the proposed mechanism, the verification of mobility, overall Jacobian matrix, the displacement analysis, reachable workspace, sensitivity of OG were described. The results are summarized as follows from those analysis and calculations:

- The (2–RRU)–URR parallel mechanism was proposed with a focus on thumb movement. This mechanism consists of three chains: two RRU chains and URR chain. Furthermore, this mechanism is designed with a perpendicular connection between the output link and a URR chain.

- To determine the DOF of this mechanism, two methods were applied: Gruebler's mobility formula and screw theory. The results of those calculations con-

firmed that the proposed mechanism has 3 DOF and it is an overconstrained mechanism.

- Based on the screw theory, the constraint wrenches and actuation wrenches were derived. With regards to the constraint wrenches, these did not relate the constraints of each chain, but rather to the whole constraint of the proposed mechanism. Moreover, the overall Jacobian, which consists of the actuation wrenches and the constraint wrenches, was derived.

- The displacement analysis of this mechanism was considered by dividing it into two parts: PMG and OG. The calculation process of each part was derived. Each part was easily calculated using the method for planar 4-bar linkage mechanisms. Finally, the whole displacement of the mechanism was considered by combining the results of the two-part. This is an original method for the proposed mechanism and it simplifies the displacement analysis.

- To verify the performance of the proposed mechanism, a numerical example was shown, in which the sensitivity of the OG and workspace of the PMG were presented.

  - From the result of the OG sensitivity, each range of the input angle θ_{H} depends on r, and its range narrows with an increase in r. Moreover, there was no rapid increase in sensitivity value in the prescribed range of target angles. For this reason, it was confirmed that no singularity occurs in the target range of orientation angles.
  - The reachable workspace was successfully obtained.

Chapter 3

Static analysis

3.1 Introduction

In this chapter, the static analysis of the proposed overconstrained mechanism, the relevant experiment, and the actuation selection for thumb rehabilitation are described. Suitable and safe actuation torques must be determined when considering for design of a mechanism. In general, the static analysis of the overconstrained mechanism can be derived from the relationship equation between force and displacement with consideration about the elastic deformation at the same time [63, 64]. To know the elastic deformation, the measurement by sensors is necessary. However, mechanism orientation and position are changed when the angles of the actuated joints move. Therefore, the elastic deformation also changes through the actuated joint's input angle, which causes the complex calculation process. Moreover, the measurement of the elastic deformation is also needed to change every time when the joint angle changes. When the actuation torque is only focused, its torque can be derived from the overall Jacobian matrix. From the redundant constraints imposed by the independent chains arranged in parallel between the end effector and the base, a sufficient number of independent constraints are selected and applied to formulate the overall Jacobian matrix, which does not include any redundant information. As mentioned in chapter 2, the independent constraint wrenches are

not directly related to each chain's constraint. The experiment was performed using an experimental apparatus and attached force sensors, and the calculation results were confirmed. The actuator selection was conducted by considering the human kinesiology for thumb rehabilitation.

3.2 Static analysis

3.2.1 Method

In this section, the method of the static analysis is described. As shown in Figure 3.1, the force equilibrium is described using two kinds of force. $\boldsymbol{F} = [\boldsymbol{f}^T \ \boldsymbol{m}^T]^T$ is the effected force on the output link from the external space and $\boldsymbol{F}_{\mathrm{M}k}$ $(k = 1, \cdots, 3)$ is the effected force on the output link from the chain k. Based on the equilibrium of the forces, the relationship between these two forces is explained in the following equation:

$$\boldsymbol{F} = \sum_{k=1}^{3} \boldsymbol{F}_{\mathrm{M}k} \tag{3.1}$$

Furthermore, $\boldsymbol{F}_{\mathrm{M}k}$ can be categorized in terms of the actuation force and the constraint force (Both forces are vectors that include the force and the moment). The actuation force is the force generated by the actuator, and the constraint force

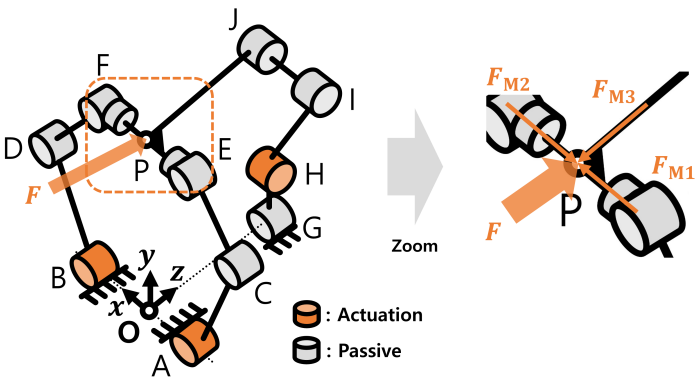

Figure 3.1: The situation of the force equilibrium.

consists of the internal forces in the link and the constraint forces of the joints. Each force consists of the magnitude of the force and its direction. Furthermore, the direction of each force is the same as the wrenches. For this reason, the direction of the forces can be described using the actuation wrenches and the constraint wrenches. As the result is the same as the result of the wrenches, there are six constraint forces and three actuation forces in the whole mechanism. From the constraint forces of each chain, the whole constraint force in the mechanism can be explained by the independent constraint wrenches ($\$'_{c,i}$) because the constraint wrenches are mutually overlapped, as mentioned above. For this reason, the forces can be described using the independent constraint and actuation wrenches. When the constraint and actuation forces are defined as $\boldsymbol{F}_{c,i}$ and $\boldsymbol{F}_{a,n}$, the forces are described as follows:

$$\begin{aligned} \boldsymbol{F}_{a,n} &= \tau_{a,n}\$_{a,n} \ (n = 1, \cdots, 3) \\ \boldsymbol{F}_{c,i} &= \tau_{c,i}\$'_{c,i} \ (i = 1, \cdots, 3) \end{aligned} \tag{3.2}$$

where $\tau_{c,i}$ and $\tau_{a,n}$ are the magnitudes of the constraint and actuation forces, respectively. Thus, these are scalar value of $\boldsymbol{F}_{c,i}$ and $\boldsymbol{F}_{a,n}$ without the direction vector. Similar to $\$'_{c,i}$, $\tau_{c,i}$ represents the virtual force without direct correspondence to the actual chain. In contrast, the actuation forces directly correspond to the active joint torques of the mechanism. Based on this, $\boldsymbol{F}_{\mathrm{M}k}$ in Equation (3.1) can be separately considered into the constraint and actuation force as in following equation:

$$\boldsymbol{F} = \sum_{i=1}^{3} \boldsymbol{F}_{c,i} + \sum_{n=1}^{3} \boldsymbol{F}_{a,n} = \sum_{i=1}^{3} \tau_{c,i}\$'_{c,i} + \sum_{n=1}^{3} \tau_{a,n}\$_{a,n} \tag{3.3}$$

This equation can be expressed in the matrix form as follows:

$$\boldsymbol{F} = \begin{bmatrix} J_{\mathrm{a}}^T \\ J_{\mathrm{c}}^T \end{bmatrix} \tau = J_T^T \boldsymbol{\tau}, \text{ where } \boldsymbol{\tau} = \begin{bmatrix} \boldsymbol{\tau}_{\mathrm{a}}^T & \boldsymbol{\tau}_{\mathrm{c}}^T \end{bmatrix}^T \tag{3.4}$$

where $\boldsymbol{\tau}_{\mathrm{a}}$ and $\boldsymbol{\tau}_{\mathrm{c}}$ are the vectors of $\tau_{a,n}$ and the vectors of $\tau_{c,i}$, respectively. Using Equation (3.4), the actuation forces τ_a can be derived. Note that the constraint forces obtained using Equation (3.4) do not correspond to the actual constraint forces of each chain, as the direct correspondence of the constraint to the actual structure of the mechanism was lost in the derivation of the overall Jacobian matrix.

3.2.2 Experimental verification

An experiment considering a numerical example was performed to verify the calculation method of the static analysis. Table 3.1 lists the kinematic parameters employed in the mechanism. Figure 3.2 shows the 3D CAD drawing of the experimental apparatus considered in the example.

Table 3.1: Numerical example parameters for static analysis.

Link length [mm]		Joint angle [Degree]		Positions (x, y, z) [mm]	
l_{AC}, l_{CE}, l_{BD}, l_{DF}, l_{JP}, l_{HI}	50	θ_{A}	110	A	(-41.5, 0, 0)
l_{EF}	82	θ_{B}	70	B	(41.5, 0, 0)
l_{IJ}	60	θ_{H}	160	G	(0, 0, 52)
l_{GH}	27.5	θ_{P}	-41.35	P	(0, 84.89, 0)

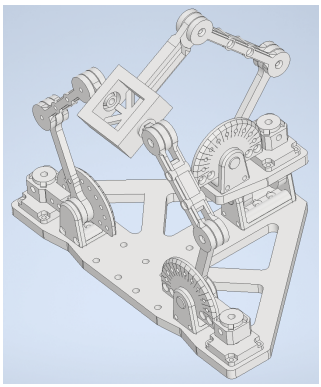

Figure 3.2: CAD drawing of the experimental apparatus.

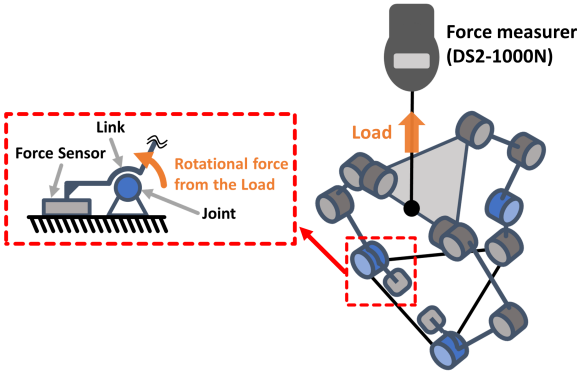

Figure 3.3: Concept of the experiments and scenario.

The experimental apparatus was manufactured using a 3D printer . The links were assembled using bolts to reduce their deformation. The angle holder, which is the part that appears as an angle protractor, was designed to provide an accurate input angle to the actuation joint. A Teflon wire was connected with the end-effector and force measurement device (DS2-1000N) to apply the load in the y-axis direction. A 27-mm-long transmission link was attached to the actuation links (i.e., AC, BD, and HI). The bolts, designed to contact the measurement point of the force sensor, were assembled on the opposite side of the link.

When the load was applied and actuation joint angle was determined, each sensor measured the given load and required torque of each actuation joint. Figure 3.3 shows the experimental procedure and measurement principle. The experiment system was controlled using a personal computer. The force measurement device communicated through RS232. Three force sensors transmitted signals, which passed through the

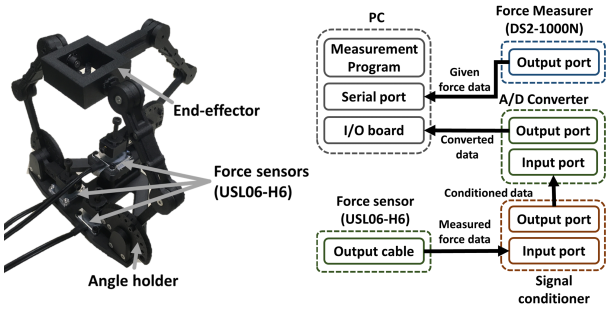

Figure 3.4: Experiment mechanism and its experiment system environment.

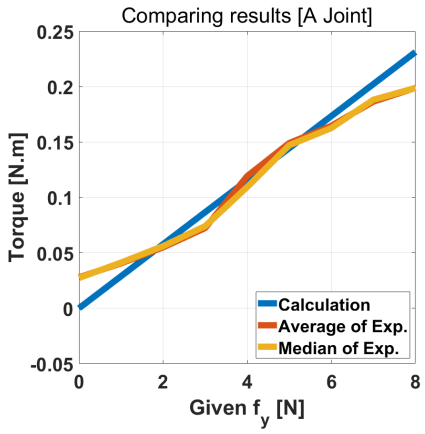

Figure 3.5: Experiment data of Joint A.

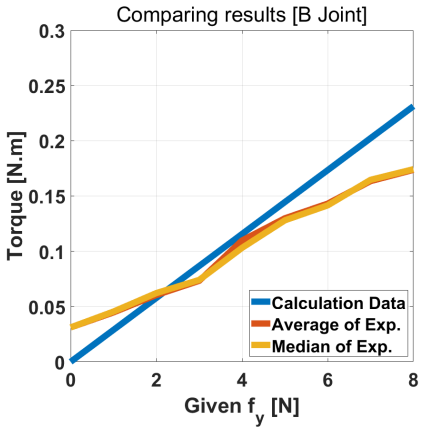

Figure 3.6: Experiment data of Joint B.

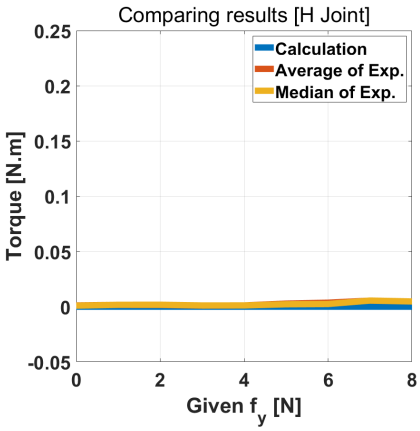

Figure 3.7: Experiment data of Joint H.

signal conditioner and A/D converter. Figure 3.4 depicts the experiment system maps. Each experiment was performed five times for 20 min, and the input loads were randomized. Every measured datum was categorized in the given load value.

Figures 3.5, 3.6, and 3.7 show the required torque of the different actuation joints. As the result, the given load was influenced more by chain1 and 2 by chain 3. The comparison of the calculation and experiment results showed that the data in Figures 3.5 and 3.6 were similar in the period 2–6 N. Even though a certain difference existed between the experimental and theoretical results, this tendencies were similar. The error was caused by environmental factors, such as the inaccurate direction of the

given load and unexpected deformation of the links. Table 3.2 presents the errors between average value and calculation data.

Table 3.2: Errors between average value and calculation data.(Unit: N.m)

f_y	0N	1N	2N	3N	4N	5N	6N	7N	8N
Joint A	0.028	0.012	0.003	0.014	0.004	0.004	0.005	0.009	0.009
Joint B	0.031	0.016	0.003	0.013	0.006	0.015	0.030	0.039	0.058
Joint H	0.001	0.002	0.002	0.001	0.001	0.003	0.004	0.006	0.005

3.3 Conclusion

This chapter described the static analysis method for the (2-RRU)-URR parallel mechanism using the overall Jacobian matrix. The analysis method used the overall Jacobian matrix to consider the actuation force from the constraint force in the overconstrained parallel mechanism with lower mobility separately. In other words, the relationship between the input torque and the external load applied to the end effector has been derived for the overconstrained mechanism with lower mobility based on the overall jacobian matrix introducing the virtual constraint wrenches. An experiment using the experimental apparatus was performed to verify the calculation result, revealing the following:

- The experiment results showed that chains 1 and 2 had a more significant effect compared to Chain 3. In joints A and B, the difference between the calculation and measurement data was small in the 2N to 6N period.
- Since this calculation should require that mechanism never deformation by the external forces, the error from the experiment anticipated that cause from deformation of material or the joint clearance. However, the tendency of the experiment result follows along with the simulation results.
- From the result of the verification experiment, the method of the static analysis was verified, and it was evident that it can be used for the actuator selection.

Based on this method, the actuator torque will be determined for designing the practical prototype.

Chapter 4

Workspace analysis and dimensional synthesis

4.1 Introduction

In this chapter, to find the suitable link length for thumb rehabilitation, the maximum torque of actuation joint is described as the design index. Based on this index, the effective workspace, which shows the effectiveness with the given link length of the mechanism, is derived. Furthermore, the dimensional synthesis of the proposed mechanism is described, and a numerical example of synthesis is demonstrated.

4.2 Effective workspace

To design the proposed mechanism for safety, an effective workspace is defined and determined using the input torques. This workspace is the sub-workspace of the proposed mechanism and it indicates the workspace that satisfied the desired range of the actuation torque of the actuation joint. To define the effective workspace, the maximum torque of the actuated joints is considered. From the result of the static analysis, the actuation torques are derived to respect the principle of virtual work. Because the actuation joints of the proposed mechanism are three, the derived torque of the actuation joint also three. There is a case where one torque of them

is unnaturally higher than the others. This may be the result when the proposed mechanism reached the singularity. Moreover, considering the practical design of the proposed mechanism, the higher torque actuator has huge volume and heavy in general. Because the proposed mechanism is designed to attach with a hand, the excessive weight of the actuator is not desirable. Furthermore, the unbalanced weight may affect the performing motion and it also has the possibility of increasing fatigue. For this reason, the same specifications and size of the actuators are desired to use in the mechanism. To recognize a suitable situation for thumb rehabilitation, the maximum torque of the actuation joint is used as a design index and it notates D as the maximum value of the three actuation torque. As the standard to judge this index, the threshold is determined based on the desired condition. In this thesis,

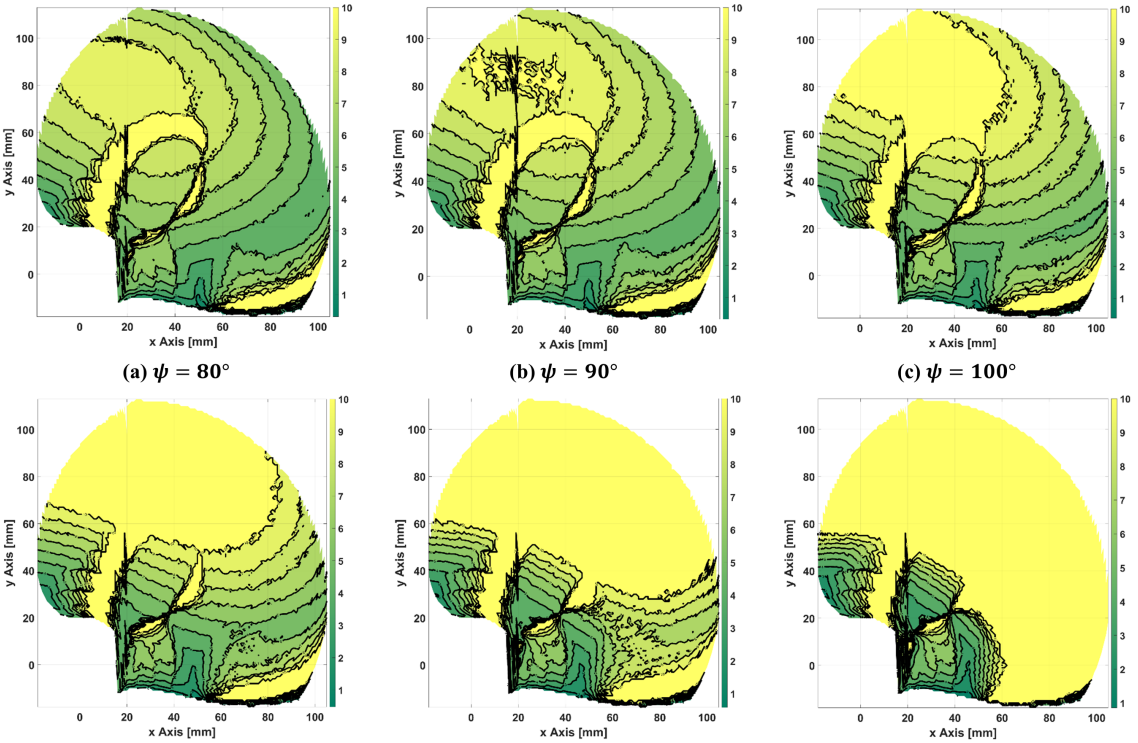

Figure 4.1: Distribution maps of D in workspace for each orientation angle Ψ. If the workspace area is the closest to yellow, then the mechanism has a higher torque difference over 10 N·m. [(**a**) $\Psi = 80$ deg, (**b**) $\Psi = 90$ deg, (**c**) $\Psi = 100$ deg, (**d**) $\Psi = 110$ deg, (**e**) $\Psi = 120$ deg, (**f**) $\Psi = 130$ deg].

the threshold value of the D was decided by the medical information and the static analysis results. When index D is equal or smaller than the threshold value, the state of the mechanism is called "effective". In opposite, the ineffective state of the mechanism is defined when D is higher than the threshold value.

As the numerical example, the effective workspace is calculated. As the parameter, Table 2.1, the external force ($\boldsymbol{F}$) was set as $\boldsymbol{F} = [f_x, f_y, f_z, m_x, m_y, m_z]^T = [6, 0, 6, 0, 0.11, 0]^T$, and the threshold value was set as 6 N·m. The effective workspace maps are shown in Figure 4.1 for each fixed orientation angle Ψ from 80° to 130° with increments of 10°. To better understand the characteristics of the mechanism, the workspace is colored according to the value of D: the area of $D \leq 10$ is colored green, while that of $D > 10$ is yellow. This range of the thresholds only helps to visualisation of the chart to make the values of the under threshold value as the green color. As the quantitative calculation results, the range of threshold value was used as 6 for counting the area of the effective workspace. From these figures, the orientation angle significantly impacts the effective workspace is known. In particular, the yellow area increases with the increase of Ψ, and it is clearly exposed in the maps of 120° and 130°.

4.3 Dimensional synthesis

Based on the effective workspace analysis result, the dimensional synthesis, which is done to find the suitable link length, is described. The idea of the synthesis is focused on the way to use the area of the effective workspace. The size of the effective workspace is expected to change depending on the design parameter. Thus, if the link lengths are given, the coverage of the green area changes consequently. At this time, the optimum value corresponded to that with the maximum coverage of the green area and minimum link length simultaneously. Based on this idea, the calculation for the suitable link length is carried out.

The numerical example was demonstrated for the sake of understanding. In this section, the square area covering the red-lined area is temporarily set as the ex-

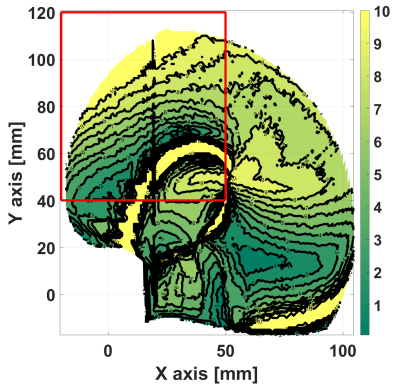

Figure 4.2: Example of the target workspace (Red square).

ample of the target workspace for computational convenience in the calculation (x: $50 \sim -10$, y: $40 \sim 120$). Figure 4.2 shows the target workspace (red square area). In the algorithm, when an arbitrary link length was specified, an appropriate candidate was selected by evaluating the proportion of the green area in the target workspace. Therefore, the design variables, constant variables, and constraints were set, as specified in Table 4.1. The constant values are referred to from Table 2.1 and the external force (F) as mentioned above. Where l_1, l_2 are design values categorized into two from the mechanism links, shown in the figure. Based on the table, the dimensional synthesis is carried out according to the following flow chart shown in Figure 4.3.

Using the numerical example using the values of Table 4.1, the dimensional synthesis is conducted. In this calculation, the range of the orientation angle was set as 0° to 40° with respecting the required range of the thumb movement for the proposed mechanism. Based on this condition, the list of the design candidates was

Table 4.1: Design variables, constant variables, and constraints.

Design variables	l_1 (l_{AC}, l_{CD}, l_{BD}, l_{DF}): $0 \sim 100$ [mm] l_2 (l_{IJ}, l_{HI}): $0 \sim 100$ [mm]	
Constraint	θ_{A}, θ_{B}, θ_{H}: $0° \sim 180°$ θ_{C}, θ_{D}: $-90° \sim 90°$	θ_{J}, θ_{I}: $-160° \sim -10°$ -
Constant value	l_{EF}: 52mm l_{JP}: 45mm	l_{offset}: 20mm l_{OG}: 8.5mm

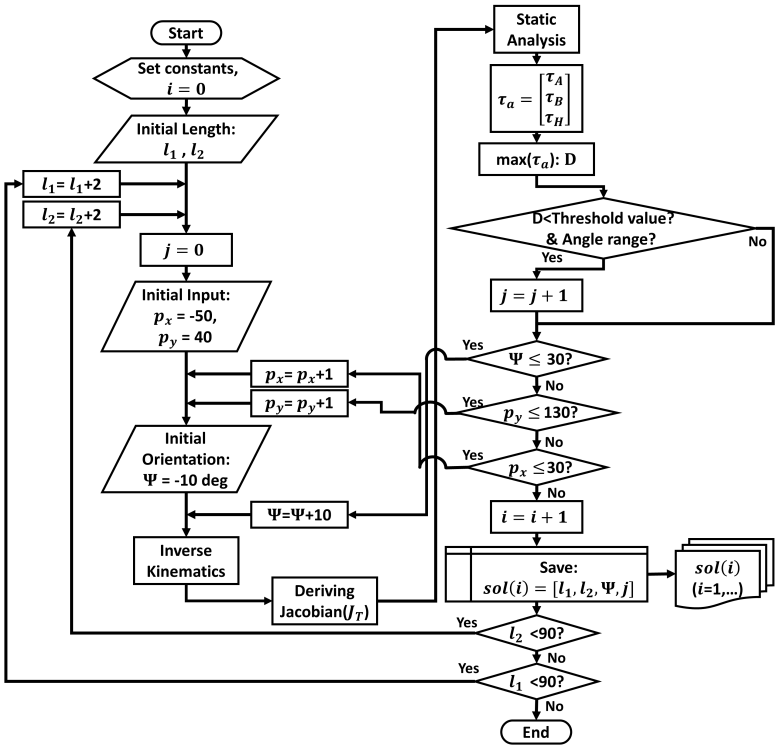

Figure 4.3: Calculation flow chart of dimensional synthesis.

listed as shown in Table 4.2 when the orientation angle Ψ of the mechanism was zero. From this table, where c_R and c_E are the coverage of the reachable workspace in the target workspace and the coverage of the effective workspace in the target workspace, respectively. When R_{area}, E_{area}, and T_{area} are set as the area of the reachable workspace in the target area, the area of the sorted effective workspace in the target area, the target area respectively, each coverage is derived as the following equations:

$$c_R = (R_{area}/T_{area}) \times 100 \tag{4.1}$$

$$c_E = (E_{area}/T_{area}) \times 100 \tag{4.2}$$

Table 4.2 shows the result of the dimensional synthesis. Because the suitable candidate is chosen in the condition that has a high c_E with high c_R, the suitable

Table 4.2: Calculation results of the numerical example.

$l_1(mm)$	$l_2(mm)$	$\psi(\circ)$	$c_R(\%)$	$c_E(\%)$
52	84	0	96.57	0.036
52	86	0	97.51	0.036
52	88	0	97.64	0.036
52	90	0	97.64	0.036
46	74	0	73.97	0.024
46	76	0	77.77	0.022
42	82	0	79.60	0.022
42	84	0	80.32	0.022
42	86	0	80.32	0.022
42	88	0	80.32	0.022
42	90	0	80.32	0.022
46	78	0	81.32	0.021
46	80	0	84.54	0.021
46	82	0	87.34	0.020
46	84	0	89.44	0.019

condition is chosen as: l_1=52, l_2=84, Ψ=0, C_R=96.57, and C_E=0.036 from the results. Based on this procedure, the link length was determined. Figure 4.4 shows the effective workspace maps when the link parameters decided as l_1=52, l_2=84. In this figure, the size of the reachable workspace is not changed in the whole cases. The non-effective area marked in yellow and the effective workspace was marked in green. When the green is getting deeper, the derived D is lower than the threshold value. From the result, when Ψ is increased, the effective workspace is increased. Using this method, the suitable link length is designed by considering the suitable torque of the actuation joint. As the next step, the design of the practical prototype will be carried out using this method.

4.4 Conclusion

To determine the link length of the proposed mechanism considering the safety issue caused by the excessive actuation torque, the difference between the maximum and minimum actuation torques was proposed as an index for it. Based on the difference, the effective workspace maps were plotted using color gradation for each

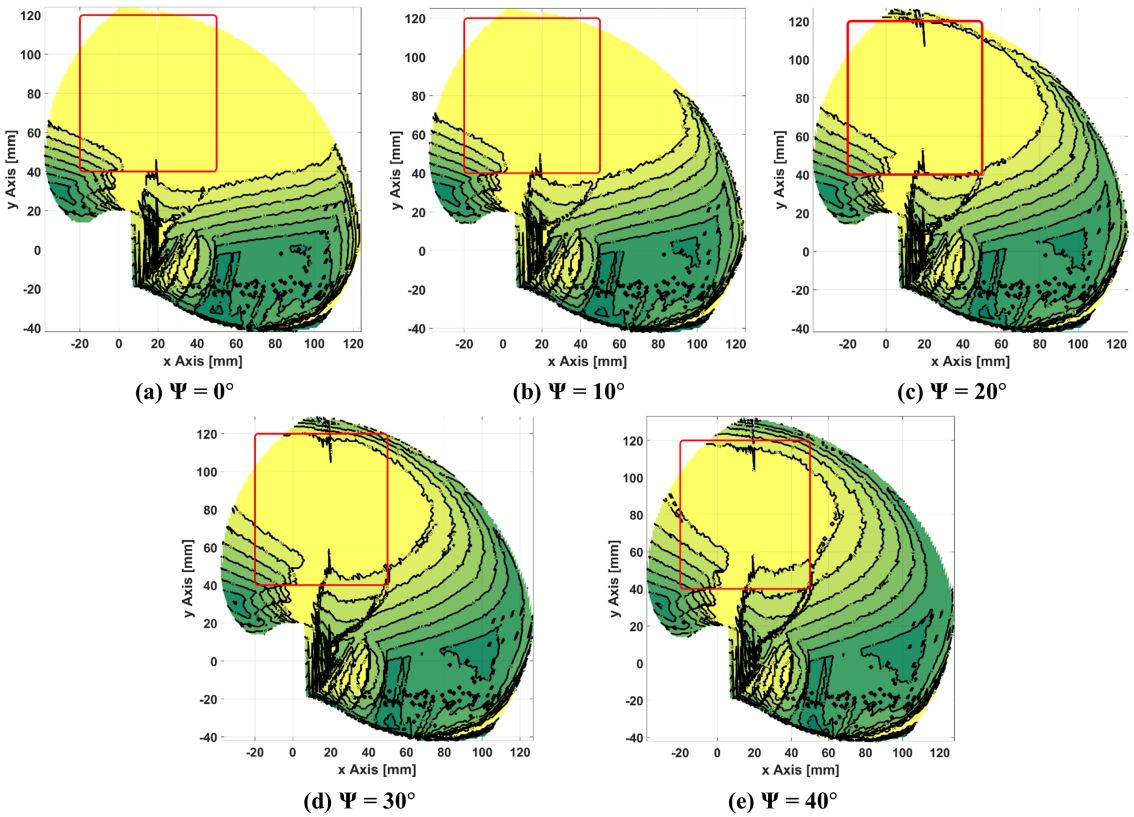

Figure 4.4: Comparison of results for target workspace (Red) and effective workspace maps of the link length optimization for each condition of Ψ: (**a**)Ψ = 20°, (**b**)Ψ = 35°, (**c**)Ψ = 50°, (**d**)Ψ = 65°, (**e**)Ψ = 80°, (**f**)Ψ = 130°

orientation angle. Furthermore, the dimensional synthesis for link length selection is conducted with the numerical example. The calculation results reveal the following:

- The effective workspace was defined by the magnitude of the maximum torques.
- From the numerical results, the decrease of the effective workspace is occurred when the orientation angle decrease.

Using this method, the suitable link length can be determined by considering the suitable torque of the actuation joint.

Chapter 5

Prototyping and experiment with users

5.1 Introduction

In the previous chapters, the concept of the mechanism was considered theoretically, and it is focused on determining the kinematic characteristics of the proposed mechanism. If the prototype is designed without any considerations to the thumb rehabilitation requirements, the prototype is not practical, and it may not be attach well to the hand. Moreover, it will not be able to provide the expected thumb rehabilitation function, and it may damage the thumb. Therefore, the investigations done through creating prototypes which are designed based on the requirements in terms of function, anatomy, kinesiology and practical implementations are very important to realize the proposed concept for the target users. The prototype is also necessary to prove the feasibility, performance and reliability of the proposed concept as well as envisage its future qualification. In this chapter, the design of the prototype with consideration of the requirements is described. Based on the measured thumb motion data and the kinesiological and the anatomical information, the design requirements and the target movement were determined. To verify the performance of the proposed mechanism, experiments were performed to measure

the trajectories of the thumb and its range of movement under two conditions; with and without attaching the prototype. The experiments involved the use of prototypes manufactured using a 3D printer. In addition, the experiment environment and system are described in terms of the specifications of each part, communication method, electrical/electronic specifications, and other aspects.

5.2 Design of prototype

5.2.1 Determination of the target workspace

Before manufacturing the prototype, the thumb measured trajectories of volunteers were measured. Certain data, such as the thumb trajectory, were measured using the motion capture system (OptiTrack Flex 13). Figure 5.1 shows the environment for the motion capture system. The obtained data were used for various purposes, such as determining the target workspace and the source of the prototype's input trajectory. Because the proposed mechanism's position moves in the xy plane by the PMG, the thumb measured data were projected onto the xy plane before use. The target workspace is the workspace in the xy plane that includes all movements of the thumb measured data, and this is used as the design workspace. The input trajectory is the expected path of the output link and it is used as the input data when the proposed mechanism is controlled. Furthermore, this is also

Figure 5.1: Measurement environment of motion capture system (adapted from [65]).

Figure 5.2: Markers for the thumb trajectory measurement.

compared with the experimental data to prove the mechanism's performance and reliability.

Because the camera used in the motion capture system detects the reflection of infrared rays, errors could easily occur due to light reflection. To reduce the reflection of infrared light on the skin surface, black gloves were used. To prevent the noise from light, shades were used around the system to block external light. Figure 5.2 shows the markers on the hand for the measurement. As shown in Figure 5.2, seven markers were used. Markers 1 and 2 were the guide markers to indicate the hand direction. Marker 6 corresponds to the origin point, and marker 7 was used to set the z-axis as the line through the origin and marker 7. Markers 3, 4, and 5 were used to measure the MP joint position and thumb tip. The thumb trajectory data was measured by using the motion capture system on twelve volunteers. The measurement safety was ensured in accordance with the experimental ethics of the university. The detailed information regarding this is presented in the experiment scenario section.

When designing the proposed mechanism, its workspace must cover the two target movements: AA and FE. Due to the difference in the hand size of volunteers, the ranges of the movements are different. The thumb measured trajectories are three-dimensional data and are not located in a plane. Considering the structure of the proposed mechanism and its mobility, its position workspace is formed in the

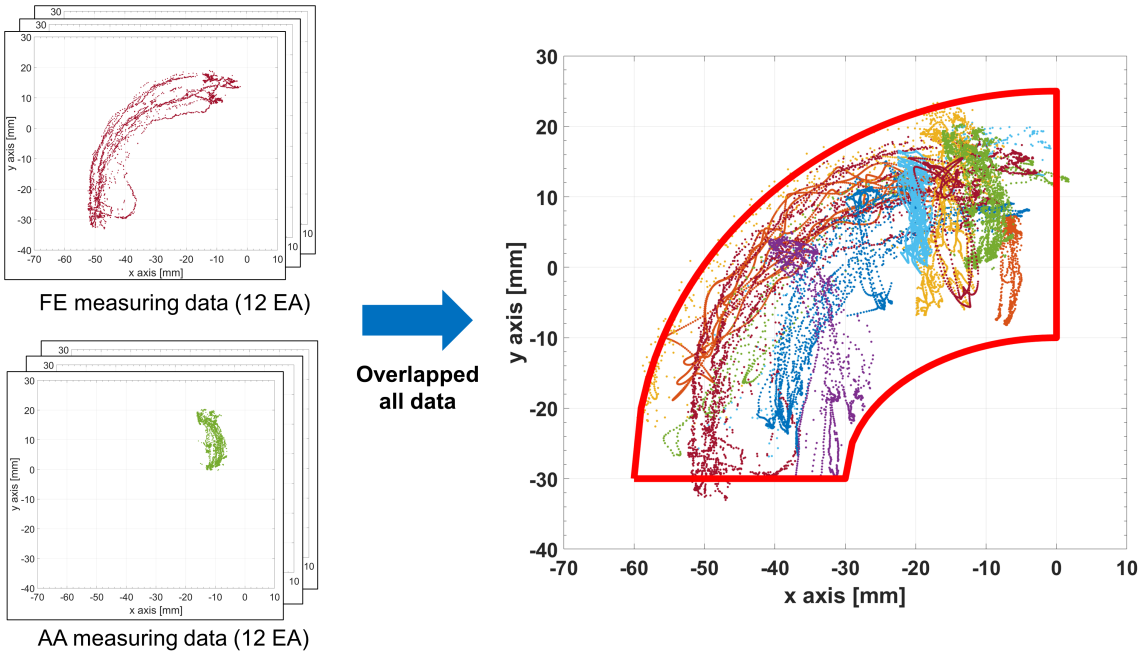

Figure 5.3: Target workspace defined by the measured trajectories of the thumb through motion capture system.

xy plane. To determine the target workspace in this plane, the measured thumb trajectories are projected onto this plane. Here, the required workspace (= target workspace) is the workspace to cover all movements from the projected thumb trajectories. Figure 5.3 shows the AA and FE measured data of twelve volunteers in the xy plane and the target workspace for PMG of the proposed mechanism. Each dot shown in this figure is was obtained through measurements for each movement. The trajectories are classified by their shape. Therefore, the near rectilinear shape is the trajectory of the AA movement and the curved shape is the trajectory of the FE movement. In this figure, the total data consists of 24 sets of data (12 volunteers $\times$ 2 required movements = 24). To cover all movements of all volunteers, all measured data were plotted in the same space, and the boundary of the target workspace was determined to be the area surrounded by the red line.

5.2.2 Actuator placement and its effect on workspace

Because of the hand's narrow space, the actuator placement should be carefully determined in the geometric design. Of the three actuators (each actuator adapted in joint A, B, and H), two actuators (A and B) are used for PMG and actuator H is used for OG. In detail, actuators A and B are installed on the palm and the hand's surface, respectively. In the yz plane of the hand, the location of those actuators is similar or overlapped. Note that the axes of the passive joint G and the active joint H are crossed perpendicularly to each other similar to a universal joint. For this reason, when the placement of the third actuator is decided, the placement of the passive joint G is also decided. Regarding the third actuator placement, if it is installed near the palm or the surface, the structure of the base part will be complex and there is the possibility that the collision between chains 3 and 1 or 3 and 2 occur. For this reason, the probable placement is chosen as near the wrist. However, because the placement of the actuator affects the size of the reachable workspace, the placement must still be considered in more detail. For the third actuator placement, two models were considered, as shown in Figure 5.4. Those candidates are designed with the third actuator placed near the wrist, but the detailed placements are different.

In the first candidate, the third actuator is placed on the side of the wrist. In the coordinate system in the figure, the third actuator's position on the xy plane matches

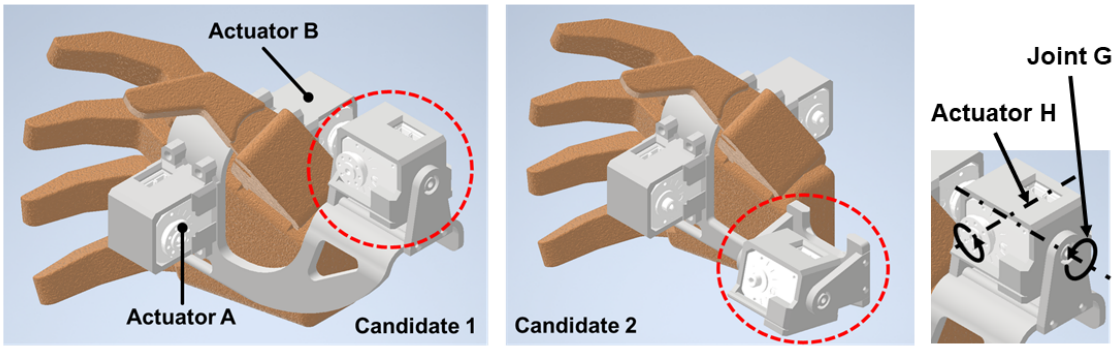

Figure 5.4: CAD images of two candidates, with the different placements of joints G and H: candidate 1 designed to be located behind the thumb, and the candidate 2 designed to be located beside the wrist.

the origin point. In the second candidate, the placement of the third actuator is designed to be near the wrist. Based on the above-mentioned coordinate system, the actuator position on the xy plane is not in the origin point. Regarding the position of the third actuator along the z axis, both design candidates are set to the same value of zero. Furthermore, an offset was included to reduce the collision of the hands and ensure the parallelization of the third chain. Figure 5.5 illustrates two candidates and their differences.

To find a suitable design, a workspace comparison of the two candidates is carried out. Table 5.1 shows the relevant parameters. On the basis of PMG, l_{AC}, l_{CE}, l_{BD},

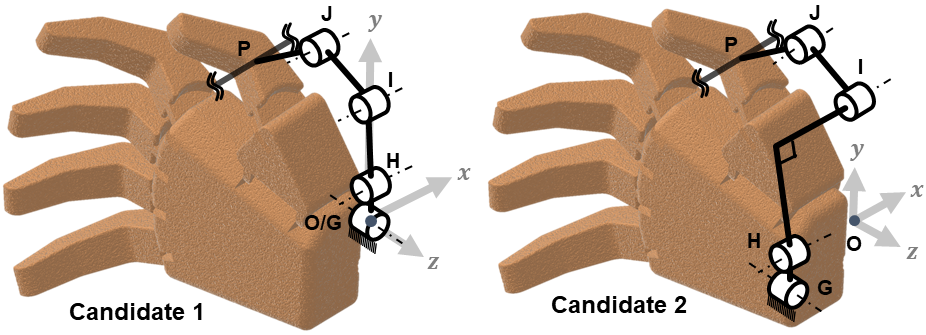

Figure 5.5: Difference of each candidate and configuration of the third chain for each candidate. (The actual distance between joint H and G is zero)

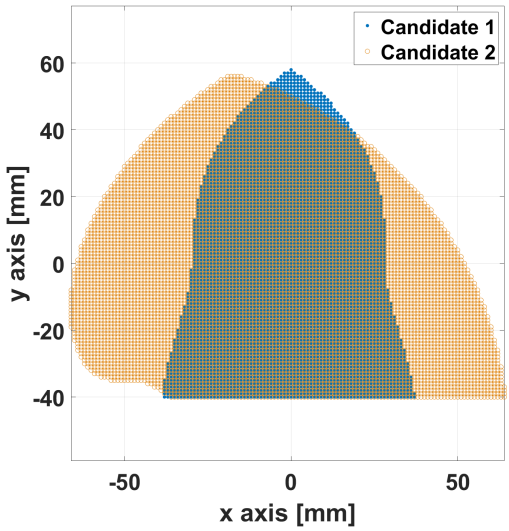

Figure 5.6: The derived reachable workspace for each candidate.

and l_{DF} were set to have the same link length. Furthermore, l_{HI} and l_{IJ} were set to have the same link length based on OG. The reason for those settings is for the simplification of the calculation for the design. Therefore, the design parameters of links are set as l_1 (=l_{AC}, l_{CE}, l_{BD}, and l_{DF}) and l_2 (=l_{HI} and l_{IJ}). The parameters, such as l_1, l_2, and joint positions for two candidates, were the same in both cases. Other parameters such as offset, l_{EF}, and l_{JP} are set as constant values with respect to the size of the hand. Moreover, the range of workspace of the output link position was given as random values. Based on these parameters, the reachable workspace of each candidate was derived. Figure 5.6 shows both reachable workspaces. The reachable workspace for the first candidate exhibits a vertical, tower-like workspace. On the other hand, the second candidate's workspace has a long width along the x-axis while having the same height as the first candidate. Each workspace is compared to the target workspace (red marked area in Figure 5.3), as shown in Figure 5.7. In terms of the target workspace, the second candidate covers more of the target workspace than the first and also completely covers the target workspace.

This phenomenon can be attributed to the structure of the proposed mechanism such as the perpendicular connection of OG with the output link, and the effect of the PMG on the OG. In the structure of the proposed mechanism, the workspace is

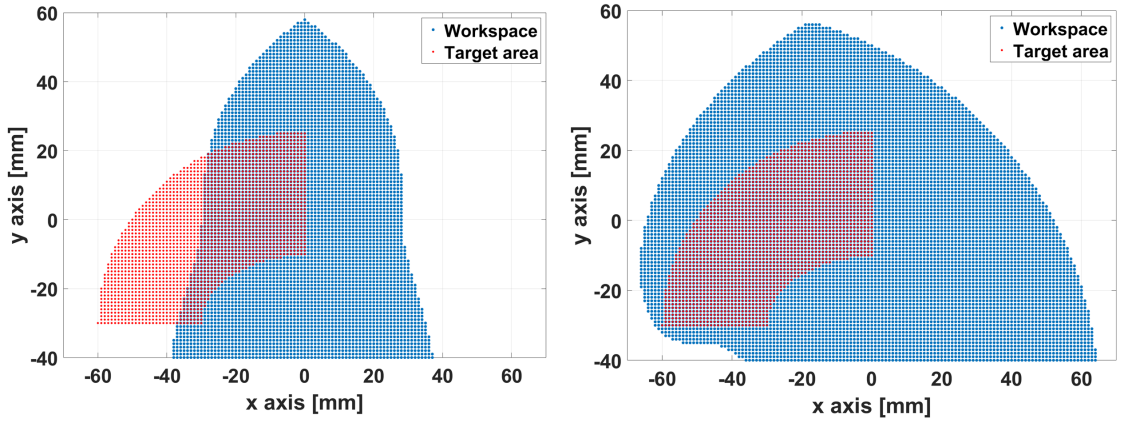

Figure 5.7: The workspace when the target workspace overlapped in the same coordinate space: (a) Candidate 1, (b) Candidate 2

Table 5.1: The parameters of two candidates.

Parameter	Common		Candidate A		Candidate B	
Joint	A	[-49,-52,-69]	G	[0, 0, 0]	G	[-50, -55, 0]
Position	B	[47.5, -52, -69]	-	-	-	-
$[x,y,z]$ (mm)	O	[0, 0, 0]	-	-	-	-
Link Length (mm)	l_1	64	Offset	0	Offset	20
	l_2	50	-	-	-	-
	l_{EF}	58	-	-	-	-
	l_{JP}	24	-	-	-	-
Given position of output link point (mm)	x	$-180 \leq x \leq 180$ (Interval: 1mm)	-	-	-	-
	y	$-40 \leq y \leq 180$ (Interval: 1mm)	-	-	-	-

generated by the PMG and the size of the workspace is determined by two parameters. The first parameter is the range of the circle drawn from the center point G/H with its radius being the distance between P and point G/H in the OG (In chapter 2, this distance was explained as d_{GP}). If there is no constraint from the other chains, the size of the circle is determined by the link lengths of OG. The second parameter is the constraint of PMG on the circle of OG. Through the constraint of the PMG, the circle size of OG is limited. In other words, the size of the workspace is related to the circle generated by OG, and the constraint of PMG determines the shape of the workspace. In the case of candidate 1, because of the position of the G/H joint located inside the loop of the PMG, the circle size of OG is decreased by the constraint of the PMG. In the case of candidate 2, the position of the G/H is located outside of the PMG loop. For this reason, the constraint of PMG is less affected by the circle size of OG than candidate 1 and the size of candidate 2's workspace is wider than candidate 1. Figure 5.8 shows the graphical explanation of two candidates to explain the circle of point P as the center of the G/H point.

Furthermore, the width of the workspace is also dependant on how far the x-axis of the G/H joint is positioned from the y-axis. In the case of candidate 1, the workspace shape is symmetric like a tower shape because the x-axis position

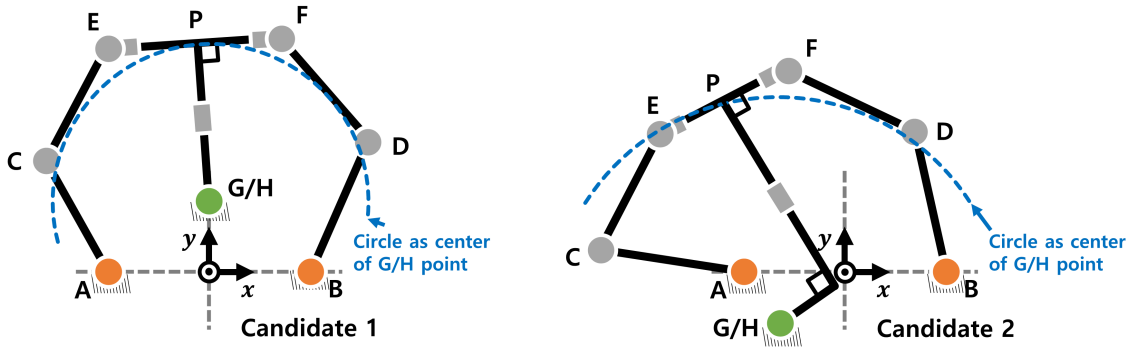

Figure 5.8: The graphical explanation of two candidates to explain the circle of point P as center of G/H point.

of the G/H joint is zero. In the case of candidate 2, the shape of the workspace is asymmetric because the position of the G/H joint along the x-axis is located in the negative value. Based on these results, the second candidate appears to be a reasonable choice for designing the prototype to be attached to the users, even though the offset makes the structure relatively complex.

5.2.3 Prototype

Considering the aforementioned results, a prototype of the proposed mechanism was developed. Figure 5.9 shows the CAD drawing of the prototype. To adapt to different hand sizes, the base module was designed to incorporate three parts. The three parts are called the upper base part 1, upper base part 2, and under base part, respectively, and each part is connected by a passive revolute joint. One actuator was installed in the upper base part 1 and the other actuators were installed in the under base part. The upper base part 2 was passively attached to the hand surface. Through this structure, the base module can wrap the hand without needing to consider differing hand thicknesses. When the mechanism is placed on the hand, the parts were fixed using a Velcro strap, as shown in Figure 5.10. In terms of hand thickness, the mechanism was designed to fit hands with a thickness of more than 33 mm, in consideration of the human measurement data. Thus, the base module can adapt be fixed to hand sizes with a high thickness. Moreover, the shape of each

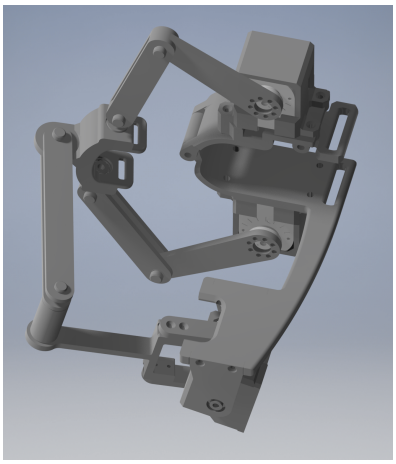

Figure 5.9: CAD drawing of the proposed mechanism.

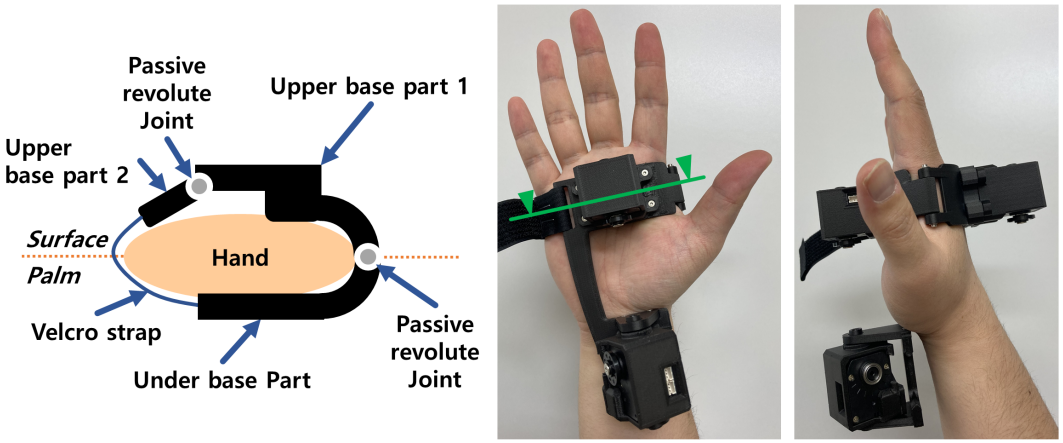

Figure 5.10: The cross-section of base parts and the attached state of the base with hand.

part is complex to provide an ergonomic shape. In order to fabricate the complex shapes, most parts of the prototype were fabricated using a 3D printer (Markforged Mark two), and the parts were reinforced with carbon fiber. Furthermore, the third actuator, connected to chain 3, was placed near the wrist and thumb CMC joint. This placement allows the center of weight of the mechanism to be close to the center of the hand. The manufactured prototype and the attachment state are shown in Figure 5.11. The weight of the prototype was 317g (including the actuators). Figure 5.12 shows the parameters of the prototype's link lengths.

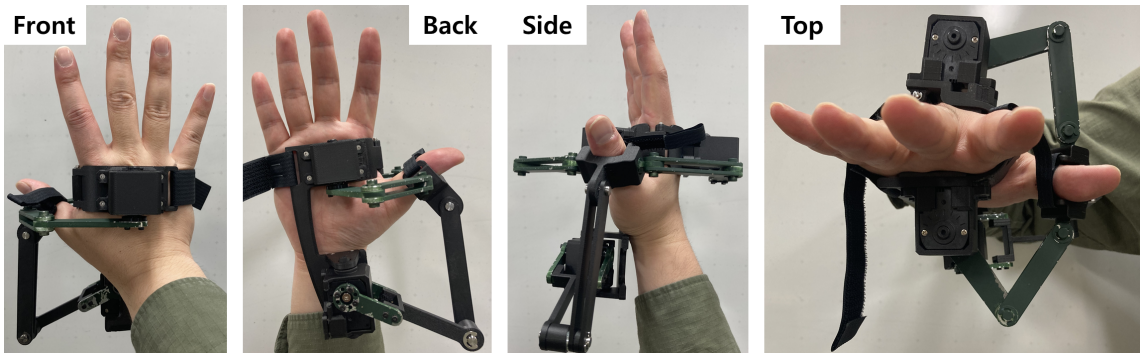

Figure 5.11: Manufactured final design of prototype.

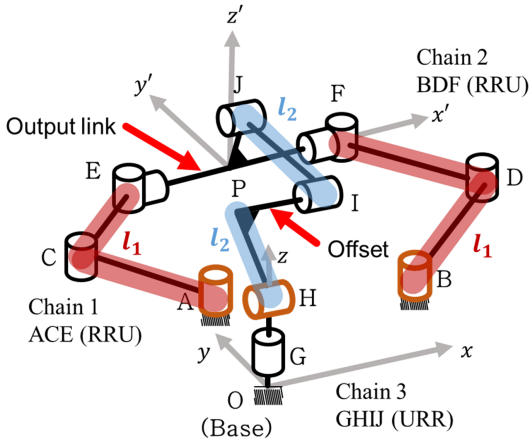

Link	length (mm)
l_1 (l_{AC}, l_{BD}, l_{CE}, l_{DF})	56
l_2 (l_{HI}, l_{JI})	87
l_{EF}	58
l_{JP}	24
Offset	20

Figure 5.12: The design variables of each link for prototype.

5.2.4 Experiment system and control

The experimental system consisted of three elements, specifically, the proposed mechanism, driving/control part, and control algorithm. The driving/control part contained all the electrical parts needed to control the mechanism. The control algorithm was the code for the position control of the actuator, and this program uploaded to the controller unit. The driving/control part consisted of the microcontroller unit (MCU), servomotor, and signal conversion board. The servomotor (KRS-3304R2 from Kondo Corporation) is a DC type motor, controlled through UART communication, with the electric power being 6.0 V/2.0 A. Table 5.2 presents the detailed actuator specifications.

Because the actuator uses only one signal line for transmitting and receiving

Table 5.2: Specification of used servo motor.

Operating power	6.0 V 2.0 A
Maximum Torque	1.1 N.m
Maximum Speed	2.51 rad/sec
Size [mm]	32.5 × 26 × 26
Weight	33.7 g
Maximum operating angle	±135°

information, circuits to realize communication between the MCU to the servomotor were established. The signal conversion board converted the two signals into one signal for the servomotor and divided the signal into two signals for the MCU. The control processor used was an Arduino UNO based on a 5.0 V logic. Figure 5.13 shows the overall connection and communication status of the driving/control parts. Position control was implemented for control of the actuators.

5.2.5 Planned trajectory and determination of required orientation angle's range

To determine the input trajectory for the prototype, trajectory planning was implemented using the measured thumb trajectory. The planned trajectory was calculated using the center point of the breadth of the raw thumb trajectory. Figure 5.14 shows the method of the planned trajectory calculation. In the case of AA, its

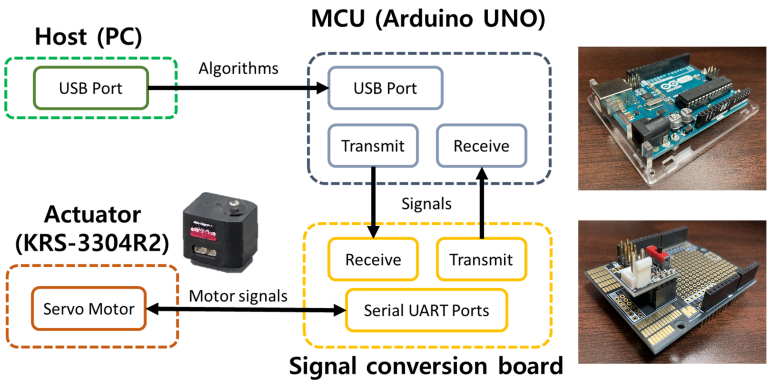

Figure 5.13: Diagram maps of the experimental system.

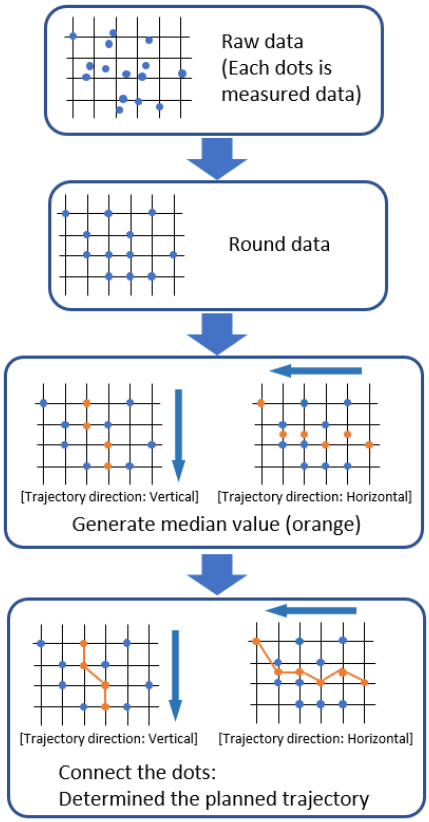

Figure 5.14: Calculation method of the planned trajectory.

form is similar to a long rectangle and the pattern of the trajectory moves along the y axis. Therefore, the planned trajectory is easily calculated from the average of the x axis value in regard to each y value. Because the form of the FE is curved, the calculation is separated into two parts. The upper part of the FE trajectory has a wide range along the x axis. The lower part has a small range along the x axis and its trajectory is formed along the y axis. For this reason, the calculation of the lower part trajectory is the same as the calculation done for AA. For the upper part, the calculation is done using the average of the y value. Figure 5.15 shows the raw measured data and calculation result of the trajectory planning. From this figure, the dots in the planned trajectory (referred to as steps) are input points for the inverse kinematics for the required position of P. In addition, the points passed on the planned trajectory were selected. Due to the FE trajectory being longer than

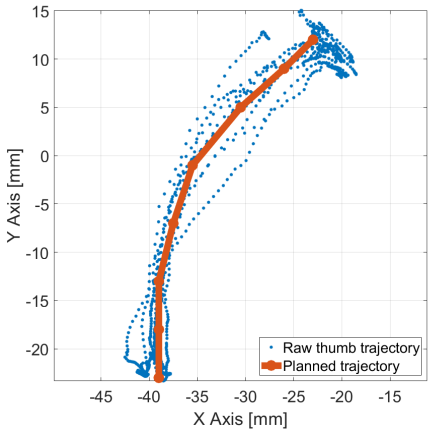

Figure 5.15: An example of the trajectory planning result of FE movement.

AA, eight and three dots for the FE and AA movement were selected, respectively. In controlling the prototype, the output link passing through dots one by one, and a time delay is given between the dots to control the trajectory speed. Using the selected dots, the required angles of the actuation joints A and B were derived through inverse kinematic analysis. It was confirmed that the planned trajectory was located within the target workspace.

In addition, the range of the orientation angle of the thumb was decided. Comparing the movements of AA and FE, AA has a larger range of thumb orientation angle compared to the FE movement. For this reason, the range of the orientation angle is determined from the range of the AA movement. In literature from [11, 12], the total range of the AA movement was reported as 40°. Considering the situation wherein the mechanism is attached to the hand as shown in Figure 5.16, the minimum orientation angle is set as zero. While the thumb can move more towards the palm, its movement is blocked by the base part. For this reason, the range of the orientation angle was set as 0° to 40° for the experiment. In the case of AA, the thumb is located in the palm of the hand and the orientation angle along the y axis (Ψ) is zero for the adduction movement. Furthermore, when the thumb moves far from the palm (abduction), Ψ increases. Therefore, the orientation angles for the three steps of AA movement were set as 0, 20, 40° from adduction to abduction

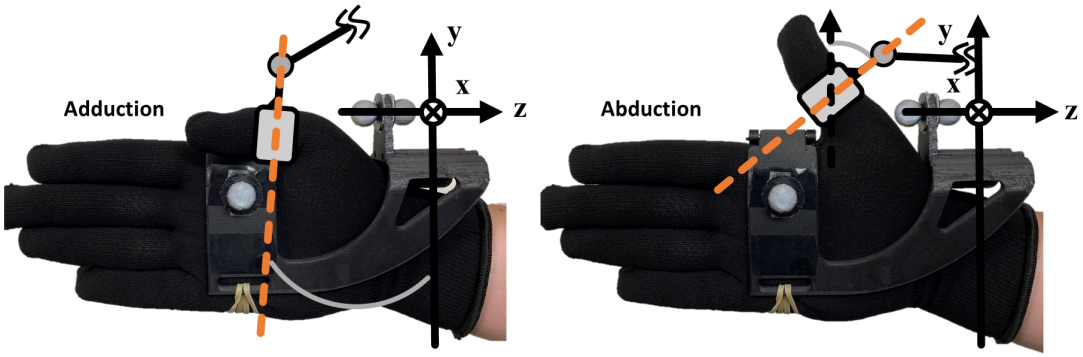

Figure 5.16: Range of the required orientation angle when thumb equipped the output link (Adduction-Abduction movement).

movement. Regarding the FE movement, a constant angle of 40° was given to all steps of the FE planned trajectory. This orientation angle was used to derive the required angle for the actuation at H through inverse kinematics.

5.3 Experiment with users

Because the proposed mechanism is to be applied for rehabilitation therapy, it was necessary to verify the presented movement while considering the effect on the human hand. In the experiment, each volunteer's planned trajectory and the range of the required orientation angle were used to control the prototype. When the output movement of the prototype is following through the input trajectory, we assume that the prototype has the feasibility of the thumb rehabilitation robot. For this reason, the control of the prototype for two movements were done and the position of the output link was measured. After measuring, the experimental data was compared with the input trajectory. Moreover, an experiment was conducted on publicly recruited volunteers to perform a performance evaluation and identify any unexpected problems by obtaining feedback through a questionnaire.

In the experiment, the two movements, namely, AA and FE, were considered. To control the prototype, the thumb trajectory, which was measured with the motion capture system in Fig. 5.1, was used. The thumb data were measured before the ex-

periment by using the prototype and these were also used in the determination of the target workspace of Fig. 5.3. Twelve people participated in this experiment and each volunteer was briefed prior to the experiment regarding the thumb measurement. Moreover, these data were considered as the target group and the measured thumb data were used for generating the planned path of the experiment. The planned path was an individual path for each user and the same path was not used for other users. Before the experiment, the user was asked to sit near the camera of the motion capture system, and the prototype was attached to his/her right hand. The movement was provided by the prototype to the user five times, for each movement. Figure 5.17 shows the experimental scenario. Because the results of the experiment were not expected to be influenced by factors such as the temperature and humidity of the room, these factors were not limited. To measure the trajectory of the prototype performance, motion markers were attached to the prototype during the experiment. Figure 5.18 shows the attached markers on the prototype. The measurement point is the middle point of four markers: 8, 9, 10, and 11. In the experiment, the following

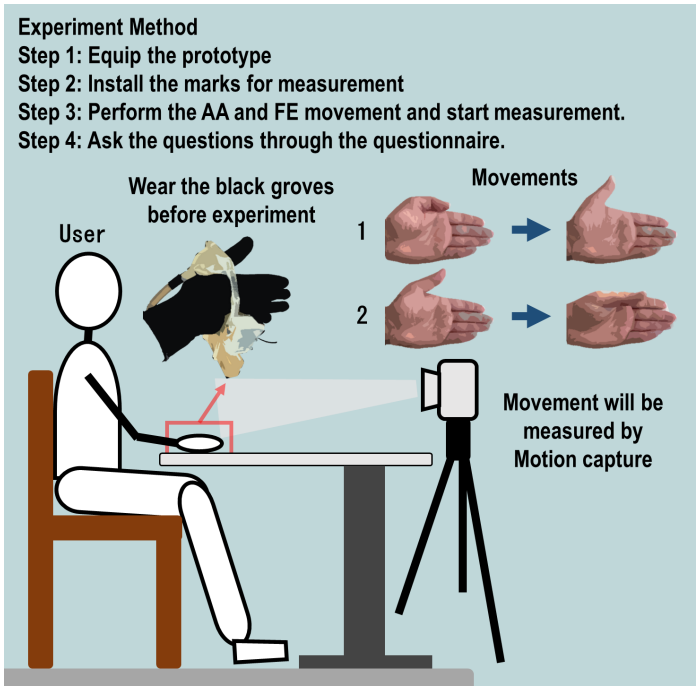

Figure 5.17: Concept of the experimental scenario.

Figure 5.18: Measurement markers on the prototype in the experiment.

safety clauses were implemented:

- The torque of the used actuator was less than that of the thumb.
- To prevent damage to the human body, mechanical and electrical safety measures were implemented, such as the installation of electrical circuits to prevent overload and electrical back-flow.
- Two emergency stop switches were used. The first emergency stop switch was provided to the users to stop operation during the experiment if they felt any pain or discomfort. The second switch was installed for the organizer of the experiment to stop the operation of the device.

The experiment scenario and safety clauses were approved by the research ethics committee of Tokyo Institute of Technology (Registration number: A19190).

Figure 5.19 shows the experiment results pertaining to the FE movement of four users which was controlled using the prototype. These experimental data were measured as three-dimensional data using the motion capture system. Because the reachable workspace was located in the xy plane, the figures are shown in the xy

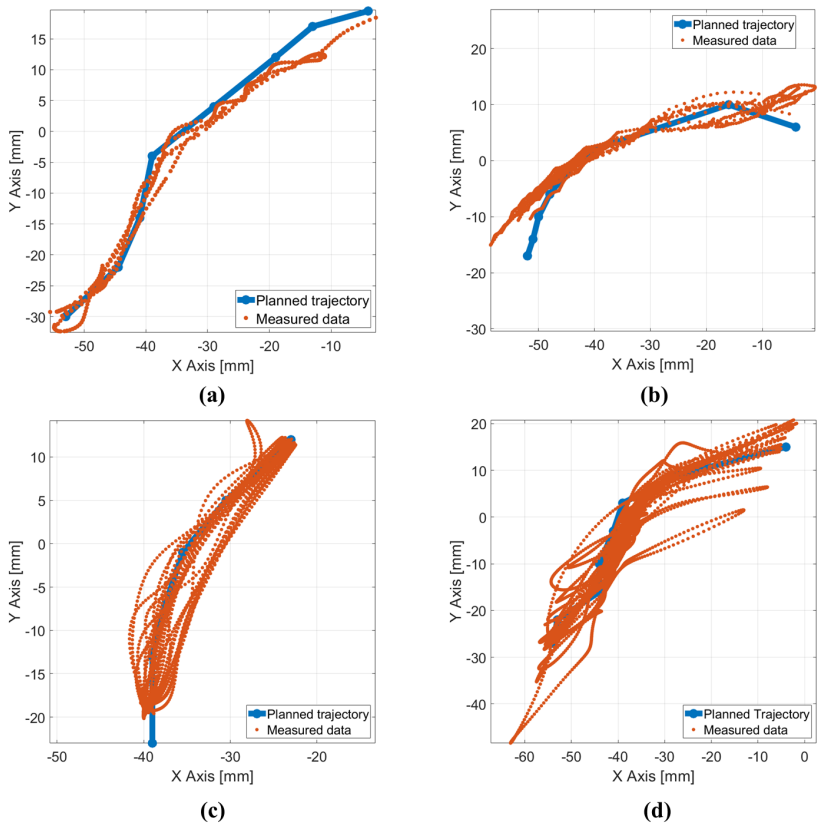

Figure 5.19: Comparison the planning trajectory and measurement data for each person in the FE movement.

plane. The blue dot and line represent the planned trajectory, which is generated from the thumb trajectory while the users did not have the prototype attached, and the orange dots correspond to the measurement data of the thumb trajectory provided by the prototype. In the figure, the orange dots indicate the difference from the planned trajectory (marked by the blue dots). From the result of figure 5.19, the position of the output link shows that the prototype generates a trajectory that is most similar to the planned trajectories. Thus, the prototype is capable of controlling the FE movement.

To confirm the FE movement in detail, the orientation angles around the z axis in the xy plane of thumb and output link were compared (this angle is not Ψ). Figure 5.20 (a) shows the explanation of the two angles, and Fig. 5.20 (b) shows the two angles: the blue line is the thumb orientation angle, and orange is the output

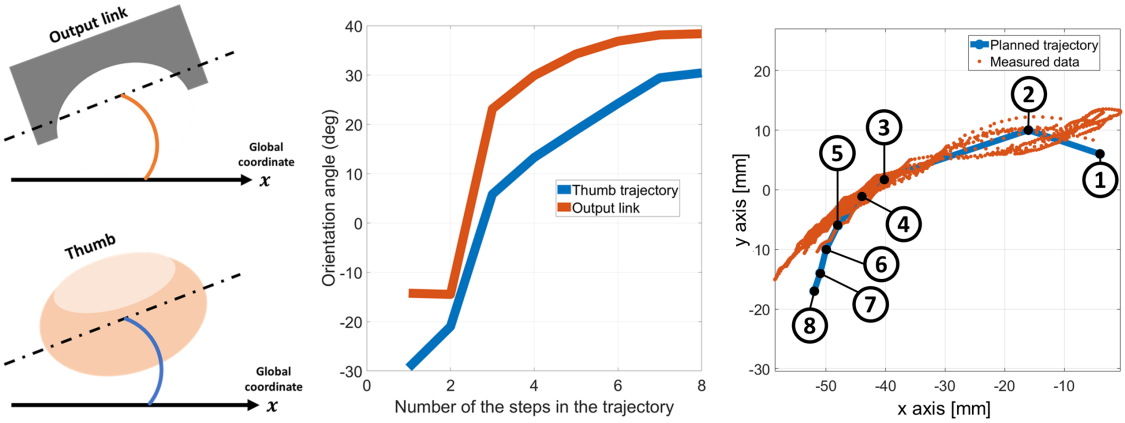

(a) Explanation of orientation angle

(b) Two orientation angles

(c) Steps in the planned trajectory

Figure 5.20: The orientation angles (around z axis in the xy plane) of the thumb measured data, and the output link of the experimental data and the explanation of the steps on the used planned trajectory: (a) explanation of orientation angle, (b) two orientation angles, (c) steps in the planned trajectory.

link orientation angle. Those two data were not simultaneously measured, but the patterns of the movements and the trajectories are largely the same. From the result of Fig. 5.20, we know that relative motion, which is the sliding motion between hand tissue and bone, between the two angles exists. Thus, the relative motions that occur between the output link and the base part were detected. Because of the relative motion effects, the tip of the trajectory of the experiment is not expected to match well with the planned trajectory in the practical experiment shown in Fig. 5.19. However, the thumb orientation angle's measured data has the possibility of being mixed in with data from other thumb movements because this data is performed by moving the volunteer's hand themselves. Therefore, the relative motion can be interpreted as proof that the possibility of providing the anatomically non-defined direction against the thumb movement when the proposed mechanism controls the thumb.

Figure 5.21 shows the results for the AA movement. The measured data are significantly smaller compared to the planned trajectory data. From this result, it is expected that the motion transmission from the actuator was not well done or

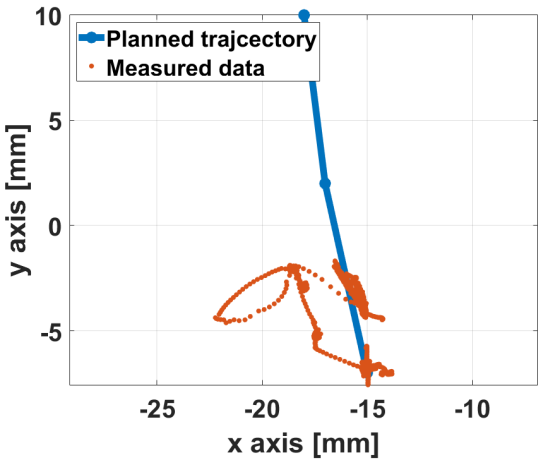

Figure 5.21: Comparison the planning trajectory and measurement data in the AA movement.

(a) P1 = (-15, -7, 0)
θ_A = 144.8 / θ_B = 70.15
θ_H = 11.8 / Ψ = 0

(b) P2 = (-17, 2, 0)
θ_A = 143.9 / θ_B = 69.48
θ_H = 16.82 / Ψ = 17.5

(c) P3 = (-18, 10, 0)
θ_A = 141.05 / θ_B = 70.28
θ_H = 21.15 / Ψ = 35

Figure 5.22: The simulation results of the planned trajectories of the above-mentioned experiment.

the actuator did not work well. This means that the prototype moved in a small range and its behaviour included vibratory motion. Figure 5.22 shows the simulation results for the planned trajectories of the above-mentioned example. The different sub-figures show the configuration of the mechanism when P is assigned with respect to the planned trajectory shown in Figure 5.21. It can be noted that the angle of actuation joint A (θ_A) does not change considerably from (a) to (c). In the (c) in the figure, link EF and link FD have formed close to the straight line. Therefore, the mechanism requires huge torques on the actuation joint because the range of the actuation joint is too small compared to the range of AA movement trajectory.

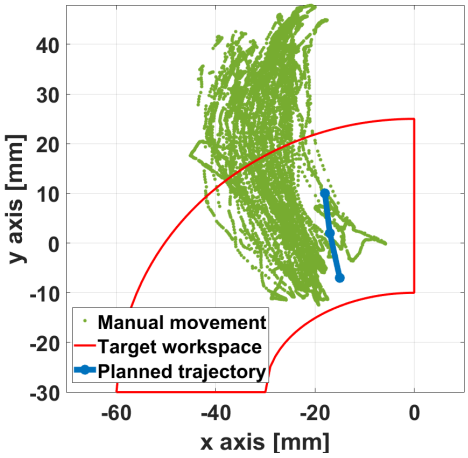

Figure 5.23: The measurement data of the AA movement in the case of the attached prototype moving by hand.

This is means that the output link of the mechanism is close to the singularity.

To confirm the ideal AA movement of the proposed mechanism, a manual movement, which provides assistance to the actuators by hand without electric power, was carried out. This was a simple test done to confirm the prototype performance when the actuators have enough torque. When AA movement was performed, the result, the target workspace, and the planned trajectory are shown in Fig. 5.23. The green dots indicate the output link position of the measured data wherein the prototype was moved by assisting the actuator by hand. Because this data was obtained while moving the actuator by hand, it does not perfectly follow the planned trajectory. From this result, it can be seen that the measured data of the manual movement has a larger trajectory, and it protrudes from the range of the target workspace. Therefore, if the actuator is capable of enough torque output, the prototype is expected to be capable of controlling AA movement.

Regarding the questionnaire, various questions such as age, feeling during the experiment, the intensity of the resistance, and the prototype's weight are asked. The six volunteers answered their experience of the experiment through the questionnaire. The age of volunteers was from late-20s to early-30s. From the questionnaire results, three volunteers answered that they feel the resistance force, and they felt it from the around of the IP joint of the thumb. From this result, the existence of

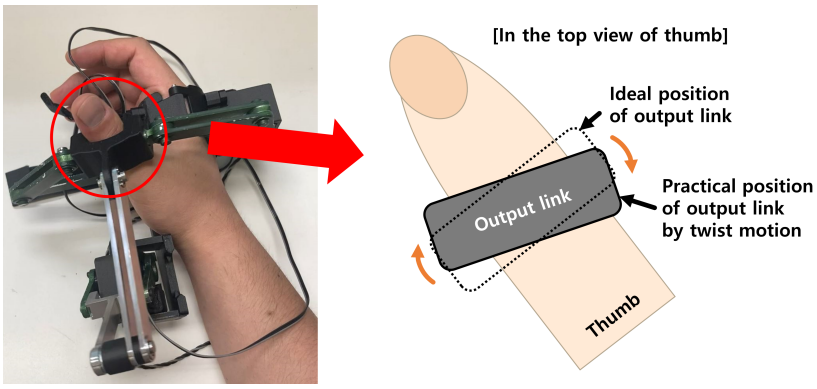

Figure 5.24: The explanation of the twist situation.

the friction between the output link and thumb was confirmed. This means that the sliding movement of the output link along the thumb finger has not worked as well as the concept idea of the proposed mechanism's design. Furthermore, a twist between output link and thumb was mentioned. In the top view of the thumb, the twist is the rotation motion of the output link around the IP joint of the thumb, and the extent of the twist is different depending on the hand size because the prototype was designed as one size. Figure 5.24 shows the explanation of the twist situation in the prototype for easy understanding. Because of this related to user's safety, the improving design to reduce this problem is required. With regards to resistance force, two participants answered that they felt a light resistance force in the AA movement, and another person was answered that a strong resistance force could be felt in both movements. Regarding the feel of the prototype, three volunteers felt the weight as moderate, and two volunteers answered that it felt a little lightweight. Only one volunteer had felt that the prototype was very light.

To sum up the results of the relative motion and the questionnaire, the mechanism has the possibility to provide the thumb with an anatomically non-defined motion (unexpected motion). This means that the sliding movement of the output link along the thumb finger has not worked as well as the concept idea of the proposed mechanism's design. The effect of the unexpected motion depends on the hand size and finger length. Since this motion is related to the safety and the accuracy of the providing motion, an improvement to solve this motion is required.

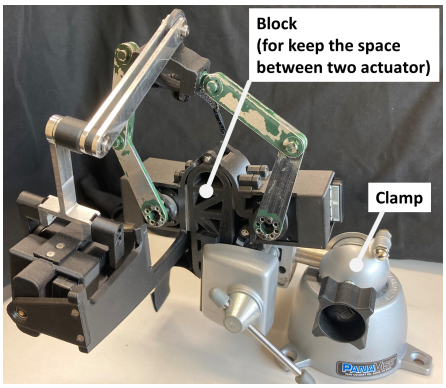

Figure 5.25: The environment of the additional experiment with higher torque actuator

In addition, the prototype's movement test using a higher torque actuator was carried out as an additional experiment as shown in Figure 5.25. The new actuator is B3M-SC-1170-A (Maximum torque: 7.6 N·m, speed: 4.82 rad/sec). Because its size is different from the previous actuator, the motor housing part was redesigned. When adapting the mechanism to this motor, motor placement was not changed. For safety, this additional experiment is carried out without thumb attachment to avoid an accident, such as an injury to the thumb. To keep the base and the position of the actuator, a block was installed in the base. For the input movement, the planned trajectories of the FE and AA from one of the measured data was used, which is

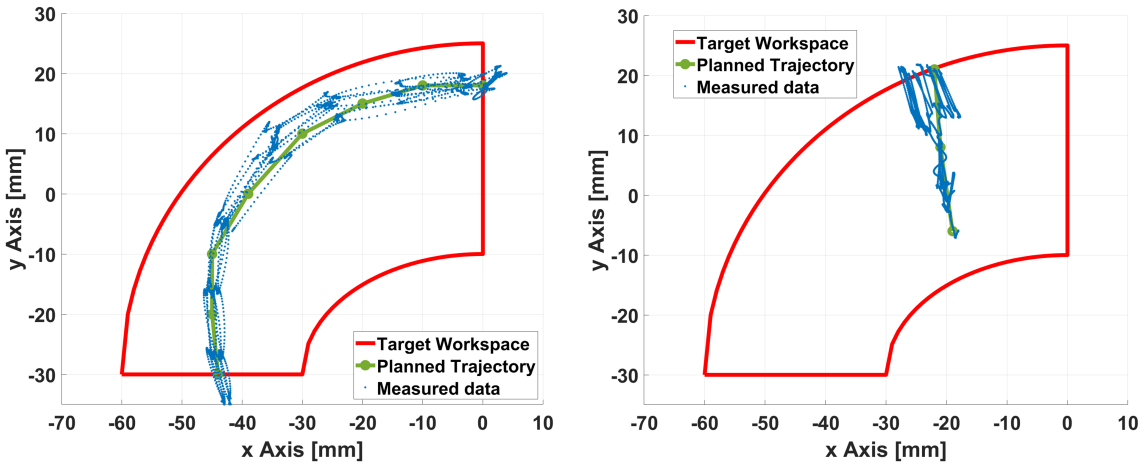

Figure 5.26: The results of the additional experiment when the planned trajectories of the FE and AA are given. (a) FE movement (b) AA movement.

taken from the thumb movement. Figure 5.26 shows the results of the experiment. In this figure, the blue dot is the position data of the output link, and the green line and dot is the planned trajectory. From this result, the measured data matched to the planned trajectory in both target movements. However, high torque must be used carefully due to safety risks.

For future work, additional analysis of the required torque while considering the weight of the prototype for thumb rehabilitation applications will be carried out.

5.4 Discussion and conclusion

In this chapter, the prototyping, and user test of the proposed mechanism were described to be adapted for application in thumb rehabilitation therapy. Two design candidates, which had different actuator placements, were considered in order to avoid collisions between the mechanism and hand. The sizes of the three workspaces (target workspace, the workspace of candidate 1, and the workspace of candidate 2) were compared while keeping the two candidates' design variables the same. Based on these, a prototype was manufactured. To prove the suitability and performance of the mechanism for application in thumb rehabilitation, user tests were carried out. User testing was performed using the prototype on volunteers. The input data were determined from the results of the trajectory planning method. Two target movements were provided: FE and AA. The results of this chapter are summarized as follows:

- Candidate 2 was found to have a wider workspace than candidate 1 while being able to cover the target workspace. For this reason, candidate 2 was selected as a suitable design.
- The results for the FE movement were largely satisfactory following the planned trajectory. Because the tip of trajectories did not match with the input trajectory well, the relative motion between the thumb and output link was compared. The results showed that a relative motion exists in both ends of the

trajectory and it causes a small effect on the control accuracy of the prototype.

- The results of the AA movement cases were not satisfactory. To investigate these, a manual moving test of the prototype using the AA movement was done by assisting the actuators by hand. Through this test, it was shown that the range of the output trajectory was longer than the planned one, and it could cover the target workspace. Thus, the prototype has the potential to perform the AA movement. To confirm the performance of the prototype within the higher torque over 1.1 N·m, an additional experiment using the higher torque (7.6 N·m) than the previous actuator in the prototype was carried out. The result of the experiment shows that the two movements are fully matched between the planned trajectory and the measured trajectory. Through this, it can be concluded that the prototype needs higher torque. For the next step, the actuation selection will be carefully considered.

- From the result of the relative motion check and the result of the questionnaire, a relative motion was detected and the resistance force was confirmed during the experiment. This means that there is a limitation to cover thumb mobility through the proposed mobility of the mechanism. The magnitude of the resistance force was dependant on the size of the hand and the length of the thumb. To reduce this issue, an improvement of the proposed mechanism is required.

To sum up the findings, the prototype has the possibility to be adapted for thumb rehabilitation, though the prototype used in this experiment has some limitations. To improve the proposed mechanism for thumb rehabilitation, actuation selection will be necessary by performing a static analysis on the prototype. Future work on the mechanism design while considering the design factors calculated from the static analysis will be required.

Chapter 6

Conclusion and discussion

6.1 Conclusion and discussion

In this thesis, a parallel mechanism has been proposed to be adapted for thumb rehabilitation therapy. Furthermore, the basic kinematics to determine the proposed mechanism's characteristics, the prototyping with the geometric design to adapt to thumb rehabilitation therapy, and the user test were described.

The necessity of the thumb rehabilitation robot can be seen from various issues such as the lack of therapists and the importance of thumb to hand dexterity. To design the wearable thumb rehabilitation robot, the complexity of the thumb CMC joint should be considered. In the previous research, various mechanisms have been reported, and their types of mechanism are classified into two types: the exoskeleton and the end-effector type. The misalignment issue occurs when there is a mismatch between the axes of the human joint and the kinematic joint, and it occurs in the exoskeleton type. On the other hand, for the end-effector type, it is not necessary to consider misalignment in its design due to its inherent structural advantage. In the CMC joint part of the previous researches, their mechanism designs are classified into three cases by their design to control two DOFs of the CMC joint. However, these did not consider the additional sliding motion when designing the mechanism.

Based on this background, the proposed mechanism called a (2–RRU)–URR par-

allel mechanism was a hybrid type, which combines the advantages of the exoskeleton and the end-effector type mechanisms. Combining the two mechanism types, the structural characteristics allow the thumb CMC joint's complexity to not to be considered in the mechanism design. Thus, the consideration of the misalignment issue is not necessary to design the proposed mechanism using the end-effector to control the thumb joint. As the structural characteristic, the proposed mechanism is an over-constrained mechanism, with three DOF: two rotational DOF and one translational DOF, and it consists of three chains, the output link, and the base. Structurally, the first and second chains are connected with the output link through a universal joint. The third chain is connected with the output link through a revolute joint.

To understand the characteristics of the proposed mechanism, the kinematics such as mobility, displacement, workspace analysis, and statics for calculating the actuation torque against the external load on the output link were analyzed. Moreover, the prototype of the proposed mechanism was manufactured by considering the kinesiological/anatomical information. The details of the research's contributions are summarized as follows:

1. Mechanism design

- The mechanism was designed in which the base attached in the palm and the multiple chains connected between base to the output link. This mechanism is classified as the hybrid type between the exoskeleton type and the end-effector type to avoid the consideration of the complex structure of the thumb CMC joint.

- The mobilities of the proposed mechanism are three: two translational and one rotational DOF. The proposed mechanism presents the target movements by combining three mobilities.

2. Mobility, Kinematic analysis, and Static analysis

- Through the results of the mobility analysis through Gruebler's mobility formula and screw theory, it is clarified that the proposed mechanism has three DOF, and it is an overconstrained mechanism.
- An original method for the proposed mechanism to simplify the displacement analysis was proposed. This method was considered by dividing it into two parts. Each part was separately calculated and the whole displacement of the mechanism was calculated by combining the two results.
- Since the proposed mechanism is overconstrained, the overall Jacobian matrix adapted to the virtual parameters (the virtual constraint force that is not related to the real constraint force) is used for deriving the geometrical relationship between the required force and the actuator torque.
- Through the result of the verification experiment, the method of the static analysis was verified.

3. Evaluation of kinematic characteristic and workspace analysis

- With regards to the design index, the effective workspace was derived from the result of the static analysis. It is used to avoid a calculation resulting in unnaturally high torque, which affects the weight of the actuator and safety, and to determine the performance of the mechanism by its actuation torque.
- The OG's sensitivity is described as the relationship between the input angle and the output angle of OG. This parameter is relative to the change of the orientation. Since the rapid change of the orientation provides loads on the joints, it is related to the singularity situation and user safety.

4. Geometric design for prototype and User test

- Two design candidates with different actuator placements, were considered in order to avoid collisions between the mechanism and hand. Through comparing the workspace of two candidates, the suitable design was selected as a suitable design.

- To prove the suitability and performance of the mechanism for application in thumb rehabilitation, user tests were carried out with the prototype. In the experiment, the results for the FE movement were largely satisfactory following the planned trajectory. On the other hand, the AA movement cases were not satisfactory. The additional experiment of the prototype with the higher torque is carried out. As the result, two movements are matched between the planned trajectory and the measured trajectory. Through this, it was determined that the prototype needs higher torque.

- Limitation of the proposed mechanism in providing the thumb movements was found through the results of the relative motion check and the result of the questionnaire.

- Prototype has the possibility to be adapted for thumb rehabilitation, though the prototype used in this paper has some limitations.

To sum up, the (2–RRU)–URR parallel mechanism is proposed for thumb rehabilitation and it is designed to avoid the consideration of the complexity of the CMC joint. From the result of the basic kinematics, the characteristics of the proposed mechanism were determined. Furthermore, the geometric design considering the anatomical/kinesiology information was carried out and user test with the prototype was carried out. From these results, the possibility to be adapted for thumb rehabilitation was confirmed even the limitations exist.

6.2 Future works

In this study, due to limitations, it was not possible to design the ideal of the proposed mechanism which could cover the whole thumb mobility. Moreover, further improvements are required to achieve such results in the future. The details of the further improvements are listed as follows:

- In the static analysis of this research, the constraint force was ignored. However, the effect of the constraint force on the hand should be considered because the base part is attached to the palm and the surface of the hand. The measurement of force through force sensors in the attachment point between base part and the hand is required.

- When the mechanism controls the AA movement, the required actuation torque is too high for a small range of the actuation joint. This means that the proposed mechanism reaches the near-space of the singularity when it performs the AA movement. To avoid the situation close to the singularity, actuation selection and design improvement are required.

- In this study, the planned trajectories (input trajectory to give the prototype) are independently given for each volunteer. However, the nominal trajectory is should be adapted to various hand sizes for the application of thumb rehabilitation. For this reason, the calculation method for the derivation of the nominal trajectory is required. Furthermore, determining the nominal size of the prototype to adapt to various hand sizes is also required. Optimization design will be carried out to design the nominal size of the proposed mechanism.

- The unexpected motion of the proposed mechanism gives the user a feeling of resistance and this is related to the issue of safety and accuracy of the performance. To avoid the unexpected motion between the output link and the hand, additional mobilities are planned to be included in the output link as a redundant system.

- From the perspective of the mechanism, this mechanism has a movement in unique from other parallel mechanisms. As the design of the output link is perpendicularly connected with the third chain, the orientation of the output link is always located perpendicularly against the line of GP. This means that the one side of the output link is always directed towards the outside. Furthermore, the output links can rotate along the x' axis of the partial coordinate. Through these structural characteristics, the proposed mechanism can be applied to other applications such as a visual inspection system, 3D scanning system, among various others.

Bibliography

[1] R. Galvin, B. Murphy, T. Cusack, and E. Stokes, "The impact of increased duration of exercise therapy on functional recovery following stroke—what is the evidence?" *Topics in Stroke Rehabilitation*, vol. 15, no. 4, pp. 365–377, 2008.

[2] J. Lee and B.-R. Kim, "Role of intensity and repetition in rehabilitation therapy," *Brain & Neurorehabilitation*, vol. 5, no. 1, pp. 6–11, 2012.

[3] G. Kwakkel, R. van Peppen, R. C. Wagenaar, S. Wood Dauphinee, C. Richards, A. Ashburn, K. Miller, N. Lincoln, C. Partridge, I. Wellwood *et al.*, "Effects of augmented exercise therapy time after stroke: a meta-analysis," *stroke*, vol. 35, no. 11, pp. 2529–2539, 2004.

[4] Who, *World health statistics 2008*. World Health Organization, 2008.

[5] J. Bernhardt, H. Dewey, A. Thrift, and G. Donnan, "Inactive and alone: physical activity within the first 14 days of acute stroke unit care," *Stroke*, vol. 35, no. 4, pp. 1005–1009, 2004.

[6] E. Taub, N. E. Miller, T. A. Novack, E. W. Cook, W. C. Fleming, C. S. Nepomuceno, J. S. Connell, J. Crago *et al.*, "Technique to improve chronic motor deficit after stroke," *Archives of physical medicine and rehabilitation*, vol. 74, no. 4, pp. 347–354, 1993.

[7] D. A. Neumann, *Kinesiology of the musculoskeletal system: foundations for rehabilitation*. Elsevier Health Sciences, 2013.

[8] P. Soucacos, "Indications and selection for digital amputation and replantation," *Journal of hand surgery*, vol. 26, no. 6, pp. 572–581, 2001.

[9] W.-h. Choi and Y. Takeda, "Geometric design and prototyping of a (2-rru)-urr parallel mechanism for thumb rehabilitation therapy," *Machines*, vol. 9, no. 3, p. 50, 2021.

[10] V. Spartacus, "Trapeziometacarpal joint: A mechanical explanation of total prosthesis failures," in *Biomechanics*. IntechOpen, 2018.

[11] M. Batmanabane and S. Malathi, "Movements at the carpometacarpal and metacarpophalangeal joints of the hand and their effect on the dimensions of the articular ends of the metacarpal bones," *The Anatomical Record*, vol. 213, no. 1, pp. 102–110, 1985.

[12] W. P. Cooney, M. J. Lucca, E. Chao, and R. Linscheid, "The kinesiology of the thumb trapeziometacarpal joint," *J Bone Joint Surg Am*, vol. 63, no. 9, pp. 1371–1381, 1981.

[13] H. Tanabe, M. Ikuta, T. Mikawa, A. Kondo, and Y. Morita, "Application of a robotic rehabilitation training system for recovery of severe plegie hand motor function after a stroke," in *Medical Robotics-New Achievements*. IntechOpen, 2018.

[14] A. M. Smith, "The coactivation of antagonist muscles," *Canadian journal of physiology and pharmacology*, vol. 59, no. 7, pp. 733–747, 1981.

[15] S. Brunnström, "Movement therapy in hemiplegia: A neurophysiological approach/1st edn hagerstown," *MD-Harper & Row*, 1970.

[16] S. Brunnstrom, "Motor testing procedures in hemiplegia: based on sequential recovery stages," *Physical therapy*, vol. 46, no. 4, pp. 357–375, 1966.

[17] S. B. O'Sullivan, T. J. Schmitz, and G. Fulk, *Physical rehabilitation*. FA Davis, 2019.

[18] D. T. Wade, V. A. Wood, and R. L. Hewer, "Recovery after stroke–the first 3 months." *Journal of Neurology, Neurosurgery & Psychiatry*, vol. 48, no. 1, pp. 7–13, 1985.

[19] J.-D. Lee, Y.-T. Cheng, L.-C. Liu, and C.-Y. Wu, "A study of evaluation parameters for stroke patients' brunnstrom recovery stages," in *TENCON 2007-2007 IEEE Region 10 Conference*. IEEE, 2007, pp. 1–4.

[20] S. Naghdi, N. N. Ansari, K. Mansouri, and S. Hasson, "A neurophysiological and clinical study of brunnstrom recovery stages in the upper limb following stroke," *Brain injury*, vol. 24, no. 11, pp. 1372–1378, 2010.

[21] I. Safaz, B. Ylmaz, E. Yasar, and R. Alaca, "Brunnstrom recovery stage and motricity index for the evaluation of upper extremity in stroke: analysis for correlation and responsiveness," *International Journal of Rehabilitation Research*, vol. 32, no. 3, pp. 228–231, 2009.

[22] S. Shah, S. Harasymiw, and P. Stahl, "Stroke rehabilitation: outcome based on brunnstrom recovery stages," *The Occupational Therapy Journal of Research*, vol. 6, no. 6, pp. 365–376, 1986.

[23] L. Yu, J.-p. Wang, Q. Fang, and Y. Wang, "Brunnstrom stage automatic evaluation for stroke patients using extreme learning machine," in *2012 IEEE Biomedical Circuits and Systems Conference (BioCAS)*. IEEE, 2012, pp. 380–383.

[24] T. Ro, T. Ota, T. Saito, and O. Oikawa, "Spasticity and range of motion over time in stroke patients who received multiple-dose botulinum toxin therapy," *Journal of Stroke and Cerebrovascular Diseases*, vol. 29, no. 1, p. 104481, 2020.

[25] R. C. Loureiro, W. S. Harwin, K. Nagai, and M. Johnson, "Advances in upper limb stroke rehabilitation: a technology push," *Medical & biological engineering & computing*, vol. 49, no. 10, p. 1103, 2011.

[26] Z. Yue, X. Zhang, and J. Wang, "Hand rehabilitation robotics on poststroke motor recovery." *Behavioural neurology*, 2017.

[27] B. Sheng, Y. Zhang, W. Meng, C. Deng, and S. Xie, "Bilateral robots for upper-limb stroke rehabilitation: State of the art and future prospects," *Medical engineering & physics*, vol. 38, no. 7, pp. 587–606, 2016.

[28] T. Endo, S. Tanimura, and H. Kawasaki, "Development of tool-type devices for a multifingered haptic interface robot," *IEEE Transactions on Robotics*, vol. 29, no. 1, pp. 68–81, 2012.

[29] O. Lambercy, L. Dovat, R. Gassert, E. Burdet, C. L. Teo, and T. Milner, "A haptic knob for rehabilitation of hand function," *IEEE Transactions on Neural Systems and Rehabilitation Engineering*, vol. 15, no. 3, pp. 356–366, 2007.

[30] C. D. Takahashi, L. Der-Yeghiaian, V. Le, and S. C. Cramer, "A robotic device for hand motor therapy after stroke," in *9th International Conference on Rehabilitation Robotics, 2005. ICORR 2005.* IEEE, 2005, pp. 17–20.

[31] L. Dovat, O. Lambercy, R. Gassert, T. Maeder, T. Milner, T. C. Leong, and E. Burdet, "Handcare: a cable-actuated rehabilitation system to train hand function after stroke," *IEEE Transactions on Neural Systems and Rehabilitation Engineering*, vol. 16, no. 6, pp. 582–591, 2008.

[32] S. Ueki, H. Kawasaki, S. Ito, Y. Nishimoto, M. Abe, T. Aoki, Y. Ishigure, T. Ojika, and T. Mouri, "Development of a hand-assist robot with multi-degrees-of-freedom for rehabilitation therapy," *IEEE/ASME Transactions on mechatronics*, vol. 17, no. 1, pp. 136–146, 2010.

[33] A. Wege and G. Hommel, "Development and control of a hand exoskeleton for rehabilitation of hand injuries," in *2005 IEEE/RSJ International Conference on Intelligent Robots and Systems.* IEEE, 2005, pp. 3046–3051.

[34] J. Wang, J. Li, Y. Zhang, and S. Wang, "Design of an exoskeleton for index finger rehabilitation," in *2009 Annual International Conference of the IEEE Engineering in Medicine and Biology Society.* IEEE, 2009, pp. 5957–5960.

[35] B. L. Shields, J. A. Main, S. W. Peterson, and A. M. Strauss, "An anthropomorphic hand exoskeleton to prevent astronaut hand fatigue during extravehicular activities," *IEEE transactions on systems, man, and cybernetics-part A: systems and humans*, vol. 27, no. 5, pp. 668–673, 1997.

[36] M. Fontana, A. Dettori, F. Salsedo, and M. Bergamasco, "Mechanical design of a novel hand exoskeleton for accurate force displaying," in *2009 IEEE International Conference on Robotics and Automation*. IEEE, 2009, pp. 1704–1709.

[37] S. Nakagawara, H. Kajimoto, N. Kawakami, S. Tachi, and I. Kawabuchi, "An encounter-type multi-fingered master hand using circuitous joints," in *Proceedings of the 2005 IEEE International Conference on Robotics and Automation*. IEEE, 2005, pp. 2667–2672.

[38] J. Iqbal, O. Ahmad, and A. Malik, "Hexosys ii-towards realization of light mass robotics for the hand," in *2011 IEEE 14th International Multitopic Conference*. IEEE, 2011, pp. 115–119.

[39] P. Stergiopoulos, P. Fuchs, and C. Laurgeau, "Design of a 2-finger hand exoskeleton for vr grasping simulation," *Eurohaptics, Dublin, Ireland*, pp. 80–93, 2003.

[40] N. Garcia-Hernandez, I. Sarakoglou, N. Tsagarakis, and D. Caldwell, "Underactuated hand exoskeleton with novel kinematics for potential use in rehabilitation," *EuroHaptics, Versailles, France*, pp. 24–27, 2014.

[41] S. Balasubramanian, J. Klein, and E. Burdet, "Robot-assisted rehabilitation of hand function," *Current opinion in neurology*, vol. 23, no. 6, pp. 661–670, 2010.

[42] Y. Yihun, R. Miklos, A. Perez-Gracia, D. J. Reinkensmeyer, K. Denney, and E. T. Wolbrecht, "Single degree-of-freedom exoskeleton mechanism design for thumb rehabilitation," in *2012 Annual International Conference of the IEEE Engineering in Medicine and Biology Society*. IEEE, 2012, pp. 1916–1920.

[43] P. Agarwal, "A hand exoskeleton with series elastic actuation for rehabilitation: design, control and experimentation," Ph.D. dissertation, The University of Texas at Austin, 2017.

[44] P. M. Aubin, H. Sallum, C. Walsh, L. Stirling, and A. Correia, "A pediatric robotic thumb exoskeleton for at-home rehabilitation: the isolated orthosis for thumb actuation (iota)," in *2013 IEEE 13th International Conference on Rehabilitation Robotics (ICORR)*. IEEE, 2013, pp. 1–6.

[45] D. Leonardis, M. Barsotti, C. Loconsole, M. Solazzi, M. Troncossi, C. Mazzotti, V. P. Castelli, C. Procopio, G. Lamola, C. Chisari *et al.*, "An emg-controlled robotic hand exoskeleton for bilateral rehabilitation," *IEEE transactions on haptics*, vol. 8, no. 2, pp. 140–151, 2015.

[46] Y. Hasegawa, Y. Mikami, K. Watanabe, and Y. Sankai, "Five-fingered assistive hand with mechanical compliance of human finger," in *2008 IEEE international conference on robotics and automation*. IEEE, 2008, pp. 718–724.

[47] M. Bouzit, G. Burdea, G. Popescu, and R. Boian, "The rutgers master ii-new design force-feedback glove," *IEEE/ASME Transactions on mechatronics*, vol. 7, no. 2, pp. 256–263, 2002.

[48] O. Lambercy, D. Schröder, S. Zwicker, and R. Gassert, "Design of a thumb exoskeleton for hand rehabilitation," in *proceedings of the 7th International Convention on Rehabilitation Engineering and Assistive Technology*. Singapore Therapeutic, Assistive & Rehabilitative Technologies (START) Centre, 2013, p. 41.

[49] F. Wang, M. Shastri, C. L. Jones, V. Gupta, C. Osswald, X. Kang, D. G. Kamper, and N. Sarkar, "Design and control of an actuated thumb exoskeleton for hand rehabilitation following stroke," in *2011 IEEE International Conference on Robotics and Automation*. IEEE, 2011, pp. 3688–3693.

[50] P. Agarwal, Y. Yun, J. Fox, K. Madden, and A. D. Deshpande, "Design, control, and testing of a thumb exoskeleton with series elastic actuation," *The International Journal of Robotics Research*, vol. 36, no. 3, pp. 355–375, 2017.

[51] K. R. Flowers and P. LaStayo, "Effect of total end range time on improving passive range of motion," *Journal of Hand Therapy*, vol. 7, no. 3, pp. 150–157, 1994.

[52] K. Haruhisa, K. Hiroki, I. Satoshi, N. Yutaka, H. Hiroyuki, and S. Hirohumi, "Hand rehabilitation support system," *Transactions of the Japan society of mechanical engineers. C.*, vol. 72, no. 720, pp. 2568–2573, 2006.

[53] L. Masia, H. I. Krebs, P. Cappa, and N. Hogan, "Design and characterization of hand module for whole-arm rehabilitation following stroke," *IEEE/ASME Transactions on Mechatronics*, vol. 12, no. 4, pp. 399–407, 2007.

[54] D. A. Neumann and T. Bielefeld, "The carpometacarpal joint of the thumb: stability, deformity, and therapeutic intervention," *Journal of Orthopaedic & Sports Physical Therapy*, vol. 33, no. 7, pp. 386–399, 2003.

[55] W. P. Smutz, A. Kongsayreepong, R. E. Hughes, G. Niebur, W. P. Cooney, and K.-N. An, "Mechanical advantage of the thumb muscles," *Journal of biomechanics*, vol. 31, no. 6, pp. 565–570, 1998.

[56] W.-h. Choi and Y. Takeda, "Kinematic analysis of (2-rru)-urr parallel mechanism performing 2r1t output motion," in *IFToMM International Symposium on Robotics and Mechatronics*. Springer, 2019, pp. 114–124.

[57] D. Stewart, "A platform with six degrees of freedom," *Proceedings of the institution of mechanical engineers*, vol. 180, no. 1, pp. 371–386, 1965.

[58] R. Clavel, "A fast robot with parallel geometry," in *Proc. Int. Symposium on Industrial Robots*, 1988, pp. 91–100.

[59] C. M. Gosselin and J.-F. Hamel, "The agile eye: a high-performance three-degree-of-freedom camera-orienting device," in *Proceedings of the 1994 IEEE international conference on robotics and automation*. IEEE, 1994, pp. 781–786.

[60] X.-J. Liu, X. Tang, and J. Wang, "Hana: a novel spatial parallel manipulator with one rotational and two translational degrees of freedom," *Robotica*, vol. 23, no. 2, pp. 257–270, 2005.

[61] J. Wang and X.-J. Liu, "Analysis of a novel cylindrical 3-dof parallel robot," *Robotics and Autonomous Systems*, vol. 42, no. 1, pp. 31–46, 2003.

[62] S. A. Joshi and L.-W. Tsai, "Jacobian analysis of limited-dof parallel manipulators," *J. Mech. Des.*, vol. 124, no. 2, pp. 254–258, 2002.

[63] Y. Takeda, H. Funabashi, and Y. Sasaki, "Development of a spherical in-parallel actuated mechanism with three degrees of freedom with large working space and high motion transmissibility: evaluation of motion transmissibility and analysis of working space," *JSME international journal. Ser. C, Dynamics, control, robotics, design and manufacturing*, vol. 39, no. 3, pp. 541–548, 1996.

[64] B. Hu, "Kinematically identical manipulators for the exechon parallel manipulator and their comparison study," *Mechanism and Machine Theory*, vol. 103, pp. 117–137, 2016.

[65] W.-h. Choi and Y. Takeda, "Displacement analysis and design of a (2–rru)–urr parallel mechanism performing 2r1t output motion for thumb rehabilitation," *Robotics*, vol. 9, no. 3, p. 67, 2020.

[66] "Size Korea 5th human measurement data," http://sizekorea.kr/, accessed: 2020-06-01.

Appendix

A.1 Hand Measurement Data

This Hand Measurement Data is reported from "Size Korea" as the fifth korean body measurement campaign [66]. This data were referred for design the prototype. The each measurement data is explained as follows:

- A: Palm width
- B: Thumb length
- C: Thickness of hand
- D: Circumference of Thumb
- E: Range of thumb angle from palm

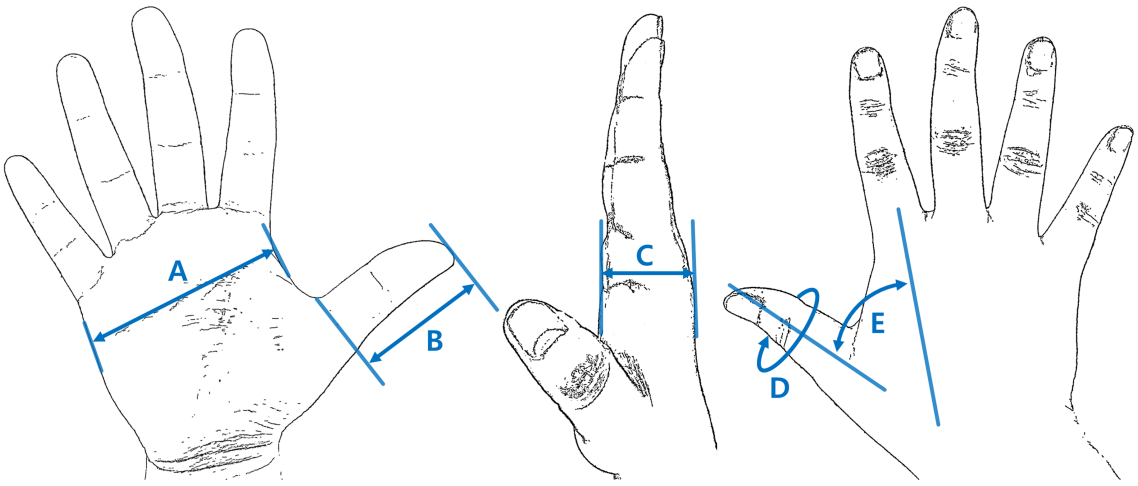

Measurement Period		April 2003 to November 2004	
Targets		505 People 50-59 years old	
A: Palm width [mm]			
Average	Standard Deviation	Minimum	Maximum
82.84	5.22	72.67	95.75
B: Thumb length [mm]			
Average	Standard Deviation	Minimum	Maximum
59.54	4.17	50.64	68.64
C: Thickness of hand [mm]			
Average	Standard Deviation	Minimum	Maximum
26.84	2.52	21	32.09
D: Circumference of Thumb [mm]			
Average	Standard Deviation	Minimum	Maximum
65.98	5.89	54	80
E: Range of thumb angle from palm [deg]			
Average	Standard Deviation	Minimum	Maximum
62.75	10.94	25	80

A.2 Control codes of prototype

A.2.1 KRS-3304 ICS

```
1  const int EnPin = 2;  //Define as Global
2  //Command definition
3  const byte ICS_POS_CMD = 0x80;
4  const byte ICS_PARA_WRITE_COMMND = 0xC0;
5  const byte ICS_PARA_READ_COMMND = 0xA0;
6  const byte SUB_ST_COMMND = 0x01;
7  const byte SUB_SP_COMMND = 0x02;
8  int pos0;
9  int pos1;
10 int pos2;
11
12 void Synchronize_slave(byte *txBuff, size_t txLength)
13 {
14   //If not defined, raise an error
15   if (Serial == false)return false;
16
17   Serial.flush();
18
19   digitalWrite(EnPin, HIGH);
20
21   Serial.write(txBuff, txLength);
22
23   Serial.flush();   //Wait for the transmission to finish
24
25   digitalWrite(EnPin, LOW);
26 }
27
28 int ics_set_pos_slave(unsigned short pos0, unsigned short pos1,
     unsigned short pos2)
29 {
30   byte tx_data[12];
```

```
31    // Create send command
32    tx_data[0] = 0x00;
33    tx_data[1] = ICS_POS_CMD;
34    tx_data[2] = (byte)((pos0 & 0x3F80) >> 7);
35    tx_data[3] = (byte)(pos0 & 0x007F);
36    tx_data[4] = 0x00;
37    tx_data[5] = ICS_POS_CMD + 0x01;
38    tx_data[6] = (byte)((pos1 & 0x3F80) >> 7);
39    tx_data[7] = (byte)(pos1 & 0x007F);
40    tx_data[8] = 0x00;
41    tx_data[9] = ICS_POS_CMD + 0x02;
42    tx_data[10] = (byte)((pos2 & 0x3F80) >> 7);
43    tx_data[11] = (byte)(pos2 & 0x007F);
44
45    //Send and receive
46    Synchronize_slave(tx_data,12);
47 }
48
49 void ics_set_sp_slave(byte spData0, byte spData1 ,byte spData2)
50 {
51    byte tx_data[9];
52    // Create send command
53    tx_data[0] = ICS_PARA_WRITE_COMMND;
54    tx_data[1] = SUB_SP_COMMND;
55    tx_data[2] = spData0;
56    tx_data[3] = ICS_PARA_WRITE_COMMND + 0x01;
57    tx_data[4] = SUB_SP_COMMND;
58    tx_data[5] = spData1;
59    tx_data[6] = ICS_PARA_WRITE_COMMND + 0x02;
60    tx_data[7] = SUB_SP_COMMND;
61    tx_data[8] = spData2;
62
63    //Send and receive
64    Synchronize_slave(tx_data,9);
```

```
65 }
66
67 void setup() {
68   Serial.begin(115200, SERIAL_8E1);  //UART communication settings
69   pinMode(EnPin, OUTPUT);            //Setting of send/receive switching
         pin
70   digitalWrite(EnPin, LOW);             //Always in receive mode
71 }
72
73 void loop() {
74   //ics_set_pos_slave(10172,4000,7400);//Left-Right phase 1
75   ics_set_pos_slave(10047,5500,6500);//Up-down phase1
76   //ics_set_pos_slave(10172,5085,7274);//Left-Right phase2 1
77   delay(1000);
78   //ics_set_pos_slave(10047,4750,6650);//Left-Right phase 2
79   ics_set_pos_slave(9847,4750,5750);//Up-down phase1
80   //ics_set_pos_slave(10047,5467,6892);//Left-Right phase2 2
81   delay(1000);
82   //ics_set_pos_slave(9900,5500,5900);//Left-Right phase 3
83   ics_set_pos_slave(9647,4000,5000);//Up-down phase1
84   //ics_set_pos_slave(9900,5649,6710);//Left-Right phase2 3
85   delay(1000);
86 }
```

A.2.2 B3M-SC-1170-A

```
1 #include <IcsHardSerialClass.h>
2
3 const byte EN_PIN = 2;
4 const long BAUDRATE = 115200;
5 const int TIMEOUT = 1000;
6 int id = 0;
7 int Ref_Time = 5000; //0.5 sec
8
9 IcsHardSerialClass B3M(&Serial1,EN_PIN,BAUDRATE,TIMEOUT);
```

```
10
11 void setup() {
12
13   B3M.begin();
14   Serial1.begin(115200, SERIAL_8N1);
15   Serial.begin(115200);
16
17   //B3M_WriteCmd(int id, int Data, int Address)
18   B3M_WriteCmd(id, 0x02, 0x28);
19   B3M_WriteCmd(id+1, 0x02, 0x28);
20   B3M_WriteCmd(id+2, 0x02, 0x28);
21   delay(500);
22
23   B3M_WriteCmd(id, 0x02, 0x28);
24   B3M_WriteCmd(id+1, 0x02, 0x28);
25   B3M_WriteCmd(id+2, 0x02, 0x28);
26   delay(500);
27
28   B3M_WriteCmd(id, 0x01, 0x29);
29   B3M_WriteCmd(id+1, 0x01, 0x29);
30   B3M_WriteCmd(id+2, 0x01, 0x29);
31   delay(500);
32
33   B3M_WriteCmd(id, 0x00, 0x5C);
34   B3M_WriteCmd(id+1, 0x00, 0x5C);
35   B3M_WriteCmd(id+2, 0x00, 0x5C);
36   delay(500);
37
38   B3M_WriteCmd(id, 0x00, 0x28);
39   B3M_WriteCmd(id+1, 0x00, 0x28);
40   B3M_WriteCmd(id+2, 0x00, 0x28);
41   delay(500);
42 }
43
```

```
44 void loop() {
45
46   //B3M_setPos(int id, int Pos, int Time)
47
48   // AA movement
49   B3M_setPos3(id,id+1,id+2,-14554,9672,11524);
50   delay(2000);
51
52   B3M_setPos3(id,id+1,id+2,-14520,9486,11196);
53   delay(2000);
54
55   B3M_setPos3(id,id+1,id+2,-14084,8755,10738);
56   delay(2000);
57
58   B3M_setPos3(id,id+1,id+2,-14520,9486,11196);
59   delay(2000);
60
61   // FE movement
62   //B3M_setPos3(id,id+1,id+2,-20866,6604,11433);
63   //delay(2000);
64
65   //B3M_setPos3(id,id+1,id+2,-19967,6803,11482);
66   //delay(2000);
67
68   //B3M_setPos3(id,id+1,id+2,-18751,7210,11515);
69   //delay(2000);
70
71   //B3M_setPos3(id,id+1,id+2,-17282,7888,11516);
72   //delay(2000);
73
74   //B3M_setPos3(id,id+1,id+2,-15482,8844,11454);
75   //delay(2000);
76
77   //B3M_setPos3(id,id+1,id+2,-14066,9800,11382);
```

```
78    //delay(2000);
79
80    //B3M_setPos3(id,id+1,id+2,-11535,11770,11155);
81    //delay(2000);
82
83    //B3M_setPos3(id,id+1,id+2,-12742,10775,11272);
84    //delay(2000);
85
86    //B3M_setPos3(id,id+1,id+2,-11535,11770,11155);
87    //delay(2000);
88
89    //B3M_setPos3(id,id+1,id+2,-14066,9800,11382);
90    //delay(2000);
91
92    //B3M_setPos3(id,id+1,id+2,-15482,8844,11454);
93    //delay(2000);
94
95    //B3M_setPos3(id,id+1,id+2,-17282,7888,11516);
96    //delay(2000);
97
98    //B3M_setPos3(id,id+1,id+2,-18751,7210,11515);
99    //delay(2000);
100
101   //B3M_setPos3(id,id+1,id+2,-19967,6803,11482);
102   //delay(2000);
103 }
104
105 int B3M_WriteCmd(byte id, byte TxData, byte Address){
106
107   byte txCmd[8];
108   byte rxCmd[5];
109   unsigned int reData;
110   bool flg;
111
```

```
112   txCmd[0] = (byte)(0x08);        // SIZE
113   txCmd[1] = (byte)(0x04);        // CMD
114   txCmd[2] = (byte)(0x00);        // OP
115   txCmd[3] = (byte)(id);          // ID
116   txCmd[4] = (byte)(TxData);      // DATA
117   txCmd[5] = (byte)(Address);     // ADR
118   txCmd[6] = (byte)(0x01);        // CNT
119   txCmd[7] = (byte)(0x00);        // SUM
120
121   for(int i = 0; i < 7; i++){
122     txCmd[7] += txCmd[i];
123   }
124   txCmd[7] = (byte)(txCmd[7]);    // SUM
125
126   flg = B3M.synchronize(txCmd, sizeof txCmd, rxCmd, sizeof rxCmd);
127
128   if (flg == false)
129   {
130     return -1;
131   }
132
133   reData = rxCmd[2];
134   return reData;
135 }
136
137 int B3M_setPos3(byte id0, byte id1, byte id2, int Pos0, int Pos1, int
      Pos2){
138
139   byte txCmd[15]={0};
140   byte rxCmd[15]={0};
141   unsigned int reData;
142   bool flg;
143
144   txCmd[0] = (byte)(15);    // SIZE
```

```
145    txCmd[1] = (byte)(0x04);    // CMD
146    txCmd[2] = (byte)(0x00);    // OP
147
148    // Motor 0 set
149    txCmd[3] = (byte)(id0);      // ID0
150    txCmd[4] = (byte)(Pos0 & 0xFF);        // POS_L
151    txCmd[5] = (byte)(Pos0 >> 8 & 0xFF); // POS_H
152
153    // Motor 1 set
154    txCmd[6] = (byte)(id1);      // ID0
155    txCmd[7] = (byte)(Pos1 & 0xFF);        // POS_L
156    txCmd[8] = (byte)(Pos1 >> 8 & 0xFF); // POS_H
157
158    // Motor 2 set
159    txCmd[9] = (byte)(id2);      // ID0
160    txCmd[10] = (byte)(Pos2 & 0xFF);        // POS_L
161    txCmd[11] = (byte)(Pos2 >> 8 & 0xFF); // POS_H
162
163    txCmd[12] = 0x2A; //ADR
164    txCmd[13] = 0x03; //CNT
165
166    for(int i = 0; i < 14; i++){
167      txCmd[14] += txCmd[i];
168    }
169    txCmd[14] = (byte)(txCmd[14]);    // SUM
170
171    flg = B3M.synchronize(txCmd, sizeof txCmd, rxCmd, sizeof rxCmd);
172
173    return 0;
174 }
```

A.3 Questionnaire form of experiment

添付資料

「 親指のウェアラブルリハビリテーションロボットの開発 」の実験後アンケート

東京工業大学　工学院　機械系
研究代表者　武田　行生
研究担当者　Choi Woohyeok

本日は実験にご協力いただきありがとうございます。もしよろしければ、可能な範囲で当アンケートにご回答いただけると幸いです。

留意事項

- ご回答いただいたアンケートの結果を学内・学外で公表することがございます。なお、アンケート結果を公表する際には、 匿名化に加工し公表いたします。
- 実験に関わった担当者は、実験を通じて知り得た個人情報や、実験データ・アンケート以外の情報を口外することはありません。

上記留意事項にご了承いただけない場合は，当アンケートにご回答いただく必要はございません

アンケート

1. 年齢と性別を教えてください。

年齢：（　　）

□ 男　　□ 女

2. 実験中に感じた不便な抵抗感がありましたか？

□ はい　　□ いいえ

あったら、どの動きの時でしたか？

□ 「屈曲・伸展」　□ 「外転・内転」　□ 両方とも

どの程度でしたか？

□ 弱い　　□ 中程度　　□ 強力　　□ かなり強力

手のどの部分でしたか？〇をつけてください。

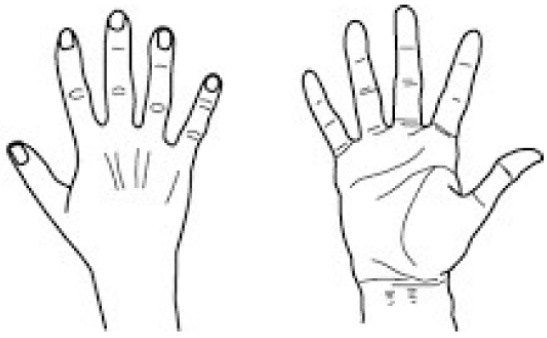

（裏面に続く）

3. ロボットの重さはどう感じましたか？

☐ 軽い　☐ ちょっと軽い　☐ ちょうどいい　☐ やや重い　☐ 重い

4. その他、何か気付いた点がございましたら、自由にご記入願います。

ご協力ありがとうございました。

A.4 Assembly drawing of the prototype

Ver. KRS-3304 ICS

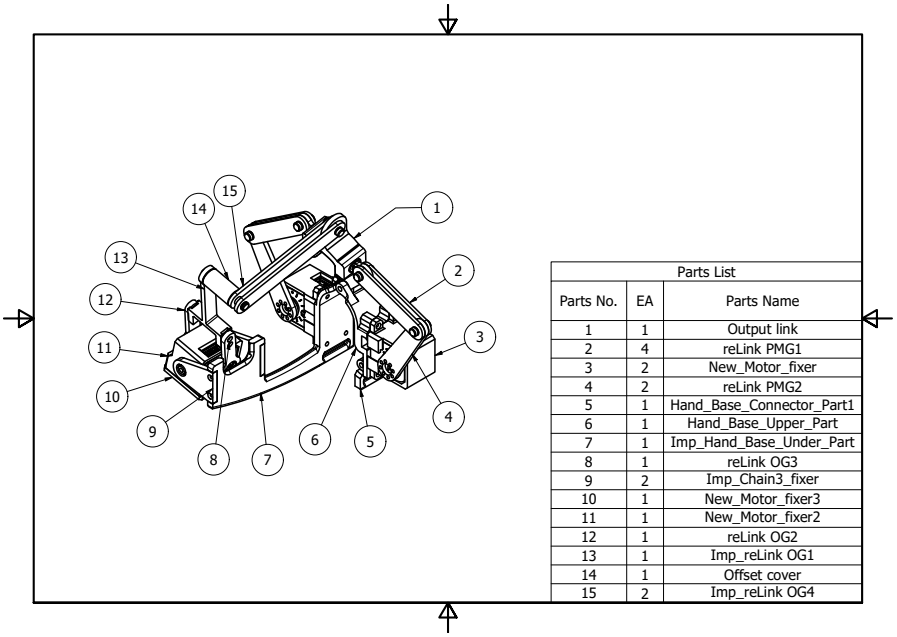

Parts List		
Parts No.	EA	Parts Name
1	1	Output link
2	4	reLink PMG1
3	2	New_Motor_fixer
4	2	reLink PMG2
5	1	Hand_Base_Connector_Part1
6	1	Hand_Base_Upper_Part
7	1	Imp_Hand_Base_Under_Part
8	1	reLink OG3
9	2	Imp_Chain3_fixer
10	1	New_Motor_fixer3
11	1	New_Motor_fixer2
12	1	reLink OG2
13	1	Imp_reLink OG1
14	1	Offset cover
15	2	Imp_reLink OG4

Ver. B3M-SC-1170-A

As shown in the following Figure, Nine parts were designed, and other parts of the previous version were reused.

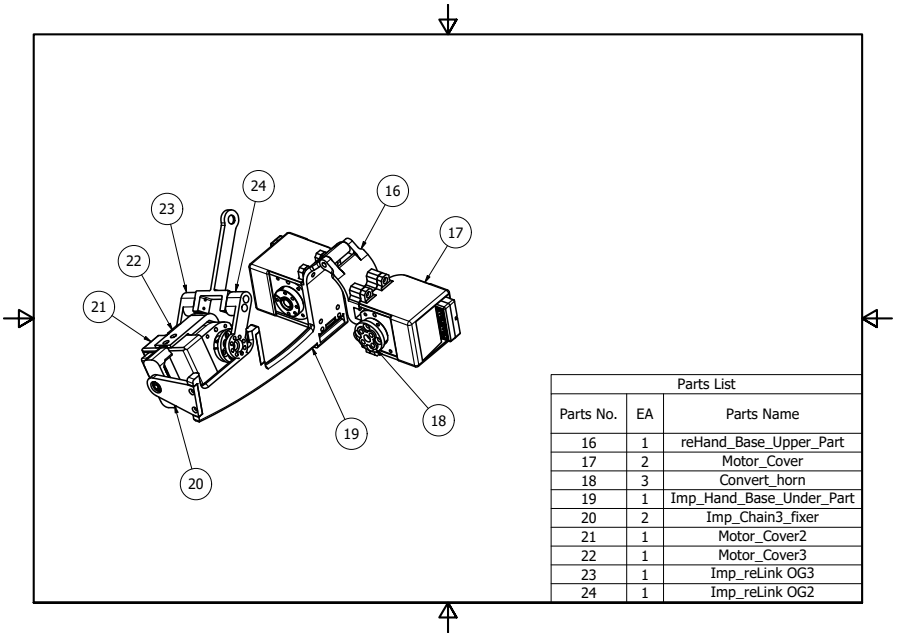

Parts List		
Parts No.	EA	Parts Name
16	1	reHand_Base_Upper_Part
17	2	Motor_Cover
18	3	Convert_horn
19	1	Imp_Hand_Base_Under_Part
20	2	Imp_Chain3_fixer
21	1	Motor_Cover2
22	1	Motor_Cover3
23	1	Imp_reLink OG3
24	1	Imp_reLink OG2

Acknowledgements

I would like to thank all those who made the accomplishment of this work possible.

First of all, I am very grateful to my supervisor and mentor Prof. Yukio Takeda, for his continuous and unconditional support throughout my research duration at the Tokyo Institute of Technology. His generosity and guidance in my work made it possible for me to promote my research ideas and achievements at international conferences and eventually awards two prizes. Also, I am grateful to Prof. Yusuke Sugahara and Prof. Daisuke Matsuura for the inspiration from them during my research.

I would also like to thank my thesis committee members, Prof. Nobuyuki Iwatsuki, Prof. Masafumi Okada, Prof. Gen Endo, and Wataru Hijikata for providing helpful feedback through the dissertation defence.

I would like to thank all participants who volunteered for our experiment to adjust their strict schedules and endure the long distance to our laboratory and the weather in spite of the difficult situation of the world. This work would have been impossible without their support.

I would like to express my thanks to the secretaries of our laboratory, Ms. Hiroko Takano and Ms. Taiko Ichinose, for providing big help not only paper-chase in the Tokyo Tech but also encourage me up. Thanks to their friendly help, I could spend lab life in a calm atmosphere.

Moreover, my special thanks go to all student members of the Mechanical Systems Design Laboratory (Takeda Sugahara Lab.) who contributed to stimulating conversations, encouraging the motivation of the research, and a pleasant working atmosphere. Especially, my sincere thanks go to Mr. Hiroshi Matsuo and Mr. Masumi Ohno, who shared the pleasures and pains during my lab life, for their discussions and support of my research and their help in daily life.

It is through the constant love, support, and patience of my family, this work

could be accomplished. My parents were always by my side whenever I needed them and inspired me not to quit when difficult, not to yield when it was tough.

I would also like to thank the funding by Grant-in-Aid for Scientific Research of Japan Society for the Promotion of Science (JSPS grant # 17H03162) and ABE TECHNO SYSTEM Co., Ltd. for supporting this research and helping me pursue my research endeavours.